Acousto-Ultrasonics for Defect Assessment of Composite Materials

Kevin M Dugmore

A thesis submitted in compliance with the requirements for the masters degree in technology in the Department of Mechanical Engineering at Technikon Natal.

Approved for final submission.

21 MAY 2002

D. Jonson	*Prof.* M. Walker	Date
MSc Eng (Natal)	*MSc Eng (Natal), PhD (Natal)*	
Supervisor	Co-Supervisor	

Durban, South Africa

January 2002

Declaration

I declare that this thesis is my own unaided work except where due acknowledgement is made to others. This thesis is being submitted for the masters degree in Technology to the Department of Mechanical Engineering at Technikon Natal, Durban, and has not been submitted previously for any other degree or examination.

Date 21/05/2002

Kevin Dugmore

Acknowledgements

I would like to thank David Jonson and Prof. Mark Walker for the opportunity to study for the Master of Technology qualification. I appreciate their help and guidance during my time at Technikon Natal.

Kentron (Pty) Ltd has funded this project and provided test specimens. It is encouraging to see their commitment to the development of skills in South Africa.

I am also thankful to my parents not only for their support and guidance but also for showing, by way of example, that success is achieved through conscientiousness.

Abstract

The experiments and their results contained herein will form the basis for the development of a portable non-destructive testing device for composite structures. This device is to be capable of detecting any of a variety of defects and assessing their severity within a short time.

A study of the acoustic emission (AE) method was initially undertaken and this brought to the attention of the researchers an alternative method, the acousto-ultrasonic (AU) method. An investigation of the AU method was then embarked upon and subsequently the focus of the project was shifted to the AU method. The propagation of sound in composites was investigated and the theoretical fundamentals of waves in plates were reviewed.

By applying the AU method in a series of experiments a repeatable test method was developed and a practical understanding of the propagation of ultrasonic waves in composite materials was gained. Furthermore, these experiments have proved that the AU method can be used to measure a material's anisotropy, identify resin content variations and determine the fibre orientation. Thereafter, the method's capability for the detecting defects in specially fabricated specimens was assessed. Limited success was achieved in the detection of impact damage and simulated delaminations. The AU method was applied in a realistic situation to 2 different components; both of sandwich construction, and skin to core delaminations were accurately identified.

The effect of the frequency of the input signal was investigated in a repeat of some of the initial experiments. By selecting a specific input frequency the detection of simulated delaminations was improved.

The development of a portable AU testing device for composite structures is feasible. However AU does have its limitations that will add to the complexity of its implementation.

Nomenclature

σ_{ij}	=	stress tensor
ρ	=	density
f	=	force
$\ddot{u}_i$	=	acceleration
ε_{ij}	=	strain tensor
$u_{i,j}$	=	displacement
λ	=	Lamé constant = $\frac{2\mu\upsilon}{1-2\upsilon}$
μ	=	Lamé constant
x	=	displacement in x direction
t	=	time
y	=	displacement in y direction
d	=	plate thickness
h	=	plate thickness
k	=	wave number
c_L	=	extensional wave velocity
c_T	=	flexural wave velocity
c_p	=	velocity of the Lamb wave mode
c_R	=	Rayleigh surface wave velocity
ω	=	circular frequency

Glossary

Arrival time	The time taken for an acoustic wave to cover the distance between the source and receiving transducers.
AU parameter	A number, determined from a recorded waveform that is used for characterising it so that it may be compared to other waveforms.
Central frequency	The centre frequency of a waveform relative to the amount of energy. Central frequency is determined by calculating the centroid of the area below the Fourier transfer curve.
Couplant	A fluid that fills the air gaps between a transducer and the material that is being tested so as to allow the efficient transmission of acoustic energy between the transducer and material under test.
Energy content	A measure of the energy of an acoustic wave, determined by calculating the area below the Fourier transfer curve[1].
Lead break method	A means of generating acoustic waves within a material and involves breaking pencil lead against the material's surface. This method can be used as an alternative to the use of a source transducer.
Peak voltage / amplitude	The highest voltage / amplitude of a recorded waveform.

[1] cf. Kiernan, M. T. and Duke, J. C. Jr., 1988. PC Analysis of an Acousto-Ultrasonic Signal. Materials Evaluation, pp 1344-1352.

Receiving transducer — A piezoelectric device that is used to detect acoustic waves within a structure and convert them to an electrical output.

Ringdown counts — Ringdown counts is defined as the number of times that a signal's voltage crosses a set voltage level (called the threshold).

Source transducer — A piezoelectric crystal, contained within a housing, that when supplied with an electrical input, emits an acoustic wave into the material to which it is coupled. Also referred to as a pulser.

Stress wave factor — A measure attenuation, often abbreviated to SWF.

SWF = GRN

where: R = the repetition rate at which the source transducer emits acoustic waves

N = number of ringdown counts counted by the counter

G = counter reset time.

Threshold — A voltage level that is set for the recording of AU waveforms such that when the voltage of a received signal exceeds the threshold, recording commences.

Trigger sensor — A transducer that is placed next to the source transducer and set to trigger the recording system as soon as an emission enters the material. Such an arrangement is used when the arrival time needs to be determined.

List of Figures

List of Tables

Contents

Introduction

Composite structures will, in all probability, be damaged while in service regardless of how carefully they are designed, operated and maintained. In addition to sustaining fatigue damage due to in service loads, composite structures are particularly vulnerable to damage from impacts. In the case of aircraft common causes of impact damage are bird strikes, the impact of tools during maintenance, hail and lightning.

Their complex manufacture processes, if not stringently controlled, leave composites susceptible to manufacture flaws. Furthermore, flaws can be introduced during the maintenance of a structure by way of a defective repair. Typical flaws include resin-starved or rich regions, weak interlaminar bonds and resin porosity.

Due to the high cost of the replacement of defective components, the implementation of repairs is essential. The design and implementation of a composite repair, especially in critical situations such as on an aircraft's airframe needs to be undertaken in a controlled and careful manner. Repair design should aim at achieving a repaired region whose mechanical properties match, as closely as possible, the properties of the surrounding material. To design a repair that results in a stronger region is seldom desirable since the increased strength may also result in local stiffening, possibly leading to premature failure.

Non-destructive evaluation methods are thus necessary for locating damage and assessing its severity so that, if necessary, repairs can be undertaken. Additionally the integrity and properties of the completed repairs needs to be assessed.

Initially, the acoustic emission (AE) method was considered and a review of the relevant literature was undertaken. Early in this study it became clear that a related method called acousto-ultrasonics (AU) would be better suited to meeting the project's aims and the focus of the study was shifted to the AU method. AE and AU do however have much in common, thus the study of the AE method was continued and much of this literature is relevant to the AU method.

The aim of this project is to establish a basis for the development of a portable device that can address the need for a non-destructive testing technique for the evaluation of composite structures. This testing device is to be capable of quickly detecting and evaluating the severity of damage and manufacturing flaws as well as evaluating repairs. To this end, an understanding of the use of AE equipment and the propagation of sound waves in composite materials is required. The capability of the AU to meet the project's aims is to be assessed.

AU is a technique based on the introduction of ultrasonic sound waves to the test structure. These waves are recorded after they have travelled through a volume of material. As it passes through the material, the wave shape is modified whereby the modification depends on the material properties and the presence of defects. Thus, with an understanding of how a particular defect or property variation affects the transmission of a sound wave, an assessment of the material can be made.

Part of the following study details the AU experiments undertaken to gain an understanding of the propagation of sound waves in composite plates. The theory that governs the propagation of waves has been reviewed. Based on this theory, dispersion curves have been plotted and comparisons with experimental results have been made.

The factors that influence the repeatability of AU tests have been identified and this has aided the development of a repeatable test method. The potential of the AU method for defect detection has been assessed with the use of damaged laminates and laminates that contain simulated defects. Encouraging results were achieved from the testing of an aircraft component and a damaged wake-board. Finally, the effect of varying the input frequency on the efficacy of the AU method has been has been investigated.

Chapter 1

Literature Review

1.1 Composite Materials

1.1.1 Introduction

Since the aim of this study is to develop a testing method for composite materials, a brief outline of composites, their advantages and their properties has been given.

In general, the term 'composite material' indicates a material that is made up of distinct parts or constituents [1]. The reason for combining materials to form a composite is to obtain a structure that posses properties that suit an application better than either of the constituents by themselves.

1.1.2 Fibre Reinforced Plastics

The types of composite materials that are relevant to this study are fibre-reinforced plastics (FRP). FRPs are a combination of a resilient, durable polymer-based resin and a strong fibrous 'cloth'.

Common types of fibre are glass, carbon and aramid. The fibres are strong, stiff and light, are the composite's primary load-carrying constituent and act as centres to suppress the propagation of cracks and defects in within the material. Fibre strands are normally woven together to form a cloth. A typical cloth may consist of fibres arranged in a single direction (uni-directional) or in 2 perpendicular directions (bi-axial mat).

Resins used in FRPs are polymer based unsaturated polyester or epoxy. Since the resin surrounds the fibres, it is often termed the 'matrix'. The purpose of the matrix is to protect the fibres, to hold them in place as well as to spread the load applied to the

composite between the individual fibres [2]. As an engineering material, polymer-based resin's major advantage is that it is supplied in a liquid form. This allows products to be cast into complex shapes thereby eliminating the need for machining operations. Furthermore, resins have a high resistance to the environment, water and other aggressive substances.

The combination of a polymer-based matrix with reinforcing fibres results in a composite that has the advantages of each of the constituents. An FRP thus has high strength and stiffness, low density, ease of moulding and a high environmental resistance.

1.1.3 The Properties of FRPs

The properties of the composite will depend on the properties of the constituents and the manner in which they are combined [3].

The properties of an FRP will depend on:
(a) the properties of the fibre,
(b) the properties of the resin,
(c) the ratio of fibre to resin,
(d) and the orientation of the fibres.

When considered in isolation both the fibres and the matrix are isotropic. However, because the fibres are long and thin and can thus only effectively transmit loads down their length, the combination of resin and fibres produces a product that is anisotropic. This is because a composite's property that is measured in the direction of the fibres is strongly dependant on the properties of the fibres. Whereas when the properties are measured at perpendicular to the fibre direction, they will be strongly influenced by the properties of the matrix.

To effectively design composite structures so as to utilise their advantages is more complex than designing using isotropic materials. However, design techniques have advanced in recent times leading to the more widespread use of composites. The need for evaluation techniques for composite structures is thus growing.

1.2 Propagation of Sound in Solids and Composites

1.2.1 Introduction

Because of their anisotropy, composites have a more complex mechanical response to applied loads, static or dynamic, than that of isotropic materials. Anisotropy introduces many wave phenomena not observed in isotropic bodies: a directional dependence of wave speed, a difference between phase and group velocity, wave skewing and three different wave speeds instead of two. An understanding of the propagation of waves in anisotropic materials is thus necessary if one is to inspect them using ultrasonic methods [4].

1.2.2 Dispersion

Associated with wave propagation in solids, is a phenomenon known as dispersion. Engineering materials at their operating temperatures are nondispersive [5], in which case the wave travels without becoming distorted. Structures however, are in some cases dispersive. Boundary conditions applied to solids, plates and rods can cause them to become dispersive. Dispersion causes wave distortion or 'spread' due to each frequency component travelling at a unique velocity. In such a case the amplitude and frequency of a received signal will vary with time. The dispersion characteristics of a material can be depicted in a plot called a dispersion curve. A dispersion curve shows the velocity of each wave mode as a function of the product of frequency and plate thickness.

1.2.3 Waves in Plates

Since many structures are geometrically plate-like it follows that when acoustic testing techniques are used, plate waves and dispersion will feature. Lamb [6] was the first derive the mathematical formulation of plate waves and plate waves have since frequently been referred to as Lamb waves.

Fowler and Papadakis [5] have introduced simulated acoustic emissions to an aluminium plate and measured the frequency spectra of various gated segments of the received signal. The results of this experiment have been compared to dispersion curves that were based on plate wave theory. A good correlation was found between the two, leading the authors to conclude that plate mode analysis is valid for describing the dispersive nature of acoustic energy in plates.

Classical plate theory, predicts the presence of 3 modes of wave propagation in a plate [7]. This theory is based on the assumption of plane stress in a thin plate and where the wavelength is large in comparison to the plate thickness. These three modes are called the extensional, flexural and the in-plane shear modes [8]. Both the flexural and extensional modes have in plane and out of plane components, however in AE and AU measurements, it is usually only the out of plane component that is detected since the transducer is coupled on the plate's surface. The in plane component can be detected by coupling the receiving transducer to the edge of the plate [9-11].

The flexural wave can be thought of as causing the plate to ripple and bend and thus has the larger of its two displacement components at perpendicular to the plane of the plate. Flexural waves (lowest order anti-symmetric or A0) are dispersive with the higher frequencies travelling at higher velocities.

The extensional component (lowest order symmetric or S0) has the larger of its two displacement components in the plane of the plate. These waves are sometimes called pressure or compression waves and have a higher velocity than flexural waves. Thus, on a waveform the extensional waves feature at the wave's leading edge. Classical plate theory only predicts an in plane displacement component for the extensional mode while higher order theories predict [12, 13] and experimental measurements verify the existence of an out of plane displacement component for this mode. This out of plane component is due to the Poisson effect from the in plane motion and thus propagates at the same velocity as the extensional wave [14]. It is due to this out of plane component that extensional waves can be detected by a transducer that is coupled to a plate's surface.

The elastic wave energy in a plate can be divided into an infinite number of modes with each mode having a unique displacement profile. Rose [15] has plotted the displacement profiles of the S0, S1, S2, A0, A1 and A2 modes in an aluminium plate (where Sn denotes the n^{th} order symmetric mode and An denotes antisymmetric modes). Work by Ditri *et al* [16] has shown that improved sensitivity to certain defects can be obtained by selecting a specific mode and displacement profile. Higher modes have what is called a cutoff frequency. Each wave mode will only exist at frequencies below its cutoff frequency. The cutoff frequencies have been shown to depend on the thickness of the plate.

By means of AU-type experiments, Egle and Brown [17] have shown that much of the energy in the received signal is concentrated at certain frequencies. These frequencies have been correlated with those predicted by Lamb wave theory. This theory shows that the cutoff frequencies and the frequencies excited within a plate are dependent on the plate's smallest dimension ie its thickness.

Kiernan and Duke [18] have also shown that a wide band pulse when input into a material will cause vibrations within few narrow frequency bands. It was found that these frequencies correlate to wavelengths that are multiplies of the material thickness. The cutoff frequency phenomenon, according to Kiernan and Duke, occurs when the wavelengths are less than the plate thickness due to coupling between the body waves. This is consistent with the constructive/destructive wave interference model proposed by Achenbach [19], in which wave interference creates plate waves at frequencies that correspond to wavelengths that are multiples of the plate thickness.

An experimental aspect of Kiernan and Duke's [18] research involved the comparison of the frequency content of a signal recorded in a four-ply laminate to that recorded in an eight-ply laminate. It was found that frequencies at 1 MHz and 3,4 MHz were dominant in the 4 ply laminate and that in the eight ply laminate the dominant frequencies were 500 MHz and 1,7 MHz. This experiment has confirmed the relation between plate thickness and the frequencies excited.

1.2.4 The AU Method for Investigating Sound Propagation in Composites

Kiernan and Duke [18] have investigated the effect that fibre orientation has on acoustic waves in composites. A series of AU tests were conducted which involved moving the sending transducer to various angular positions around the receiving transducer and recording waveforms at each position. The recorded signal's energy content and central frequency were plotted as a function of the direction of travel relative to the fibre orientation. The energy content was found to be at a maximum when the wave travelled parallel to the fibre direction and a minimum when the wave travelled perpendicular to the fibre direction. It was found that the signals central frequency was also influenced by the fibre orientation and was highest when the signal travelled at 15° to the fibre direction.

Talreja [20] has run a similar set of experiments to those of Kiernan and Duke so as to investigate the effect of fibre angle on sound waves. AU measurements have been taken in a radial pattern on unidirectional composite specimens and 5 parameters (as defined in section 1.4.3) were derived from the AU data. A correlation between the RMS value (equal to $\sqrt{SWF_1}$) and the elastic modulus of the material in the signal's direction of propagation was found. No clear variation in the parameters SWF_2 and SWF_3 was evident, indicating the basic frequencies of the stress wave are maintained for all directions of signal propagation. The ratio SWF_3 / SWF_4 is a measure of the stress wave irregularity and was found to decrease with increasing off-axis angle. SWF_5 was found to increase as the off axis angle increased, indicating an increase in the skewness of the stress wave.

Early experiments by Kroll [21] showed that both flexural and axial vibration modes were excited by a source in thin rods and that both transducer and specimen resonances were evident in the detected signal.

Egle and Brown [17] have conducted a series of simulated acoustic emission experiments the aim of which was to assess the effects of structural geometry on the

detection of emissions. They used a pulser and receiver arrangement on thin aluminium plates and bars and found that the received signals were frequency selective with much of the energy concentrated near the specimen's resonant frequencies. Lamb wave theory has been used to predict these frequencies and shows that the resonances are dependent on the thickness of the plate. The predicted and observed resonance frequencies were found in most cases to correlate. Each frequency corresponds to a different wave propagation mode and has a unique displacement and stress field. The number of resonances was found to increase as the thickness of the specimen was increased. The findings of the study are that a signal contains both specimen and transducer resonances and that the detection equipment must be capable of detecting the specimen's resonant frequencies.

1.2.5 Conclusions

The complexities associated with the propagation of sound in composite materials have been outlined. This has shown the importance of interpreting data from AU tests with consideration for dispersion, the directional dependence of wave speed and the wave modes present and their cutoff frequencies.

In the case of plate-like structures, due to dispersion, one can expect the frequencies of the received signals to occur in narrow bands where each band can be associated with a particular wave mode. It has been shown that these bands are related to the thickness of the plate. Furthermore, the characteristics of the receiving transducer and the resonances of the structure will also be imprinted on the received signal.

The characteristics of the receiving transducer and recording system are of paramount importance since this will govern the wave modes that are recorded. It is important that the receiving transducer can detect the resonances of the test piece. Furthermore, it has been suggested that improved defect detection may be achieved by isolating a particular wave mode.

1.3 Acoustic Emission

Initially it was thought that the acoustic emission method could be used to meet the project's objectives. Thus a review of the literature on acoustic emission principles and practice was undertaken. It however soon became apparent that the acousto-ultrasonic method would be more appropriate and thus the focus of the literature review shifted to the acousto-ultrasonic method. Nevertheless a summary of the AE literature reviewed has been included and is relevant since many aspects of the AE method can also be applied to the AU method.

1.3.1 Introduction

Acoustic emissions are pulses of elastic strain energy that are released when a loaded material fails locally so as to relieve stresses. The information contained in these energy pulses can be used to determine the failure mechanism that caused the emission, the rate at which damage is occurring and the location of the damage within a structure.

Acoustic emissions are normally ultrasonic (their frequency falls within the range 30 kHz to 30 MHz) and thus can only be detected by means of sensors that are attached to the component's surface. AE sensors (or transducers) are in principle high frequency microphones, which are coupled with a fluid (called a couplant) to the surface of the structure to be monitored so that the best possible acoustic transmission is achieved. These AE sensors convert the acoustic emissions to electrical signals, which are then transmitted to a data capture and storage system that records them. Software enables one to playback and analyse the recorded AE signals.

1.3.2 The Development of the AE Technique

The first AE instruments were the seismological equipment used to measure the oscillations of the earth's crust as a result of earthquakes. In the 1950s, the AE method was first applied to metals and wood by Joseph Kaiser [22]. With his

instruments he was able to hear sounds in the specimen as it deformed and he is widely accepted as being the originator of AE as an NDT method.

1.3.3 AE Testing of Composite Materials

The use of AE techniques on fibre-reinforced structures is more complex than on metal structures. Composites are anisotropic and have a layered structure. These characteristics cause a directional dependence of wave speed and a more complex response to a sound wave. Thus, when compared to the AE testing of metals, source location and the interpretation of waveforms is more difficult. Furthermore the many fibre/matrix interfaces cause rapid signal attenuation meaning that more transducers are needed to effectively cover a component's geometry. However, if the AE method is applied correctly, damage mechanisms such as matrix cracking, fibre fracture, fibre/matrix disbonding and bond failure in assembled joints (for example, nozzles, manways, etc.) can be identified [22].

1.3.4 Early AE Concepts and Practice

The early AE studies were based on differing concepts to those used in recent times. The earlier studies primarily used an amplitude analysis for characterizing signals while in the later studies the analysis of the signals is based on the principles of wave propagation.

From its first use in the 1960s until about 1995, AE technology did not record waves since most of the wave was filtered out through the use of a resonant sensor. Resonant sensors have superior sensitivity, however they give a weak response at all frequencies other than at the sensor's resonant frequency. Thus the recorded information is reduced to whether damage has occurred at a particular time or not.

Old AE concepts assume that the AE wave has the shape of a damped sine function. Amplitude analyses were carried out and the parameters ringdown counts, event duration, event amplitude and rise time comprised the basic data set. An amplitude analysis of this type is easy to implement and since it seems indicate the failure mode present has been the focus of many studies in the past [23-26]. However this

approach but has led to findings that contradict one another and its validity is thus doubtful. For example, some studies have found that low amplitude events can be associated with matrix cracking and high amplitude events with fibre breakage [23, 24], however other researcher's findings have contradicted this [25, 26]. Thus it seems improbable that a particular failure mode can be unambiguously associated with an AE event of particular amplitude [27]. Furthermore Pao [28] has stated that there is no theoretical basis for the use of the parameter-based approach. The conflicting findings arising from the amplitude-based analyses have led to a loss in confidence in the AE method and since 1988 support for AE research has dwindled [29].

1.3.5 Recent AE Concepts and Practice

An effort to derive the fundamental principles of AE was undertaken in the 1970s [30-33] and new AE technology has been based on these principles. The fundamental principles are based on Mindlin plate theory, assumed displacement theories and thin rod and beam theory.

The main characteristic of the new technology is that waves that are an accurate indication of the particle motion within the material are recorded and analysed. Since acoustic emissions excite waves with numerous frequency components, a wide band sensor is required. Wide band sensors respond equally to a wide range of frequencies and when used with a high sampling frequency and advanced electronics that do not distort the signal, waveforms can be accurately captured. The shape of the waveforms and their velocities are analysed in terms of the material's wave propagation characteristics in an attempt to identify and locate the emission source. However, these advanced AE practices are difficult to implement outside the laboratory and are have thus not been widely used [29].

1.3.6 The Use of AE for Condition Assessment

Acoustic emission techniques can be applied to components in a proof type test to gauge the component's condition. Many researchers have demonstrated the AE method's capability for condition assessment and several ASTM standards on this topic exist.

The ASTM standard (ASTM E 1067-96) [34] provides guidelines to determine whether tanks or vessels have become significantly damaged as a result of in-service loading. A similar standard exists for the AE testing of small parts (ASTM E 1932-97) [35]. These standards specify the application of a controlled and measured stress and that the counts (the number of times that the AE signal exceeds a threshold voltage) be monitored. Trends in count data are used for evaluation i.e. an exponentially increasing count rate indicates uncontrolled, continuing damage and impending failure. An accept or reject criteria, based on the count rate, can thus be established to determine whether a particular component should be removed from service [36].

Morrás and co-workers [37] have applied similar methods to those described in the above ASTM standards to filament-wound GFRP pipes that have been exposed to corrosive media. Several pipes were made and then exposed to either hydrochloric acid or sodium hypochlorite. Samples from each pipe were then loaded in compression and the emissions were monitored with an AE system. The AE hits versus time plot for each sample was found to be different depending on the type of corrosive medium and exposure time. Therefore, this type of test could be used on GFRP samples that have been in service in corrosive environments for the purpose of determining their condition and remaining safe life.

Cheng and co-workers [38] have trained an artificial neural network to memorise acoustic emission behaviour of magnesium alloy specimens during tension–tension type fatigue loading. The network had two inputs which corresponded to cumulative AE average voltage and total counts while the neuron in the output layer corresponded to crack length. The neural network has successfully been used to

automate the interpretation of the trends in the AE data to determine the length of the cracks present and hence the remaining life of the specimen.

Hill *et al* [39] have demonstrated the AE method's capability for assessing the fibre to matrix bond strength. To cause bond failure at the fibre to matrix interface, tension specimens with a fibre bundle at perpendicular to the load direction were used. A range of interfacial bond strengths was achieved by the use of a variety of post cure procedures or by treating the fibres prior to the manufacture of the specimen. The ringdown counts per event was monitored by the AE system and was found to vary depending on the post cure and fibre treatment procedure used.

1.3.7 Failure Mode Discrimination

Acoustic emissions have been analysed by numerous researchers in an attempt to establish what failure mechanism caused the emission. There are several methods available to the researcher for the analysis of AE data. While the practical techniques used most of the studies reviewed are essentially the same it is the manner in which the data is analysed that is differs in each study.

Valentin *et al* [25] have conducted a study whose aim was to discriminate between various failure mechanisms by analysing the amplitudes of acoustic emissions. Both unidirectional and cross-plied carbon fibre-reinforced epoxy composites were loaded at various angles with respect to the fibre direction. By loading the specimens at various angles, one of three different failure processes were initiated, each of which dominate at a particular load angle. The results of this study indicate that high amplitude emissions correspond to matrix cracking parallel to the fibres, smaller amplitude emissions correspond to fibre breakage and that matrix cracking normal to the fibre direction does not produce significant emissions.

In a similar study to Valentin's, Kanji Ono has monitored both the amplitude and the duration of emissions from carbon fibre-reinforced epoxy specimens [26]. The specimens tested contained pre-cut laminae, arranged so as to cause either fibre fracture or delamination. The findings of this study can be summarised as follows:

(a) Short duration (< 100 μs), low amplitude (< 50 dB) events were associated with fibre fracture.
(b) Medium amplitude signals (50 – 70 dB) with average event durations of 120 μs indicated the initiation and slow growth of a delamination.
(c) Rapid advances of the delamination, accompanied by a load drop have long (200 μs) event durations and high amplitudes (70 dB).
(d) Splitting or cracking along the fibres produced low to medium amplitude events with a long duration (> 100 μs).

Barnes and Ramirez [40] have also analysed acoustic emissions in terms of their amplitude and duration. This analysis was applied to emissions generated in an offshore drilling riser made of carbon fibre reinforced plastic. Emissions due to delamination were found to have a long duration and low frequency content while those due to fibre breakage had a shorter duration, higher amplitude and a broader frequency content. A second part of this study involved the comparison of the AE activity of a glass fibre riser with that of a carbon fibre riser. It was found that the carbon fibre riser produced more emissions of both high and low amplitude.

Shiwa *et al* [41] have shown that the emission rate can be used to determine the failure mechanism. In his study notched glass-fibre specimens were subjected to cyclic loads during which the AE parameters amplitude, energy and duration were recorded. It was found that the failure of the specimens could be divided into four separate stages: fibre breakage, fibre pull out, matrix cracking (tension) and matrix cracking (compression). These four failure mechanisms were found to correspond to each of four emission stages, each characterised by a differing event rate and energy count rate. The emission rate can thus be used as an indicator of failure mechanism and furthermore the remaining safe life of a glass-fibre component.

A more advanced analysis technique called 'the wavelet transform' has been applied to AE data by Qi and his co-workers [42]. The wavelet transform replaces the more commonly used Fourier transform but instead of expressing the signal in the frequency domain at a fixed resolution, the wavelet transform transforms the signal to the time-frequency domain such that the higher the frequency the finer the resolution. The signals are expressed as a number of wavelet levels, each with

frequency limits and energy content. As a result of applying the wavelet transform, Qi *et al* found that the energy was concentrated in three wavelet levels and that each could be related to a failure mode. The energy in the 250 to 310 kHz range made up 75 % of the total energy and was due to fibre failure. The energy in the 150 kHz to 250 kHz range was due to fibre-matrix debonding and the energy in the 50 to 150 kHz range was attributed to matrix cracking.

Numerous studies exist [5, 9, 10, 43-45] in which the researchers have analysed the waveform in terms of the amplitudes of the flexural and extensional waves. In these studies, the extensional wave mode has been recognised in the waveform as the high frequencies that feature at the wave's leading edge.

Gorman [9] has recorded flexural and extensional waves modes caused by lead breaks on the edge and the surface of a plate and documented their relative amplitudes. This study has shown that a pencil lead break on the edge of a plate produces much larger extensional than flexural waves, while a pencil lead broken on the surface will produce a larger flexural than extensional mode. Gorman and Ziola then extended this study [43] and found that the extensional wave was the predominate wave mode arising from transverse matrix cracking because transverse matrix cracking produces motion in the plane of the plate.

Following on from these studies, Gorman and Prosser [10] have investigated the waves from pencil lead breaks conducted at a variety of angles relative to the plane of the plate. Flexural and extensional waves were evident in the recorded signals and it was found that their relative amplitudes could be related to the angle at which the lead was broken. The authors have suggested that this phenomenon may be used to determine the orientation of acoustic emission sources as well as the angle of impacts.

Gorman and Ziola [43] have also analysed AE waveforms in terms of the their flexural and extensional components for the purpose of determining the location of the emission source. They found that by selecting a preamp filter that filtered out the flexural wave the location accuracy of the system could be improved.

1.3.8 Conclusions

The above review of the AE method has shown the method's capabilities. Furthermore, some of the difficulties that are to be expected when the method is applied to composite materials have been highlighted.

The differences between the early and the more recent AE concepts have been outlined. This has shown the importance of selecting a recording system that minimises wave distortion and analysing the data in terms of the principles of wave propagation. It was discovered that conflicting findings might result if a simple amplitude analysis of AE data is used.

Of primary relevance to this study is the finding that the AE method can only detect changes in materials. Thus defects already present, e.g. a crack, cannot be revealed unless the size of the crack increases under load. Therefore to determine whether there are defects present, the component needs to be loaded while being monitored by the AE system. The need for loading increases the complexity of the AE method as a means for defect location and assessment. Furthermore, a manufacturing flaw may not cause emissions and would thus be missed by the AE method. Thus the AE method is not ideally suited for defect location and assessment in the manner required by this project's objectives. Hence the focus of the literature review was shifted from the AE method to the AU method.

1.4 Acousto-Ultrasonics

1.4.1 Introduction

Acousto-ultrasonics (AU) is a non-destructive testing method that uses induced ultrasonic sound waves to assess the condition of a structure or component. AU is a combination of aspects of the acoustic emission and the ultrasound materials testing techniques. The term acousto-ultrasonics is a contraction of "acoustic emission simulation with ultrasonic sources" [46].

Basically, AU is concerned with the measurement of the attenuation of acoustic energy. The attenuation is a measure of the efficiency of strain energy transfer and strain redistribution during loading. Low attenuation indicates efficient dissipation of stress wave energy away form crack nucleation sites, ensuring that the energy is not focussed or localised in a way that causes catastrophic failure. Thus low attenuation implies increased strength and fracture resistance [47]. AU is a comparative method whereby the assessment of a volume of material is made by comparing its attenuation characteristics to that of a similar material that is known to be defect-free. Differing attenuation is indicative of either differing mechanical properties or the presence of defects [48].

The AU method was first used by Alex Vary in 1979 [49] in an attempt to address some of the difficulties in testing composite materials. He used a piezoelectric transducer to excite a mechanical disturbance in a carbon fibre reinforced epoxy plate. A second transducer was placed on the same surface of the plate and was used to monitor the disturbance. A correlation was found between the ringdown counts of the received signal and the laminate's mechanical properties. Numerous researchers have since used the AU technique for locating defects, impact damage, and material property variations as well as for assessing the condition of structures that have degraded while in service.

1.4.2 A Comparison Between the AU, AE and Ultrasound Methods

AU, AE and ultrasound have all been used as NDE methods and the equipment and methods used in each of these techniques are similar. All three methods involve the use of ultrasonic sound waves. It is either the source of the waves or the manner in which they are interpreted that differs between the three methods.

Whereas the AE method involves acoustic energy that is emitted due to damage occurring within a structure under load, the AU method uses simulated emission sources. Furthermore AE is concerned with source location and characterisation whereas AU is aimed at the location of defects and mechanical property variations and their cumulative effect on the structure's integrity.

Ultrasonic flaw detection uses well-defined wave reflection and propagation paths, whereas AU uses a received signal that is a result of multiple reflections with the material microstructure and the flaws contained within the volume of material between the sending and receiving transducers. One of the limitations of ultrasonic testing is that the wave normally passes through the thickness of the material. This means that access to both surfaces is required and that only a small volume of material is evaluated per test. The AU technique however does not require access to both faces and a larger volume of material can be evaluated per test since tests are run with a greater distance between the transducers.

1.4.3 Signal Analysis

An AU waveform appears as a damped sinusoid in which both frequency and amplitude vary with time. A direct comparison of such waveforms is impossible, thus for comparison and to use them as a measure of attenuation, waveforms need to be analysed to characterize them in terms of single number or a set of numbers. A variety of analysis methods have been developed. The signal analysis techniques used in the studies reviewed are: the RMS value of the waveform [50, 51, 53-55] the stress wave factor [50-53, 56-59], ringdown counts [50, 51, 60], the peak voltage [50, 51, 60], energy content [18, 48, 50, 51, 61, 62] and the central frequency [18, 48, 50 -52, 61, 62].

The ASTM standards that relate to AU [50, 51] (ASTM E 1495-97 and ASTM E 1736-97) recommend measurement of attenuation in terms of any of the following:

(a) ringdown counts,

(b) peak voltage,

(c) energy content,

(d) or weighted ringdown, which accounts for both the number of oscillations and their amplitude.

Furthermore these standards point out that the simplest measures of attenuation (peak voltage and ringdown counts) have frequently correlated with defect conditions.

Kiernan and Duke [48] have developed software for the analysis of a digitised AU waveform. This software is capable of performing a frequency analysis, moment analysis and determining transfer functions. The moment analysis routine uses the frequency domain, determined by applying the Fourier transform function to the waveform, to calculate AU parameters. Parameters that have been calculated as part of the study are the signal's energy content, central frequency and distortion factor.

In a similar manner to Kiernan and Duke, Talreja *et al* [52] have used five parameters to characterise AU signals. These parameters were based on a moment analysis and are defined as follows:

(a) SWF_1 is the mean square value of the signal

(b) SWF_2 is the central frequency of the signal

(c) SWF_3 is the frequency of the mean value crossings

(d) SWF_4 is the frequency of the peaks in the signal

(e) SWF_5 is a measure of the bias in the spectral density function.

Basically the above parameters characterize the power spectral density distribution in terms of a location parameter, a scale parameter and a set of shape parameters.

1.4.4 AU for Defect Detection

Sundaresan [53] *et al* have investigated the AU method by using filament wound spherical pressure vessels that contained various types of simulated defect. The stress wave factor and the RMS voltage have been used to characterize the recorded signals. It was found that the accuracy of the method is dependent on the type of couplant used, normal pressure on the transducer and instrumentation settings. In this study the AU method could detect delaminations, defects associated with dry windings and winding tension variations. While other manufacturing flaws, such as those due to macro spheres (simulated voids), alternate winding patterns and the use of fibres of a differing modulus were not consistently detected. As part of this study the AU technique, brittle coating technique and thermography were compared. It was found that AU is best in terms of accuracy, reliability of flaw detection and suitability for automation.

Kiernan and Duke [18] have evaluated the AU method for detecting delaminations. Their method involved using a Teflon patch to simulate a delamination in a graphite-epoxy laminate. They have conducted AU tests on this laminate such that the transducers straddled the Teflon patch. The results of this test were compared to those from a test on a laminate that does not contain Teflon. The received signals consisted of a 1MHz and a 3,4 MHz peak. It was found that the presence of the Teflon caused rapid attenuation of the signal and that 3,4 MHz peak was affected more than the 1MHz component.

Lo *et al* [54] have found a correlation between a carbon-epoxy specimen's tensile strength and the AU signal. In their research a baseline tensile specimen was made, a similar specimen was exposed to natural weather for one year and a third specimen was made with a 10° fibre misorientation. Each specimen was divided into five portions along its length and an AU test was conducted on each portion. The RMS value of the amplified AU signal was reported. The specimens were loaded to failure in tension and the failure location (along the specimen's length) was found, in every case, to correlate with the portion of the specimen with the lowest RMS value from the AU test. The authors have concluded that the presence of subtle defects or flaws caused the failure in each case and that the AU signal's RMS value can be used as an indicator of such flaws.

The specimen with the fibre misorientation had a lower tensile strength and this was reflected in the AU data by way of lower RMS values. It was furthermore concluded that the AU signal's RMS value provides an indication of the composite's tensile strength.

Talreja *et al* [52] have applied the AU technique to an impact damaged carbon-epoxy plate. SWF_1 was found to drop significantly as the test moved from the undamaged to damaged material. The irregularity factor (SWF_3 / SWF_4) and the skewness factor (SWF_5) were also found to be good indicators of the damage.

1.4.5 AU for Condition Assessment

Tang *et al* [61] have used the AU technique on filled polymer rocket propellant specimens to determine the damage state of the specimens. With the source and receiving transducers attached to the specimen, the specimen was loaded in tension. The results show that the energy content parameter effectively characterises the damage in the specimens. Both energy content and central frequency were found to decrease as damage grew within the specimen.

Talreja *et al* [55] have applied the AU technique to carbon-epoxy specimens and shown a correlation between the signal's RMS value of the stiffness of the specimen. They have concluded that since stiffness is related to the internal state of damage, the correlation provides a means for the assessment of the damage state in composites.

ASTM standards relating to the AU method have been compiled. ASTM E 1495-97 [50] relates to the assessment of composites, laminates and bonded joints while ASTM E 1736-97 [51] relates to filament-wound pressure vessels. It is stated in these standards that the AU method can be used to detect and assess diffuse defect states, damage conditions and mechanical property variations.

Henneke *et al* [63] have successfully used the AU technique to locate weak regions in composite laminates. These weak regions could not be detected with sophisticated ultrasonic c-scan equipment.

Srivastava [56] has applied the AU technique to glass-fibre specimens and has shown that the interface bond strength can be related to the stress wave factor of the recorded waveforms.

Phani *et al* [57] have conducted AU tests on jute-glass fibre hybrid composites that have been exposed to boiling water. The exposure to boiling water causes hydrothermal ageing and a reduction in the flexural strength of the composite. In an AU test, stress wave factor measurements were taken after various exposure times. The specimens were then bend tested to determine their flexural strength. The stress wave factor was an accurate indicator of flexural strength reduction due to hydrothermal ageing.

Tiwari and colleagues [62] have designed and experimented with a real-time AU system that monitors the change in certain AU parameters, as a specimen is loaded. Notched composite specimens were either compression loaded to failure or subjected to compression-compression type fatigue loads. The predominate failure modes were micro-buckling and longitudinal splits and caused acoustic emissions. Thus the recorded data contained both the acoustic signals input into the specimens by a pulser (as part of the AU system) and emissions due to failure events. The parameters energy content and central frequency were calculated at one-second intervals and plotted as function of time. The energy content of the AU signal decreased during the course of the test due to the accumulation of damage. Localised peaks were present in the energy plots; these were attributed to emissions due to failure events and verified by video recordings taken during the course of the test. The authors have demonstrated the capability of the AU method for real-time monitoring of structures and concluded that the energy of the AU signal is a sensitive indicator of the amount of damage occurring.

Fahr *et al* [60] have investigated the AU technique's potential for evaluating adhesive bond strength. Single-lap shear specimens were made by bonding steel plates together with an epoxy adhesive. A range of bond strengths was achieved by exposing the specimens to elevated temperatures. An AU parameter (called AUP), based on both signal amplitude and ringdown counts was developed. AU tests were conducted on each specimen such that the signal travelled through the adhesive. The strength of the bonds was determined by running destructive shear tests. A good correlation was found between the AUP and the shear strength of the adhesive bond. This correlation suggests

that the AU technique can be used to monitor or assess the strength degradation of adhesively bonded joints during or after exposure to elevated temperatures.

Vary and Bowles [58] have run AU tests on graphite-polymide composite specimens in which the stress wave factor was determined for each specimen. This study has shown that higher values of the stress wave factor correspond with greater interlaminar shear strength.

Vary and Bowles have since furthered their earlier study [59] and produced graphite-polymide composite specimens with a range of mechanical properties. A range of properties was achieved by using a different cure pressure for each specimen and these variations were confirmed by conducting ultrasonic through transmission amplitude scans. AU tests were conducted so as to determine the stress wave factor for each specimen. Their findings show that the weaker panels had lower stress wave factor values and that the stronger panels were associated with higher stress wave factor values. The authors have concluded that good transmission of ultrasonic energy, associated with higher values of the stress wave factor, denote good transmission of dynamic stresses and loads and hence improved strength.

1.4.6 Cautions and Limitations

Possibly the AU technique's biggest limitation is the fact that it is a comparative method. The method's comparative nature means that AU data from a component that is known to be defect-free needs to be obtained. Thereafter a test on a component of unknown condition will only indicate whether or not it is of worse condition than the defect free component. If a more detailed assessment is required then a database of AU measurements, each corresponding with a particular defect state needs to be established. The establishment of such a database can be costly and time consuming.

ASTM E 1495 [50] has cautioned that composites frequently have rough or textured surfaces and that these superficial factors can imprint on the received signal. Furthermore, substrate variations can obscure the effects of volume variations. It is suggested that these surface and substrate effects can be overcome by running trials to select the frequency bandpasses that isolate and eliminate these variables.

Kiernan and Duke [18] have cautioned that, in conducting AU tests in which readings are compared for various transducer positions, localised material variations may influence the readings. Thus the signals may be influenced by the material immediately below the transducers and not indicative of the material between the transducers. Vary [47] has concurred with this notion and stated that AU becomes vulnerable to material vagaries that affect probe sensitivity and signal reproducibility.

AU readings are related to structural resonances, thus the constraints on a particular structure can alter results [64]. Therefore the same piece of material, depending on its placement in relation to the structure's constraints, may yield differing AU values [18]. To account for the effect of constraints increases the complexity of AU testing.

The presence of a transducer on an elastic solid modifies the vibration characteristics of the solid in the region of the transducer [33, 65]. This is due to the weight of the transducer that acts on the medium over the area of the transducer's mounting face. Thus the recorded waveforms differ from the true particle motions of the media had the transducer not been present on the material's surface. Thus to determine the true particle motion the effect of the transducer needs to be accounted for.

1.4.7 Conclusions

The basic differences between the AU method and 2 similar NDE methods (AE and ultrasound) have been outlined. As compared to the ultrasound technique, the AU technique is favourable since access to only one surface is required and a larger volume of material can be interrogated per test.

The AU method has several important advantages when compared to the AE method. The most significant of these is the fact that AU uses simulated emissions, which implies that the component under test does not have to have loads applied to it. Thus, frequently a component can be assessed with the AU method without having to remove it from the structure in which it operates. This also implies that the AU method is better suited to automation.

Furthermore, in a comparison with the brittle coating technique and thermography, Sundaresan [53] *et al* have shown that the AU technique is better in terms of accuracy, reliability of flaw detection and suitability for automation.

The AU method is capable of detecting a wide variety of defects and material conditions and many different AU data analysis techniques have been used. The studies reviewed have formed a valuable guide for the experimental component of this project.

The above literature review has also revealed that the AU method has several limitations, the most significant of which is that it is a comparative method. Other limitations, which add to the difficulty of the use of the AU method, are as a result of surface and substrate effects and the resonances of the test structure.

1.5 Coupling Issues

1.5.1 Introduction

A couplant is a thin layer of fluid that is applied between the transducer mounting face and the material that is being tested. Its purpose is to fill the air gaps at the interface, thereby ensuring the efficient transmission of sound between transducer and test material.

The AU technique is a comparative method and its reliability depends on establishing repeatable coupling. Without consistent coupling, signal variations due to defects may become confused with those that are due to coupling variations.

1.5.2 Recommended Couplants

Vary [46] has suggested the following couplants for use in AU tests: glycerin, gel, silicone grease or shear wave couplant.

Physical Acoustics Corp. (PAC) recommends the following couplants [66]; 'high vacuum stop cock grease', 'petroleum grease', water, 'Dow Corning 200 fluid', 'dental cement', 'Nonaq stop cock grease' and 'saol'.

1.5.3 Coupling Recommendations

There is consensus in the literature that, in terms of transducer to specimen attachment, that the following factors affect AU signals [50, 53, 63, 66]: applied pressure, type and amount of couplant, specimen surface roughness and transducer alignment.

ASTM E 1495 [50] states that the following factors influence the repeatability of AU results: improper selection of type and amount of couplant, couplant thickness variations and bubbles, specimen surface roughness and texture, sensor alignment and pressure, sensor resonances, insufficient damping and insufficient instrument bandwidth. This standard recommends that the transducers be held in a rigid fixture so

that the sensor spacing can be maintained and sufficient pressure applied to effectively couple the transducers to the specimen. The standard also states that an optimum coupling pressure exists which is dependent on the combination of the sensor, the couplant type and the specimen.

ASTM E 1495 mentions an alternative to the use of a fluid called dry coupling. Dry coupling involves the use of a soft elastomer pad instead of a fluid. Dry coupling can be used to allow coupling to rough or curved surfaces or to avoid fluid infusion into porous materials. Coupling can also be improved by reducing the transducer to specimen contact area to a fraction of 1 cm^2. The reduced coupling area can be achieved by bonding truncated conical cones to the transducer faces.

Breckenridge *et al* [65] have found that inconsistent transducer performance can arise as a result of variations in the thickness of the couplant, the couplant being too viscous to be squeezed to a thin layer or due to dirt trapped within the couplant. Breckenridge has suggested that the variations in the couplant thickness can be minimised by ensuring that the transducer mounting face and the test specimen are flat and smooth. However, he also found that even when extreme care is taken to eliminate the variable effects of couplant thickness, captured dirt, variable loading force and roughness of the structure and mounting face, for some transducers the inconsistency persists.

In preliminary experiments, before applying the AU technique, Henneke *et al* [63], determined the repeatability of stress wave factor measurements. The best repeatability achieved in this study was $^{+}/_{-}$ 10 % and the major contributor to this variation was the coupling.

1.5.4 Conclusions

The findings of the above researchers and recommendations of the ASTM standards indicate that the coupling between transducer and specimen is of critical importance. They also indicate that there are numerous factors that affect the repeatability and imply that the elimination of variations due to inconsistent coupling is not always possible.

The factors that affect repeatability should be investigated, thereby identifying a test configuration that would provide the best repeatability. A procedure for coupling the transducers and conducting AU tests can then be developed so that the optimum accuracy and repeatability is maintained for every test.

Chapter 2

Development of a Repeatable Test Method

2.1 Introduction

An essential element of any experiment is that it is repeatable. The initial AU experiments in this study were hampered with a lack of repeatability. These initial experiments did however show that there are numerous variables that affect the results and repeatability. It soon became clear that a repeatable test method needed be developed and for this to be achieved an understanding of the variables that affect the repeatability was necessary.

2.2 Coupling

The major obstruction to achieving repeatable results is in the coupling of the transducers to the test specimen. With the source transducer emitting acoustic energy into the laminate and with the recording system running, each of the recorded waveforms was found to be virtually identical. However, if two sets of waveforms were recorded such that the first set was recorded before and the second set after either the source or receiving transducers were removed from the laminate and then re-coupled, the two sets of waveforms would be significantly different. This indicates that the recordings are strongly influenced by the coupling of the transducers to the laminate. The recorded signals are so sensitive to the nature of the coupling that even a small movement of the transducer applied by pulling lightly on its signal cable may cause significant changes to the shape of the waveforms recorded. In an effort to optimise the consistency of the coupling, the factors that influence the coupling have been identified and investigated.

2.2.1 The Selection of a Couplant

A variety of couplants are commercially available and the repeatability of AU tests was found to be dependent on the type used [67]. Therefore a study has been conducted, the

purpose of which was to evaluate 5 different couplants, in so doing, determining which provides the best repeatability. Initially the settling time of each couplant was determined. Thereafter a repeatability experiment was conducted in which the correct settling time was allowed for each couplant.

The five couplants investigated in this study are:

1. Glycerine
2. 'Kendon Laboratories cc' Ultra-gel
3. Petroleum jelly
4. 'Dow Corning' 340 heat sink compound
5. 'Dow Corning' high vacuum grease

Settling Time

The settling time experiment was conducted to determine the effect that a particular couplant has on the time that the experimental setup takes to produce consistent waveforms. For this experiment, the source transducer and WD sensor were coupled to a uni-directional glass fibre/epoxy laminate with 100 mm distance between them. To determine the effect of transducer contact pressure, the settling time experiment was run twice for each couplant. For the first run, a 1 lb weight was placed on top of each of the transducers, while in the second run the weights were not used. Beginning as soon as possible after the transducers were coupled to the laminate and the weights were in place, waveforms were recorded at 20-second intervals until the test had been run for 3 minutes. The recorded waveforms were then compared to one another to determine how much time elapsed before consistent waveforms were produced. This amount of time is the couplant's settling time.

Repeatability

To determine which of the couplants will produce the most repeatable results, the WD sensor and source transducer were again coupled to a uni-directional laminate with 100 mm separation. For the couplants that were found to require a settling time in the previous experiment, the appropriate time interval was allowed to pass before recording commenced. One waveform was then recorded after which the transducers were removed and the 'used' couplant was cleaned off the laminate and the transducers. The transducers were then replaced on the laminate with fresh couplant and the settlingtime

allowed to elapse before a second waveform was recorded. This procedure of recording a waveform, renewing the couplant and then recording the next waveform was repeated five times for each couplant. Thus five waveforms were generated per couplant.

To quantify their repeatability, the standard deviation of each couplant's five waveforms, from its mean, was calculated. The couplant with the lowest standard deviation has the best repeatability since a low standard deviation indicates that its waveforms are similar. The method used to determine the standard deviations is as follows:

The A/D converter converts the analogue voltage-time signal to the digital domain by sampling the voltage value at a sample interval Δt. 1024 voltage points were sampled for each waveform. Specifically, each voltage reading v_i can be related to a associated time t_i by the equation:

$$t_i = i\Delta t \qquad i = 1,2,3,....1024$$

Each couplant was found to produce waveforms that have different maximum amplitudes. To enable a meaningful comparison, each set of waveforms was expressed as a fraction of their maximum as shown below:

$$v_{ij} = \frac{V_{ij}}{v_{\max}} \qquad j = 1,2,3,....5$$

where V_{ij} is one of the five voltage values recorded at time t_i.

For each set of five waveforms (one set per couplant), a mean waveform $\bar{v}_i$ was determined using the following equation:

$$\bar{v}_i = \frac{\sum_{n=5}^{j=1} v_{ij}}{5}$$

The standard deviation of the voltages at each time interval was determined using:

$$s_i = \frac{\sum_{j=5}^{5} (v_{ij} - \bar{v}_i)^2}{j-1}$$

The average standard deviation was then determined for each couplant from:

$$s_{ave} = \frac{\sum_{i=1}^{1024} s_i}{1024}$$

Results and Conclusions

The effect of two different couplants is shown in figure 2.2.1. In each case a single waveform was recorded, the 'used' couplant removed and then fresh couplant applied. Thereafter a second waveform was recorded. Because the 2 waveforms in figure 2.2.1 (a) are almost identical while those of figure 2.2.1 (b) are significantly different, glycerine can be said to provide more repeatable results than vacuum grease.

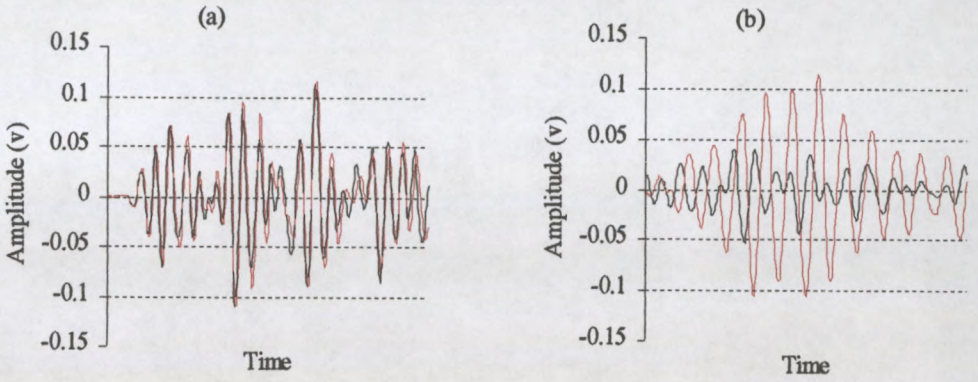

Figure 2.2.1. Effect of two different couplants on recorded waveforms (a) Glycerine (b) Vacuum Grease

The results of the settling time experiment are summarised in table 2.2.1. Petroleum jelly, heat sink compound and vacuum grease were not used in the repeatability experiment with weights because the weights prolonged their settling time beyond 3 minutes.

Couplant	Settling time with weights	Settling time without weights
glycerine	No settling time required	No settling time required
Ultra-gel	40 seconds	20 seconds
Petroleum jelly	More than 3 minutes	No settling time required
'Dow Corning' 340 heat sink compound	More than 3 minutes	No settling time required
'Dow Corning' high vacuum grease	More than 3 minutes	No settling time required

Table 2.2.1. Effect of different couplants and transducer weights on settling times.

The values of the average standard deviation of each couplant are shown in table 2.2.2. The couplant that has the lowest average standard deviation and has thus provided the most consistent set of waveforms is glycerine when used without weights. Thus all future experiments and tests will use glycerine as a couplant.

Couplant	Average Standard Deviation
Glycerine (no weight)	0.0484
Glycerin (with weight)	0.0783
'Dow Corning' 340 heat sink compound	0.0886
Ultra-gel (no weight)	0.1113
Ultra-gel (with weight)	0.0821
Petroleum jelly	0.0523
'Dow Corning' high vacuum grease	0.2156

Table 2.2.2. Average standard deviation values for each couplant

In general terms, the more viscous couplants have lower repeatability qualities. A more viscous couplant will however, transmit a greater percentage of the acoustic energy that is causing in plane particle displacement than a less viscous couplant. Thus, in using the relatively less viscous glycerine, the sensitivity of the recording system to in plane particle motion will be reduced. Glycerine was nevertheless selected since improved repeatability is more important than sensitivity to in plane motion [67].

2.2.3 The Thickness of the Couplant

The thickness of the coupling film between the transducer and the test specimen has an effect on the recorded waveforms. Thus, a means of keeping the thickness of the coupling layer constant from test to test is needed. A small device whose purpose is to accurately control the thickness of the layer of couplant between the transducer and the laminate was designed and manufactured and is shown in figure 2.2.2.

The transducer is bonded to a spindle that is held into the holder's body with a thread and locknut. The thread and locknut allow the distance between the transducer's mounting face and the specimen to be set, thereby controlling the thickness of the couplant.

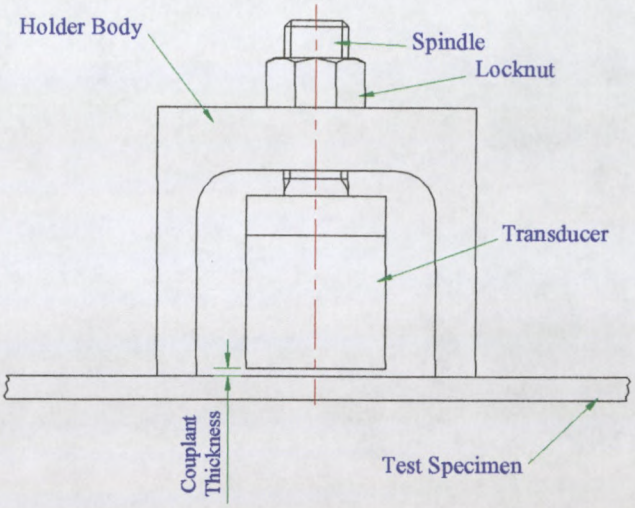

Figure 2.2.2. Couplant thickness controller.

A series of repeatability experiments were run with the use of the couplant thickness controller. These experiments showed that this device does not improve the repeatability of the recordings and its use was thus discontinued.

Suitable repeatability of the thickness of the couplant layer was achieved by dropping a single drop of glycerine onto the test specimen with the use of a cotton bud. The transducer was then placed onto the drop and seated squarely on the specimen with a light downward pressure that was applied manually. This consistently produced a thin film that covered the entire transducer contact face and is the method that was used for all experiments in this project.

2.3 An Object in Contact with the Laminate's Surface

An object that touches the laminate on the wave's path from the source transducer to the recording transducer has been found to influence the recorded waveform. This phenomenon was discovered when a trigger transducer was placed between the source and receiving transducers. In this case the recorded waveforms were significantly

different to those that were recorded without the transducer on the wave's path. The weight of the transducer alters the vibration characteristics of the surrounding material, thereby affecting the waveforms.

To avoid this unwanted effect, the trigger sensor must be placed to the side of the wave path. Furthermore any unnecessary objects must not be allowed to touch the test specimen, especially on the wave's path. By implementing the above finding the repeatability of the recordings was improved.

2.4 Support Type

A test specimen needs to be supported on a surface that acoustically isolates the specimen from its surroundings during the running of AU tests. Numerous materials and support arrangements are available. Whether the support type influences the repeatability of the recordings has been investigated.

Three support types were investigated and the differences in the recorded waveforms were noted. These support types are a soft sponge, a closed-cell rubber mat and an arrangement in which the specimen was unsupported. The unsupported arrangement was achieved by using a closed-cell rubber mat with a hole cut in it such that the material being tested was unsupported.

In terms of repeatability, the results for each support type are very similar. Thus the repeatability cannot be improved by using a particular one of the 3 support types investigated. The soft sponge support was selected and used in this project since it is the softest and would thus provide the most even support for laminates that are slightly twisted.

3.5 The Radial Dependence of the Transducers

The output of the source transducer and the response of the receiving transducer have been measured to determine whether variations are present as the angular position around the transducer is changed.

2.5.1 Source Transducer

The output of the source transducer has been measured at various angular positions around it. To do this, the WD transducer was moved in 45° increments on a 100 mm radius around the source transducer and at each position 5 waveforms were recorded. The WD sensor's 0° direction (see figure 2.5.1) was pointed toward the source transducer in each case and the source transducer was not moved during the course of the experiment. The energy content (see Glossary) of the waveforms has been calculated from which the average energy of the 5 waves at each transducer position was determined.

2.5.2 Receiving Transducer

In a similar manner to the test of the radial dependence of the source transducer's output, the WD sensor's response as a function of the direction of the source has been determined. The source transducer was moved in 45° increments, on a 100 mm radius, around the WD sensor and 5 waveforms were recorded at each location. It was ensured that, in each recording position, the source transducer's 0° direction (see figure 2.5.2) pointed toward the recording transducer. The WD sensor was not moved during the course of the test and again 5 waves were recorded at each location. Thereafter, the average energy of the 5 waves was calculated for each location of the source transducer.

2.5.3 Results and Discussion

The results of the test on the source transducer (figure 2.5.1) indicate that the most energy is emitted in the 45° direction and the least at 225°. The percentage range between the two is 26,6 %.

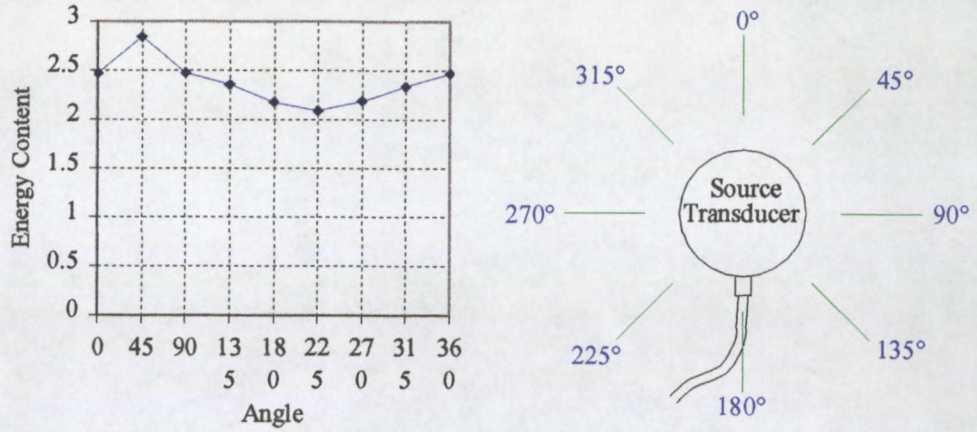

Figure 2.5.1. Radial dependence of the source transducer's output.

Figure 2.5.2, the results of the experiment on the WD sensor, show that the strongest response is in the 45° and 270° directions and that the weakest response at 0° and 1 35°. The percentage range between the strongest and weakest response is 15,6 %.

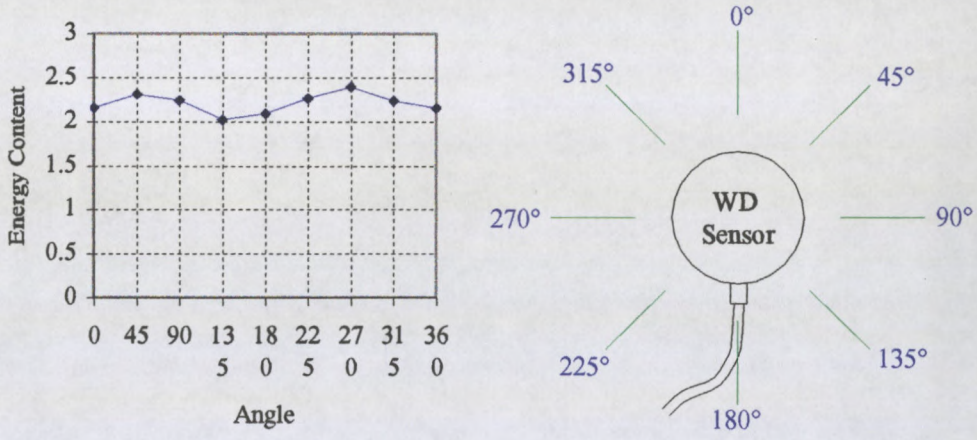

Figure 2.5.2. Radial dependence of WD sensor's response.

If, each time an AU experiment is conducted, the transducers are arbitrarily placed on the specimen then a different amount of energy will be emitted onto the path between the transducers. Furthermore the response of the receiving transducer will vary depending on its rotation relative to the source transducer.

To overcome this problem and improve the AU method's repeatability, each time that the transducers are recoupled to a specimen they need to be pointing in the same

direction relative to one another. A holder for the two transducers has been designed and made (figure 2.5.3) for this purpose. This holder consists of a Perspex bar to which a strip of polyurethane foam has been bonded. The polyurethane foam's purpose is to acoustically isolate the transducers from the Perspex, thereby preventing acoustic energy from travelling through the Perspex. The transducers are bonded to the polyurethane such that each of their 0° directions (as defined in figures 2.5.1 and 2.5.2) are pointing toward each other. Besides keeping the transducers at identical relative rotations it also ensures that the distance between the transducers remains constant and helps to seat them squarely on the test specimen. The use of this transducer holder has improved the repeatability of the recordings and was thus used throughout the project.

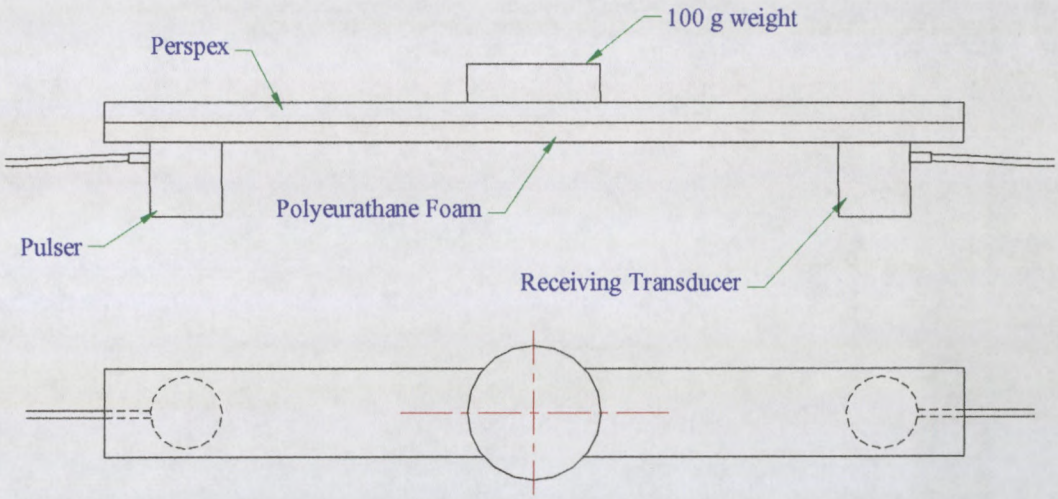

Figure 2.5.3. Transducer holder.

2.6 Securing the Transducers

In a further attempt to improve the repeatability, rubber bands were used to hold the transducers onto the test specimen. A rubber band was stretched over the test specimen and transducer so as to hold it against the laminate. This technique did not improve the repeatability of the results and was thus discontinued.

2.7 Transducer Contact Pressure

A range of pressures between the transducer and test specimen have been tried in an effort to improve the repeatability. This was done by placing weights of between 100 g and 2 kg on top of the transducer holder and determining the repeatability with each arrangement.

Increasing the weight on the holder was found to increase the amount of energy in the recorded signal. However as weight was increased, the repeatability was found to remain constant until the weight was sufficient to cause the test specimen to bend. The bending of the specimen caused a loss of square contact between the transducers and the specimen and a reduction in the repeatability. 100 g was found to be sufficient weight to seat the transducers in the glycerine without bending the laminate. A 100 g weight, bonded to the mid-span of the transducer holder (figure 2.5.3.) was thus used.

2.8 The Achieved Repeatability

The above investigation has improved the repeatability of the AU experiments. With the findings implemented, an experiment has been run to determine how repeatable AU results can be expected to be.

With the use of the transducer holder, the 100 g weight, glycerine as a couplant and the sponge support, a waveform was recorded on a glass fibre laminate. Thereafter the transducers were removed from the laminate and the glycerine was cleaned off the laminate and the transducer mounting faces. The transducers, on their holder, were then re-adhered, as before to the laminate and a second waveform was recorded. This process was repeated 10 times and the parameters peak voltage, ringdown counts, central frequency, energy content and wave speed were determined for each of the waves. The minimum and maximum values for each of the parameters as well as their percentage range are shown in table 2.8.1.

Parameter	Max Value	Min Value	Percentage Range
Peak Voltage (V)	0.13733	0.086367	$^{+}$/-18,6 %
Ringdown Counts	60	53	$^{+}$/- 5,8 %
Central Frequency (kHz)	362	349	$^{+}$/- 1,8 %
Energy	1.3766	1.08	$^{+}$/-10,8 %
Arrival time (s)	7.37	6.88	$^{+}$/- 3,3 %

Table 2.8.1. The repeatability of various parameters.

The parameter peak voltage has the poorest repeatability due to the fact that peak voltage is a single voltage reading whereas the entire waveform is considered in determining the other parameters. The repeatability that has been achieved for the other 4 parameters is comparable to that achieved by Henneke *et al* [63] who conducted repeatability experiments for stress wave factor values and achieved an optimum of $^{+}$/- 10 %.

The parameters arrival time and central frequency are the most repeatable and should, where possible, be used for the assessment of materials. In the cases where arrival time and central frequency are not related to the material's condition, ringdown counts or energy content should be used.

2.9 Equipment Details and Settings

The equipment and settings have been selected to capture waveforms as accurately as possible and minimise their distortion. Thus the widest band preamp filter and the widest band software filter have been selected with the highest possible sampling frequency. Furthermore, of the transducers available, the transducer with the widest sensitivity range has been used. Exact details of the equipment and settings used are shown in the following list. Unless otherwise specified, these settings have been used in every one of the experiments of this project.

Receiving transducer	Physical Acoustics Corporation Wide Band Sensor, WD-616
Source transducer	Physical Acoustics Corporation, no specifications available.
Source transducer input signal	Physical Acoustics Corporation 3000 Acoustic Emission Computer
Waveform capture system	Mistras 2001, AEDSP-32/16 Mistras transient recorded and analysis software **Software Settings:**
	Threshold fixed, various settings used
	Sample Rate 8 MHz
	Filter bandpass100 – 1200kHz
	Pre trigger 20 μs
	Hit length 3 k
	HLT 1000 μs
Preamp	Physical Acoustics Corporation: 1220A Acoustic Emission Preamplifier
	Gain 40 dB
	Filter highpass 100 kHz

Variable waveform generator	Hewlett Packard 33120A	
	Settings:	Sine wave
		Amplitude 0.4 V
		Frequency: Variable

Chapter 3

AU Testing of Thin Laminates

An investigation of the propagation of acoustic energy in thin glass fibre laminates has been carried out. The aims are to determine how laminate thickness, percentage resin content and ply orientation affect the value of the AU parameters. Furthermore the depth to which AU waves penetrate into a thin laminate will be investigated.

3.1 Specimen Preparation

6 different thin laminates have been designed and made for these experiments. Each of the 6 laminates has been constructed with differing numbers and orientations of glass fibre layers. The SP Systems LR-20/SLC30 epoxy resin system and 440g/m^2 uni-directional glass fibre cloth has been used for the construction of each of these laminates. All laminates were vacuum bagged and post-cured for 18 hours at 40°. The resin content of each laminate has been determined in accordance with SABS 141:1992. The stacking sequence and resin content of each laminate is shown in table 3.1.1 below.

Laminate Name	Stacking Sequence	Percentage Resin (wt)
UD3	0_3	54,34 %
UD5	0_5	37,70 %
UD3b	0_3	54,69 %
090	$0_1/90_1/0_1$	54,88 %
909	$90_1/0_1/90_1$	51,43 %
45	$0_1/45_1/90_1/-45_1/0_1$	54,92 %
452	$0_1/-45_1/45_1/90_1$	54,08 %

Table 3.1.1. Laminate details.

3.2 Test Procedure

The recording sensor was located at the centre of the laminate and the pulser was moved to various angular positions on a 100 mm radius around the recording transducer. At each angular position a waveform was recorded. Most laminates consist solely of layers at 0° and 90°, in these laminates waveforms were recorded at 30° increments. Laminates 45 and 452 have layers at 45° and -45° included in their construction so as to record signals that travel parallel to these layers, laminates 45 and 452 were tested at 15° increments.

As a measure of the test method's repeatability the curves have been discussed in terms of their symmetry with respect to the fibre direction. Since the value of any of the 5 parameters at an angle α° should be equal to the value of that parameter at $\alpha^{\circ} \pm 180^{\circ}$, differences can be attributed to inconsistencies inherent in the testing method.

In some cases a direct comparison between the results of 2 laminates has been made. The results of laminate UD3 have been compared to the results of laminate UD5 for the purpose of determining the effect of increasing the thickness of a laminate. Likewise the results from laminate UD3 have been compared to the results from laminate UD3b to determine the effect of a lower resin volume fraction.

3.3 Laminate UD3

3.3.1 Peak Voltage

The shape of the peak voltage curve (figure 3.3.1) shows that the wave's peak voltage is strongly related to its direction of travel relative to the fibre angle. The peak voltage is highest when the wave travels parallel to the fibre direction and lowest when travelling perpendicular to the fibre direction. The highest peak voltage of 0,0711 V was recorded at 180° while the lowest peak voltage of 0,0137 V was recorded at 270°. The percentage difference between the maximum and minimum peak amplitudes is 80,7 %.

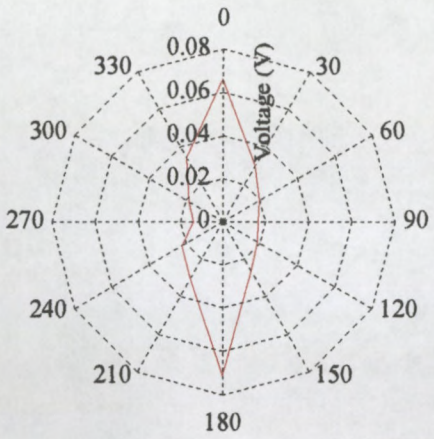

Figure 3.3.1. Variation of peak voltage in laminate UD3.

3.3.2 Ringdown Counts

The ringdown counts (figure 3.3.2) curve has maximum values when the wave travels parallel to the fibre direction (at 0° and at 180°). The lowest numbers of counts were recorded when the wave travelled perpendicular to the fibre direction. The maximum number of ringdown counts was 29 (recorded at 180°) while the minimum of 1 count was recorded at both 90°and at 270°. This variation expressed as a percentage is 96,5 %.

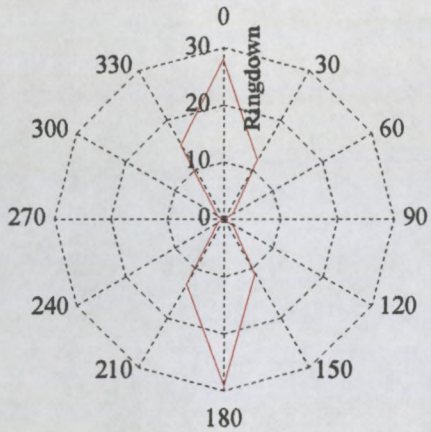

Figure 3.3.2. Variation of ringdown counts in laminate UD3.

3.3.3 Energy Content

The variation of energy content versus direction of wave travel is shown in figure 3.3.3. The curve shows that the most energy is transmitted in directions close to the fibre direction. The highest energy recorded (757 990) was at 180° while the signal with the lowest energy (189 680) was recorded (at 60°). The percentage range between the maximum and the minimum energy contents is 74 %.

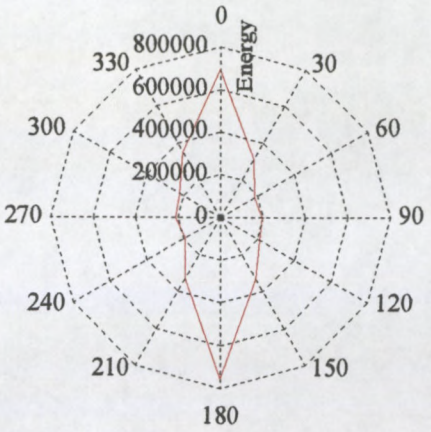

Figure 3.3.3. Variation of energy content in laminate UD3.

3.3.4 Central Frequency

Figure 3.3.4 shows that there is a weak relation between the signal's central frequency and the signal's direction of travel. The curve's trend indicates that the central frequency is higher when the wave travels parallel to the fibre direction. The highest central frequency recorded (377 kHz) was at 0° and the lowest central frequency (327 kHz) was recorded at 270°. The percentage variation between the maximum and minimum central frequencies is 13,3 %. Although there are peaks in the central frequency versus angle plot at 0° and at 180° and the lowest central frequency was recorded at 270°, this curve is not symmetric. This is illustrated by the fact that there is a 7,3 % difference between the central frequency values at 90° and 270°

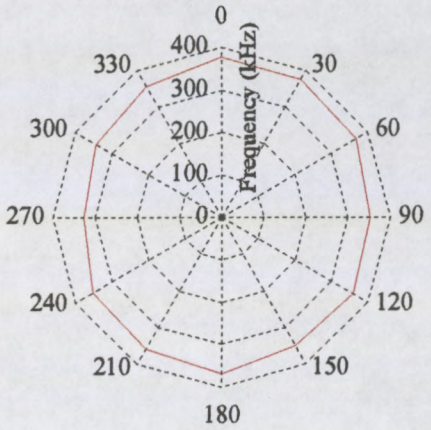

Figure 3.3.4. Variation of central frequency in laminate UD3.

3.3.5 Arrival Time

The arrival time curve (figure 3.3.5) indicates that a relationship exists between the wave's travel time and the wave's direction of travel relative to fibre angle. The shortest

travel times are found at angles that are closest to the fibre direction while the longest times were recorded when the wave was travelling at perpendicular to the fibre direction. The shortest travel time was 16,8 μs (at 0°) and the longest was 29,8 μs (at 270°). The percentage variation between the longest and shortest arrival times is 43,6 %.

Figure 3.3.5. Variation of arrival time in laminate UD3.

3.3.6 Summary of Main Features

In laminate UD3 the parameters peak amplitude, ringdown counts, energy content and arrival time are all strongly influenced by the direction of wave travel relative to the direction of the fibres. Peak amplitude, ringdown counts and energy content have their maximum values when the wave travels parallel to the fibre direction and their minimum values at angles that are perpendicular to the fibre direction. The arrival time graph is however different as it's longest times are at perpendicular to the fibre direction and it's shortest times when the wave travels parallel to the fibre direction. There appears to be a weak relationship between a signal's central frequency and its direction of travel. At wave travel directions that are parallel to the fibre direction, the central frequency is slightly higher.

All 5 curves are approximately symmetric with respect to the fibre direction and the normal to the fibre direction. The range of the peak amplitude, ringdown counts and energy content is large (80,7 %, 96,5 % and 74 % respectively) while the range of the arrival times and central frequencies is much less at 43,4 % and 13,3 %.

3.4 Laminate UD5

3.4.1 Peak Voltage

The curve in figure 3.4.1 depicts the variation in peak voltage in laminate UD5 and has maxima when the signal travels parallel to the fibre direction and minima when the signal travels perpendicular to the fibres. Apart from the 26,2 % difference between the peak voltages at 150° and 330°, the curve is approximately symmetric. The highest peak voltage of 0,1178 V was recorded at 0° and the lowest (0,0433 V) was recorded at 90°. The percentage difference between the maximum and minimum is 63,2 %.

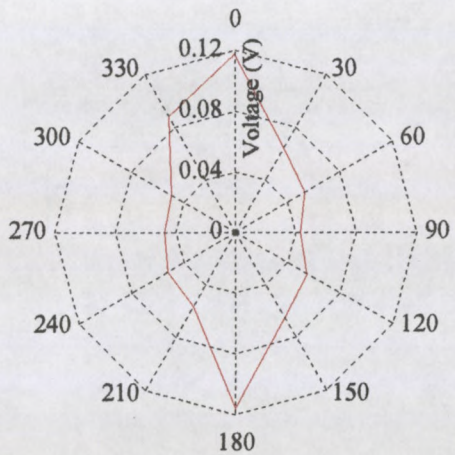

Figure 3.4.1. Variation of peak voltage in laminate UD5.

3.4.2 Ringdown Counts

The ringdown counts curve (figure 3.4.2) has peaks at both 0° and at 180 ° and is not perfectly symmetric. The peak at 0° is 12,5 % lower than the peak at 180° and the trough at 90° is 23,8 % lower than the trough at 240°. The trough between 180° and 360° is centred at 240° whereas for symmetry one would expect this trough to be located at 270°. Despite the deviations from symmetry there is a clear relationship between the number of ringdown counts and the wave's direction of travel. The maximum number of ringdown counts (56) was recorded at 180° while the minimum (16) was recorded at 90°. The percentage difference between the maximum and minimum values is 71,4 %.

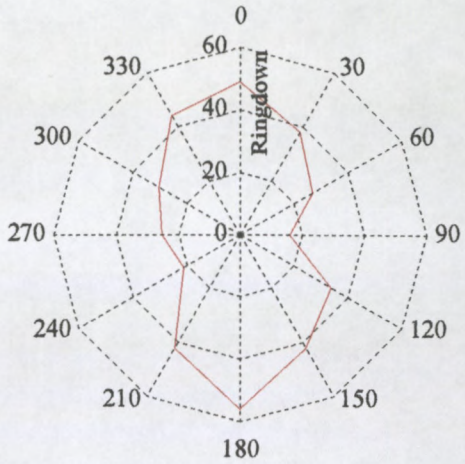

Figure 3.4.2. Variation of ringdown counts in laminate UD5.

3.4.3 Energy Content

The variation in energy content is shown on figure 3.4.3 and shows that the most energy is transmitted in directions closest to the fibre direction. This curve is fairly symmetric; the greatest deviation from symmetry is the 10,9 % difference between the energy contents at 0° and 180°. The highest energy content was 1464400, recorded at 180° while the lowest energy content of 465200 was recorded at 240°. This represents a range of 68,2 %.

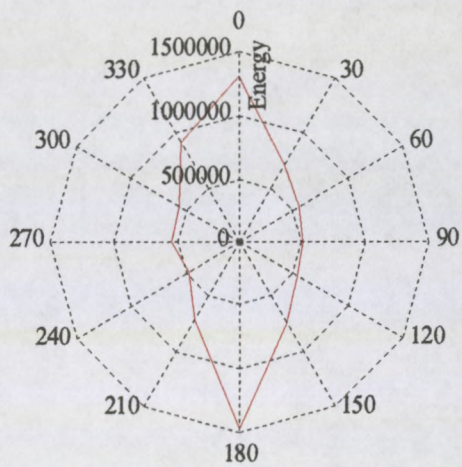

Figure 3.4.3. Variation of energy content in laminate UD5.

3.4.4 Central Frequency

The central frequency curve, on figure 3.4.4, is oval indicating that the signals have their highest central frequency when the direction of wave travel is aligned with the fibre direction. The highest central frequency of 314 kHz was recorded at 180°, while

the lowest central frequency of 270 kHz was recorded at 270°. The percentage variation between the maximum and minimum central frequencies is 14 %.

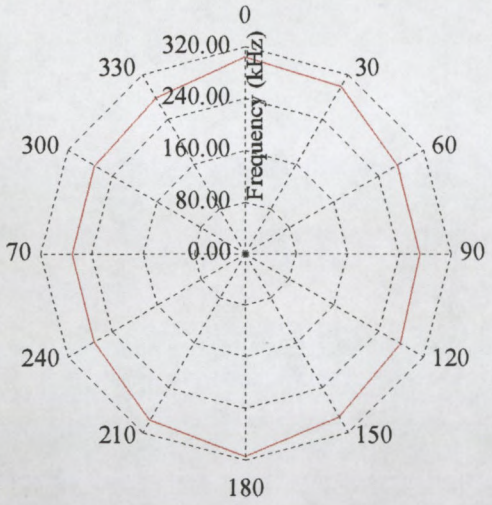

Figure 3.4.4. Variation of central frequency in laminate UD5.

3.4.5 Arrival Time

Figure 3.4.5 depicts arrival time as a function of fibre angle and has troughs at 0° and 180° and peaks at 90° and 270°. The curve is almost perfectly symmetric and the relationship that exists between fibre angle and arrival time is clearly evident. The shortest arrival time recorded was 16,6 μs (at 180°) and the longest recorded was 28,3 μs (at 90°). This range, expressed as a percentage is 41,3 %.

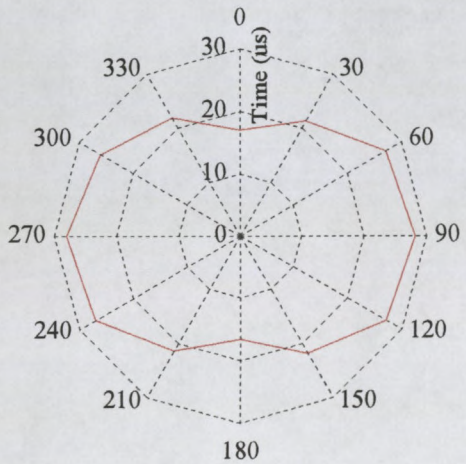

Figure 3.4.5. Variation of arrival time in laminate UD5.

3.4.6 Summary of Main Features

The value of peak amplitude, ringdown counts, energy content, central frequency and arrival time are all related to the wave's direction of travel. All parameters apart from arrival time have higher values when the wave travels parallel to the fibre direction and their lowest values at directions that are perpendicular to the fibre direction. The arrival time is shortest when the wave travels parallel to and longest when the wave travels perpendicular to the fibre direction. The range of the peak amplitude, ringdown counts and energy content is large (63,2 % 71,4 % and 68,2 % respectively) while the range of the central frequencies and arrival times is less (14 % and 41,3 % respectively).

3.5 Comparison of the results for UD3 and UD5

3.5.1 Parameter Comparison

The shapes of the graphs of each of the 5 parameters as a function of the wave's travel direction for laminates UD3 and UD5 are very similar. The average value of peak voltage, ringdown counts and energy content is greater in laminate UD5 than in UD3. However, the average of the central frequencies is higher in laminate UD3 than that in UD5. Apart from between 140° and 160° where their arrival times are the same, the arrival time in UD5 less than that in UD3. The comparison of laminates UD3 and UD5 has been summarised in table 3.5.1.

Parameter	Range UD3	Range UD5	Comparison of average values.
Peak Voltage	80,7 %	63,2 %	55 % higher in UD5
Ringdown Counts	96,5 %	71,4 %	70 % higher in UD5
Energy Content	74 %	68,2 %	54,1 % higher in UD5
Central Frequency	13,3 %	14 %.	20 % higher in UD3
Arrival Time	43,6 %.	41,3 %	3,7 % higher in UD3

Table 3.5.1. Comparison between UD3 and UD5.

3.5.2 Spectrum Comparison

The effect of increasing the laminate thickness on the signal's frequency content has been investigated. This was achieved by comparing the Fourier transforms of signals

recorded in the 0° direction in laminates UD3 and UD5 (figure 3.5.1). These Fourier transforms have peaks in identical positions, indicating the frequencies transmitted in each laminate are similar. The most notable difference between the two is the presence of frequencies in the 400 kHz to 500 kHz band in laminate UD3 that are present but at a very low amplitude in laminate UD5. It is the presence of these frequencies that have caused laminate UD3's central frequency to be higher than that of UD5. A second difference is that the maximum amplitude in UD3 was at 140 kHz whereas in UD5 the maximum amplitude was at 280 kHz.

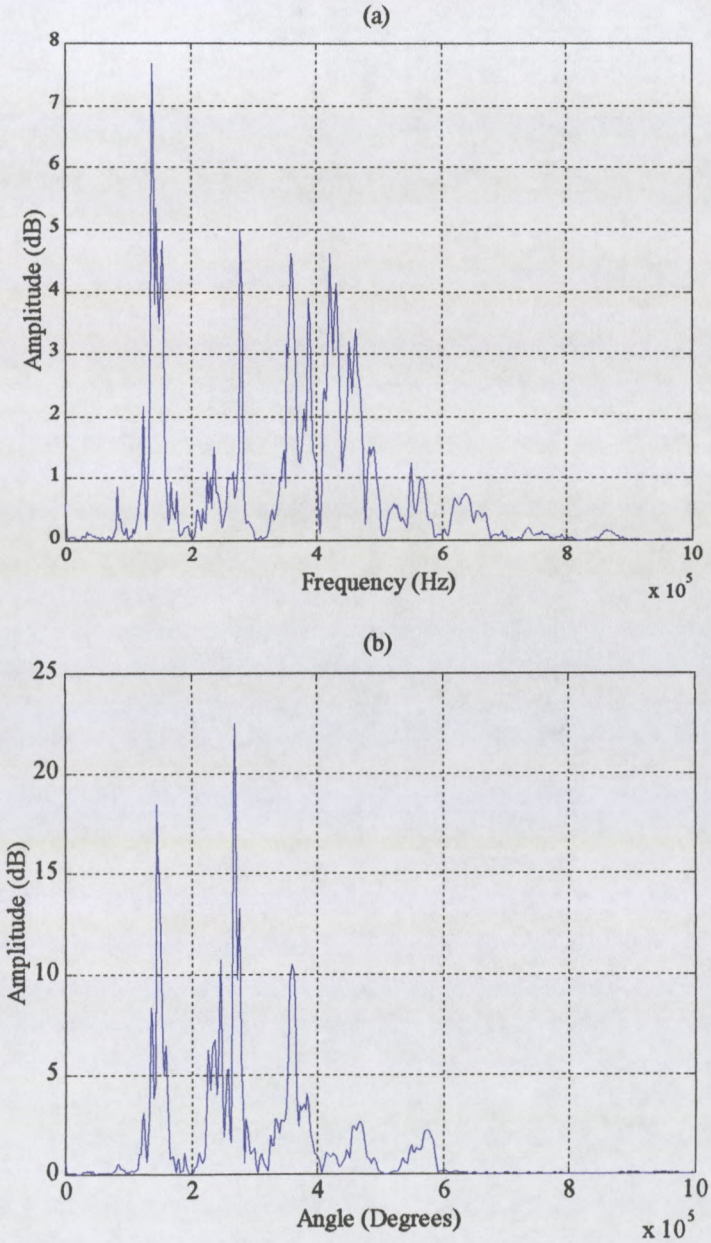

Figure 3.5.1. A comparison of the frequency components present in laminates (a) UD3 and (b) UD5.

3.6 Laminate UD3b

Preliminary tests indicated that in laminate UD3b the rate of attenuation was high. Therefore, to allow recording it was necessary to reduce the threshold level to 25 dB. Ringdown counts is the only parameter that will be affected by a change in threshold level. Because of the lower threshold setting the ringdown counts for laminate UD3b cannot be compared to the ringdown counts of the other laminates.

3.6.1 Peak Voltage

Figure 3.6.1 shows the peak voltage curve and indicates a strong relationship between the peak voltage and the direction of wave travel relative to the fibre direction. The highest peak voltage of 0,0208 V was recorded with the wave's travel direction parallel to the fibre direction i.e. at 180°. The lowest peak voltage of 0.0034 V was recorded at 90° to the fibre direction. The percentage difference between the highest and lowest peak voltages is 83,7 %.

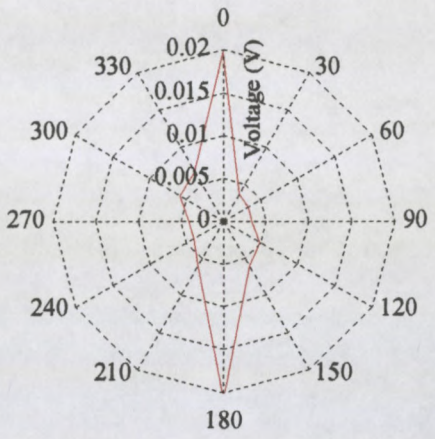

Figure 3.6.1. Variation of peak voltage in laminate UD3b.

3.6.2 Ringdown Counts

The ringdown counts curve (figure 3.6.2) shows a definite relationship between the direction of wave travel and the number of ringdown counts. The curve is not perfectly symmetric; the number of counts in the 0° to 90° quadrant are noticeably fewer than in either of the other 3 quadrants. The highest number of ringdown counts (75) was recorded when the wave travelled parallel to the fibre direction (at 180°). The lowest number of ringdown counts (12) was recorded at 30°. The percentage variation between the maximum and minimum number of ringdown counts is 84 %.

Figure 3.6.2. Variation of ringdown counts in laminate UD3b.

3.6.3 Energy Content

As shown by figure 3.6.3 peaks at 0° and 180° dominate the shape of the energy content curve. The curve's largest deviation from symmetry is the 31,9 % difference between the energy content at 0° and 180°. The maximum energy content of 301180 was recorded at 180° while the minimum energy of 48705 was recorded at 60°. This range, expressed as a percentage is 83,8 %.

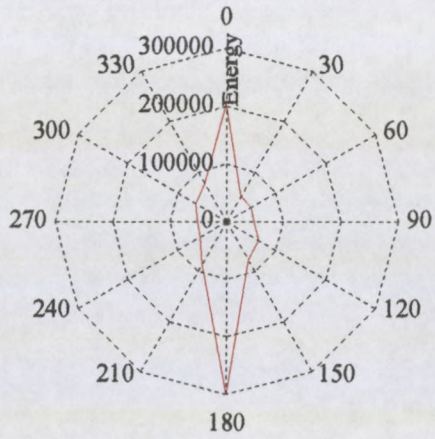

Figure 3.6.3. Variation of energy content in laminate UD3b.

3.6.4 Central Frequency

The central frequency curve (figure 3.6.4.) has an oval shape with its higher values at in the 30° to 90° region and also in the 240° to 270° region. The signals with the lowest central frequency were recorded at perpendicular to the fibre direction. The highest central frequency of 477 kHz was recorded at 30°, while the lowest central frequency of 355 kHz was recorded at 180°. This range, expressed as a percentage is 25,5 %.

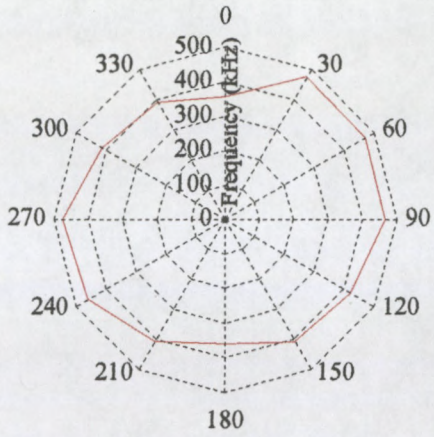

Figure 3.6.4. Variation of central frequency in laminate UD3b.

3.6.5 Arrival Time

Figure 3.6.5 depicts the variation in arrival time for different directions of wave travel. The curve is symmetric and indicates longer arrival times at perpendicular to the fibre direction (90° and 270°). The shortest arrival times were recorded at parallel to the fibre direction (0° and 180°). The minimum arrival time of 13,2 μs was recorded at 180°. The maximum arrival time of 33,4 μs was recorded at 270°. The percentage variation between the maximum and minimum arrival times is 60,5 %.

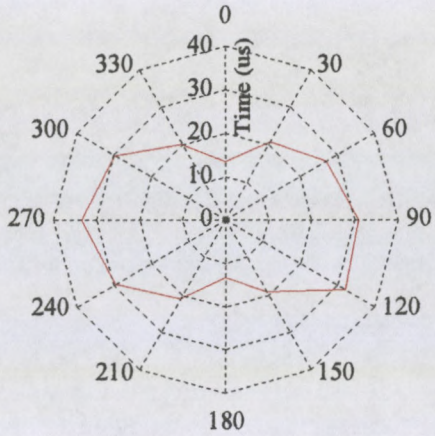

Figure 3.6.5. Variation of arrival time in laminate UD3b.

3.6.6 Summary of Main Features

The magnitudes of all 5 parameters show a relationship between the wave's direction of travel relative and the fibre direction. Peak voltage, ringdown counts and energy content have their highest magnitude when the wave travels parallel to the fibre direction and their lowest magnitude at perpendicular to the fibre direction. The central frequency and arrival time have their highest values at angles that are perpendicular to the fibre direction. The percentage variation in the peak voltage, ringdown counts, energy content and arrival time are 83,7 %, 84 %, 83,8 % and 60,5 % respectively. The variation in central frequency is much less at 25,5 %.

3.7 Comparison of the test results for UD3 and UD3b

A quantitative comparison of results from laminates UD3 and UD3b is shown in table 3.7.1. The shapes of the peak voltage and energy content curves in laminates UD3 and UD3b are very similar, with their highest values at parallel to the fibre direction and their lowest values at perpendicular to the fibre direction.

There is a significant difference between the shapes of the central frequency curves. In laminate UD3 the central frequency is highest in directions that are parallel to the fibre direction whereas in laminate UD3b the central frequency is highest at angles that are to perpendicular to the fibre direction.

The arrival time curves for UD3 and UD3b are similar in that they both show the shortest arrival time at parallel to the fibre direction. However in laminate UD3b, at parallel to the fibre direction the arrival time is less than that in laminate UD3, whereas at perpendicular to the fibre direction the arrival time is longer in laminate UD3b than in UD3.

Parameter	Range UD3	Range UD3b	Comparison of average values.
Peak Voltage	80,7 %	83,7 %	75,8 % higher in UD3
Ringdown Counts	Comparison not possible because of differing threshold settings.		
Energy Content	74 %	83,8 %	71,8 % higher in UD3
Central Frequency	13,3 %	25,5 %	6,9 % higher in UD3b
Arrival Time	43,6 %	60,5 %	3 % higher in UD3

Table 3.7.1. Comparison between UD3 and UD3b.

3.8 Laminate 090

3.8.1 Peak Voltage

Figure 3.8.1 shows the peak voltage curve for laminate 090 and has maxima at 0°, 90°, 180° and 270°. The peaks at 0° and 180° (the direction with 2 layers of fibre) are higher than the peaks at 90° and at 270° (the direction with 1 fibre layer). For the graph to reflect the symmetry of the laminate's stacking sequence it would be expected that the peak voltage at 0° would be equal to the peak voltage at 180°, however this is not the case and the peak voltage at 0° is 14,4 % higher than that at 180°. Likewise, contrary to expectation, the peak voltage at 270° is 19,2 % higher than the peak voltage at 90°. The curve has minima at 60°, 120°, 240° and 300°. The angles at which all of these minima occur are between the directions in which the fibres are aligned and closer to the direction that contains one layer. The percentage variation between the maximum and minimum peak voltages is 81 %.

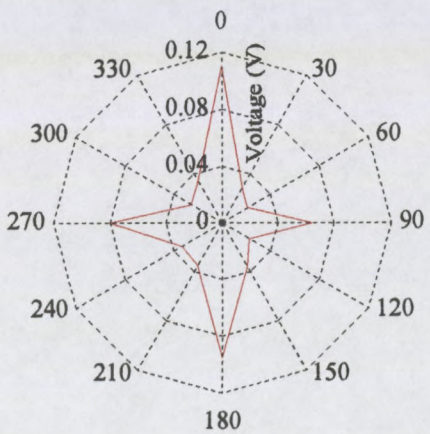

Figure 3.8.1. Variation of peak volage in laminate 090.

3.8.2 Ringdown Counts

The ringdown counts curve (figure 3.8.2) has peaks at 0°, 90°, 180° and at 270°. The peaks in the direction that that is aligned with the 2 layers (at 0° and 180°) are higher than the peaks in the direction that contains 1 layer. The number of ringdown counts at 30° and 60° are noticeably lower than the number recorded at the vertically opposite angles (210° and 240°). This difference is the graph's only significant deviation from symmetry. The percentage difference between the minimum and maximum number of ringdown counts is 93,9 %.

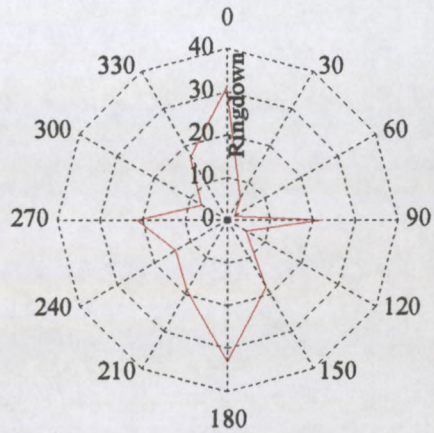

Figure 3.8.2. Variation of ringdown counts in laminate 090.

3.8.3 Energy Content

Figure 3.8.3 shows the variation in energy content as a function of direction of wave travel and is approximately symmetric. Large peaks are present at 0° and at 180° while smaller peaks are present at 90° and 270°. The highest energy content of 868 000 was recorded in one of the directions that contain 2 layers of glass fibre ie at 180°. The lowest energy content of 246 000 was recorded at 60°, which is between the two fibre directions but closer to the direction of the single layer. The percentage variation between the maximum and the minimum energy content is 70,9 %.

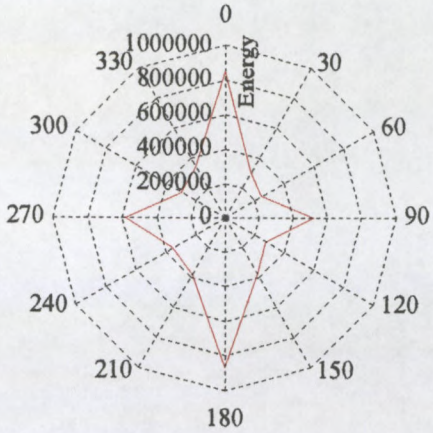

Figure 3.8.3. Variation of energy content in laminate 090.

3.8.4 Central Frequency

The trend in the central frequency curve of figure 3.8.4 indicates that at angles that are close to the fibre direction the central frequency will be higher. The curve is not symmetric as the central frequencies in the 120° to 240° region are lower than those in the 300° to 60° region. The highest central frequency of 380 kHz was recorded at 0° while the lowest central frequency of 337 kHz was recorded at 120°. The difference between the maximum and minimum central frequencies is 11,2 %.

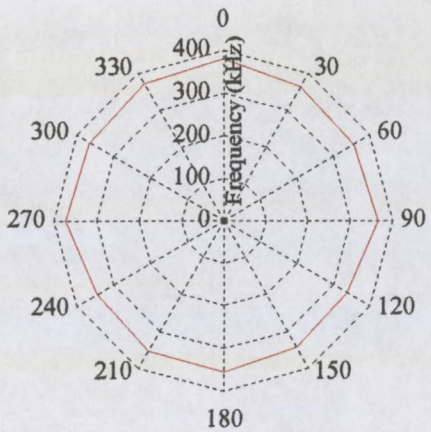

Figure 3.8.4. Variation of central frequency in laminate 090.

3.8.5 Arrival Time

Figure 3.8.5, the arrival time graph for laminate 090, indicates that the shortest arrival times occur in the direction of the two layers (0° and 180°). The average of the arrival times in the direction of the single layer (90° and 270°) is 15,1 % longer than those in the direction of the two layers. The longest times were recorded between the direction

of either of the layers and closer to the direction of the single layer i.e. at 60°, 120°, 240° and 300°. The arrival time curve for laminate 090 is almost perfectly symmetric. As an indication as to how symmetric this curve is, the difference in arrival time between the 0° and 180° directions is only 1,5 % and the difference in arrival time when comparing the 90° direction to the 270° direction is 2,6 %.

The shortest arrival time was 19,3 μs (at 0°) and the longest recorded was 24,8 μs (120° and at 240°). The percentage difference between the maximum and minimum arrival times is 22,2 %.

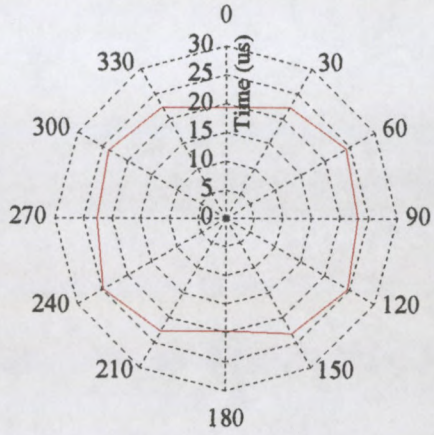

Figure 3.8.5. Variation of arrival time in laminate 090.

3.8.6 Summary of Main Features

In laminate 090 the signal's peak amplitude, ringdown counts, central frequency and energy content are all have higher values when the wave travels parallel to the fibre direction. Thus the curves for the 4 above-mentioned parameters all have peaks at 0°, 90°, 180° and 270°. The peaks at the angles that have only 1 layer (90° and 270°) of glass fibre are lower than the peaks at the angles that have 2 layers (0° and 180°). The peak amplitude, ringdown counts and energy content curves are similar in terms of their ranges and the location of their maxima and minima. However the low number of ringdown counts at 30° and 60° are not evident in the peak voltage and energy content curves. The arrival time curve is the most symmetric curve and shows the shortest travel times when the wave travels in the direction of the two layers. The range of the peak voltages, ringdown counts and energy contents is large; 81 %, 93,9 % and 70,9 % respectively. The range of the central frequencies and arrival times are much lower at 11,2 % and 22,2 % respectively.

3.9 Laminate 909

3.9.1 Peak Voltage

The peak voltage (figure 3.9.1) curve has its biggest peaks in the direction in which the 2 layers are aligned (90° and 270°) and smaller peaks in the direction that that has 1 layer (0° and 180°). The curve is not perfectly symmetric; the peak at 0° is 10,9 % higher than the peak at 180° and the peak at 90° is 14,7 % higher than the peak at 90°. The difference between the highest and lowest peak amplitudes is 69,4 %.

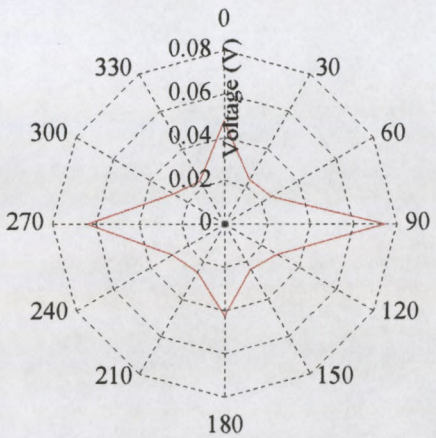

Figure 3.9.1. Variation of peak voltage in laminate 909.

3.9.2 Ringdown Counts

Figure 3.9.2, the ringdown counts curve for laminate 909, has its biggest peaks at 90° and 270° and lesser peaks at 0° and 180°. The curve is not perfectly symmetric; the peak at 90° is 7,4 % higher than the peak at 270°, the peak at 180° is 15,4 % higher than the peak at 0° and the number of counts at 210° and 330° is noticeably low. The percentage difference between the maximum and minimum number of counts is 88,9 %.

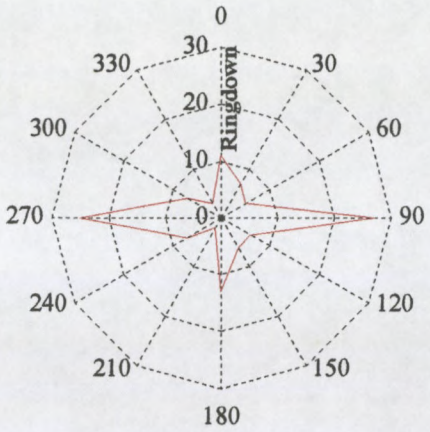

Figure 3.9.2. Variation of ringdown counts in laminate 909.

3.9.3 Energy Content

The energy content curve (figure 3.9.3) for laminate 909, is dominated by peaks at in the directions that contain 2 layers of glass fibre (90° and at 270°). Lesser peaks are present in the directions that contain a single layer of glass fibre (0° and at 180°). The maximum energy content of 601 000 was recorded at 270°. The minimum energy content of 218 000 was recorded at 210°, an angle that is closer to the orientation of the single layer than the orientation of the 2 layers. This range, expressed as a percentage is equal to 64,2%.

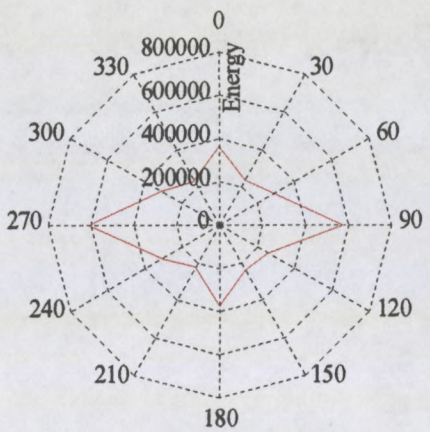

Figure 3.9.3. Variation of energy content in laminate 909.

3.9.4 Central Frequency

The variation in central frequency is shown in figure 3.9.4. The curve shows some relation to the fibre direction, with a higher central frequency at angles that are closer to the fibre direction. The central frequency at 210° deviates from the general trend and is noticeably higher than would be expected. There are peaks present in this curve at 0°,

90°, 210° and 270°. The maximum central frequency of 377 kHz was recorded at 90° while the minimum of 347 kHz was recorded at 150°. This represents a range that is equal to 7,82 %.

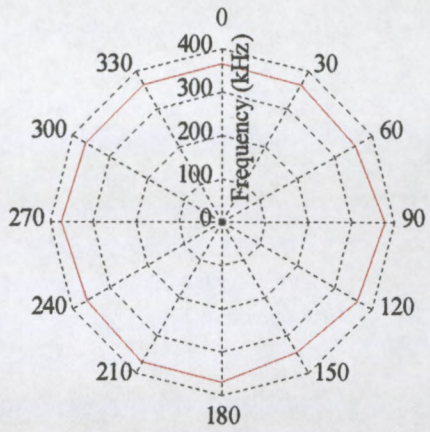

Figure 3.9.4. Variation of central frequency in laminate 909.

3.9.5 Arrival Time

Figure 3.9.5 shows that the shortest arrival times were recorded in the direction of the two layers (90° and 270°). The arrival times in the direction of the single layer (0° and 180°) are 15,2 % longer than those in the direction of the two layers. The longest times were recorded between the direction of either of the layers and closer to the direction of the single layer i.e. at 30°, 150°, 210° and 330°.

As a measure of the graph's symmetry the difference in arrival time between the 0° and 180° directions is 5,8 % and the difference when comparing the 90° direction to the 270° direction is 3,6 %. The shortest arrival time recorded was 18,6 μs (270°) and the longest arrival time recorded was 24,2 μs (210°). This range of speeds expressed, as a percentage is 22,7 %.

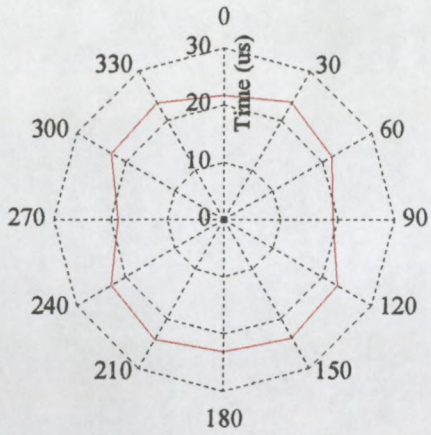

Figure 3.9.5. Variation of arrival time in laminate 909.

3.9.6 Summary of Main Features

The values of peak voltage, ringdown counts, energy content and central frequency are related to the wave's direction of travel relative to the fibre angle. These 4 parameters have peaks at 0°, 90°, 180° and 270°. The peaks in the directions of the single layer (0° and 180°) of glass fibre are lower than the peaks in the direction of the 2 layers (90° and 270°). Apart from the noticeably low number of ringdown counts at 210° and at 330°, the peak voltage, ringdown counts and energy content curves have similar shapes. The signal's arrival time is also influenced by the fibre orientation and is shortest when the signal travels parallel to the two layers of fibre.

3.10 Laminate 45

3.10.1 Peak Voltage

The variation in peak voltage is shown in figure 3.10.1. This figure shows higher peak voltages at between 0° and 30° and between 180° and 285°. The shape of the peak voltage curve appears to have been influenced by the orientation of the fibres since there are peaks present in the curve at 0° and at 180° (the direction aligned with both the top and bottom layers). The curve also has distinct peaks at 30° and at 285°, the presence of which is unexpected since there is not a fibre layer in either of these directions. The highest peak voltage of 0,1172 V was recorded in the 285° direction. The lowest peak voltage of 0,0397 V was recorded at 60°. The percentage variation between the maximum and the minimum peak voltages is 66 %.

The average of the peak voltages in the 135° and 315° directions (the orientation of the 2nd layer) is 0,0731 V. The average of the peak voltages in the 90° and 270° directions (the orientation of the 3rd layer) is 0,0841 V. Furthermore the average of the peak voltages in the 45° and 225° directions (the orientation of the 4th layer) is 0,0852 V. Stated differently, the peak voltage in the directions of the 4th layer is higher than that in the directions of the 3rd layer and likewise the peak voltage in the 3rd layer is higher than that in the 2nd layer.

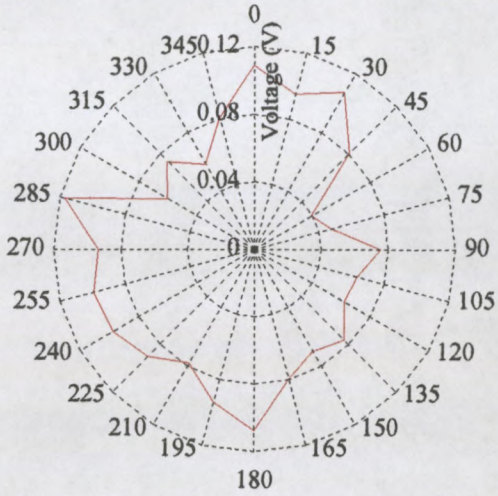

Figure 3.10.1. Variation of peak voltage in laminate 45.

3.10.2 Ringdown Counts

The ringdown counts curve on figure 3.10.2, has its highest peaks at 0° and at 180 °. The number of counts at angles between 195° and 285° is noticeably high. The maximum number of ringdown counts (39) was recorded at 165° and at 180° while the minimum number (15) was recorded at 60°. The percentage difference between the maximum and minimum number of ringdown counts is 61 %.

The average of the ringdown counts in the 135° and 315° directions (the orientation of the 2nd layer) is 29. Likewise the average of the ringdown counts in the 90° and 270° directions (the orientation of the 3rd layer) is 32. Furthermore, the average of the ringdown counts in the 45° and 225° directions (the orientation of the 4th layer) is 31. In other words the number of ringdown counts in the directions of the 2nd layer is less than the number in the directions of the 3rd and 4th layers.

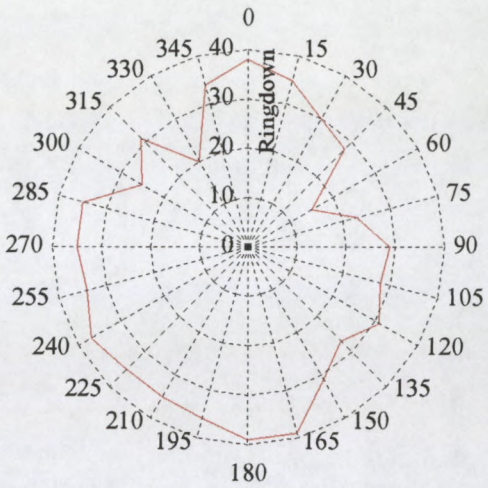

Figure 3.10.2. Variation of ringdown counts in laminate 45.

3.10.3 Energy Content

Peaks at 0° and at 180° (the orientation of the top and bottom layers) dominate the energy content curve (figure 3.10.3), indicating that the energy content has been affected by the fibre orientation. The energy contents at 60°, 315° and 330° are noticeably low. The highest energy content of 1 093 000 was recorded in one of the directions that contain 2 layers of glass fibre ie at 180°. The lowest energy content of 428 100 was recorded at 60°. This range, expressedas a percentage is 60.8 %.

The average of the energy contents in the 135° and 315° directions (the orientation of the 2nd layer) is 653 000. Likewise the average of the energy contents in the 90° and 270° directions (the orientation of the 3rd layer) is 667 000. Furthermore the average of the energy contents in the 45° and 225° directions (the orientation of the 4th layer) is 701 000. More energy has thus been transmitted in the direction of the 4th layer than in the direction of the 3rd layer. Likewise more energy has been transmitted in the direction of the 3rd layer than in the direction of the 2nd layer.

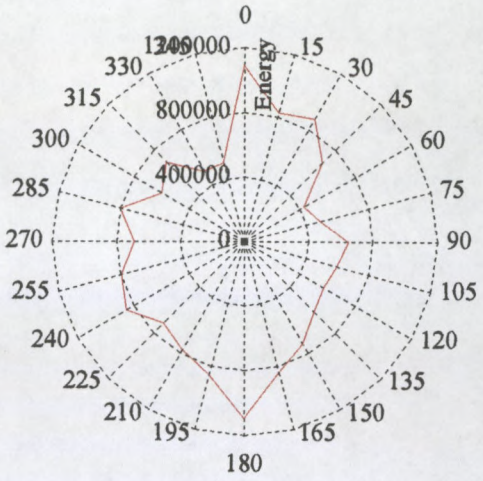

Figure 3.10.3. Variation of energy content in laminate 45.

3.10.4 Central Frequency

Figure 3.10.4 shows the variation in central frequency and has peaks at 30°, 225° and in the 330° to 345° region. The maximum recorded central frequency is 292 kHz, (at 330° and at 345°) while the minimum recorded was 265 kHz (at 105°). This difference, expressed as a percentage is 9,3 %. There does not appear to be any correlation between central frequency and direction of wave travel.

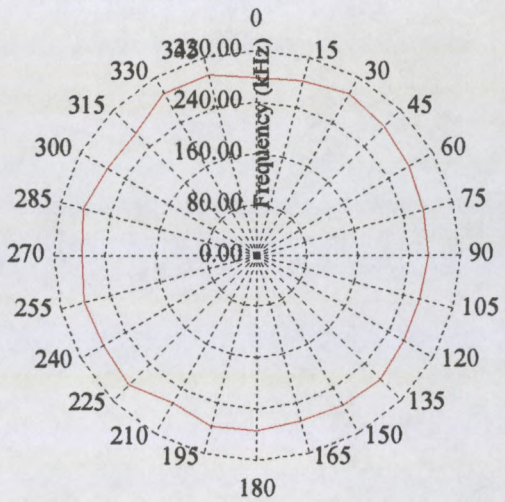

Figure 3.10.4. Variation of central frequency in laminate 45.

3.10.5 Arrival Time

The arrival time graph for laminate 45 (figure 3.10.5) has an oval shape with shorter wave travel times between 330° and 30° and between 135° and 210°. These regions of shorter travel time coincide with the alignment of the top and bottom layers. Longer

travel times were recorded in the 60° to 120° region and also in the 240° to 300° region. The longer times coincide with the alignment of the 3rd layer. The shortest travel time (23,5 μs) was recorded at 0° and at 210° while the longest travel time (28,8 μs) was recorded at 105°. The range between the longest and shortest arrival times expressed as a percentage is 18,4 %.

The average of the arrival times in the 0° and 180° directions (the orientation of the top and bottom layers) is 23,9 μs. Likewise average of the arrival times in the 135° and 315° directions (the orientation of the 2nd layer) is 25,7 μs. Furthermore the average of the arrival times in the 90° and 270° directions (the orientation of the 3rd layer) is 27,6 μs and the average of the arrival times in the 45° and 225° directions (the orientation of the 4th layer) is 26,5 μs. The above can be summarised as: the shortest wave travel time is present in the direction of the top and bottom layer. The second shortest travel time was observed in the direction of the 2nd layer, the third shortest time in the direction of the 4th layer and the longest travel time was recorded in the direction of the 3rd layer.

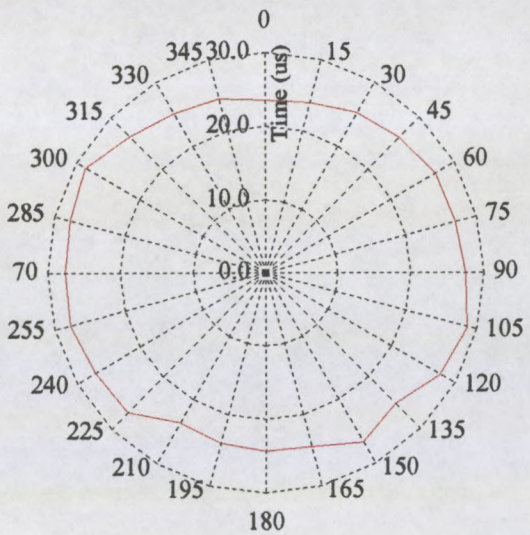

Figure 3.10.5. Variation of arrival time in laminate 45.

3.10.6 Summary of Main Features

The value of ringdown counts, peak voltage and energy content are all related to the direction of wave travel relative to the fibre angle. Each of these 3 curves have peaks at 0° and 180° (the directions that contain both the top and bottom layers).

Table 3.10.6 summarises the relative magnitudes of peak voltage, ringdown counts and energy content in terms of the depth of the layer that is aligned with signal's direction of travel.

	Top and bottom layers (Average of 0° and 180°)	2nd layer (Average of 135° and 315°)	3rd layer (Average of 90° and 270°)	4th layer (Average of 45° and 225°)
Peak Voltage	Highest	Lowest	Med-low	Med-high
Ringdown	Highest	Lowest	Med-high	Med-low
Energy	Highest	Lowest	Med-low	Med-high

Table 3.10.6. The relative magnitude of peak voltage, ringdown counts and energy.

The percentage variation in the peak voltage, ringdown counts and energy content curves is large at 66 %, 61 % and 60,8 % respectively. The range in the central frequency and arrival time is smaller at 9,3 % and 18,4 % respectively. There does not appear to be a correlation between the central frequency and the wave's direction of travel relative to the fibre angle.

More energy and a higher peak voltage were recorded in the direction of the 4th layer than in the direction of the 3rd and 2nd layers. A lower number of ringdown counts was recorded in the direction of 2nd layer than was recorded in the direction of the 3rd and 4th layers.

3.11 Laminate 452

The aim of making and testing laminate 452 was to discover how well each direction transmits acoustic energy in terms of the depth below the testing surface of the layer that is aligned with the wave's direction of travel. The laminate was made with a single layer aligned in each of 4 equi-spaced directions ($0_1/-45_1/45_1/90_1$). The thinking behind the selection of this stacking sequence was that since there is only one layer in each direction, the strength of the signal would be solely dependant on the depth of the layer that is aligned with the testing direction.

3.11.1 Peak Voltage

Figure 3.11.1 shows the variation in peak voltage and is approximately oval with its major axis in the 60° / 240° direction. The peak voltage has its highest values between 45° and 60° and in the 225° to 270° region. These higher voltages approximately coincide with the alignment of the 3rd and 4th layers. The lowest peak voltages are present in the 135° to 150° region as well as in the 315° to 0° region. The lower peak voltages approximately coincide with the alignment of the 1st and 2nd layers. The maximum peak voltage of 0,1088 V was recorded at 270° while the minimum peak voltage (0,0471 V) was recorded at 135°. This range expressed as a percentage is 56,7 %.

The peak voltage graph is not symmetric. The lack of symmetry is illustrated by the fact that there are large differences between the peaks voltage at 0° and 180° (49,2 % difference) as well as between those at 90° and 270° (39,6 % difference).

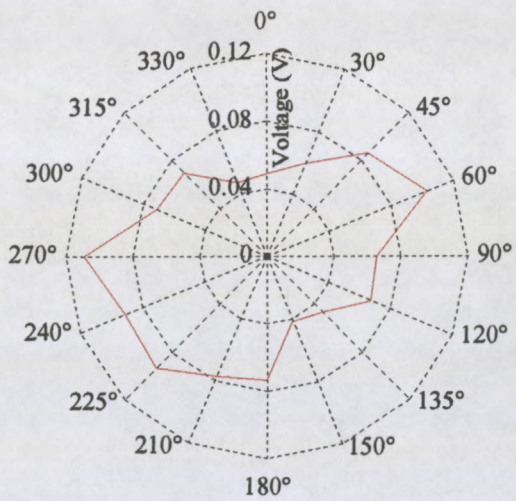

Figure 3.11.1. Variation of peak voltage in laminate 452.

3.11.2 Ringdown Counts

The variation in ringdown counts in laminate 452 is shown in figure 3.11.2. The highest numbers of ringdown counts were recorded at 60° and at 225°, which is approximately aligned with the direction of the 3rd layer. Low numbers of ringdown counts were recorded at 0° and at 150°. The maximum number of ringdown counts (55) was recorded at 225°. The minimum number (34) was recorded at 150°. This range expressed as a percentage is 38 %.

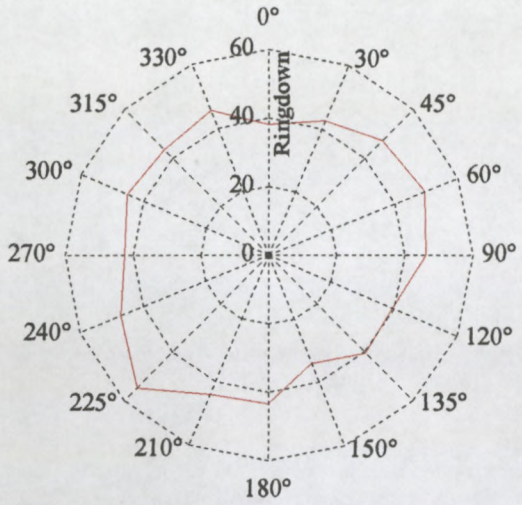

Figure 3.11.2. Variation of ringdown counts in laminate 452.

3.11.3 Energy Content

The radial plot of the energy content is oval with its highest values in the 45° to 60° region as well as in the 210° to 270° region. These higher energy contents coincide approximately with the alignment of the 3rd layer. The lowest energy contents were recorded in the 330° to 0° region and in the 135° to 150° region. These low energy contents coincide with the alignment of the 2nd layer. The maximum energy content (916985) was recorded at 225°. The minimum number (521567) was recorded at 135°. This range expressed as a percentage is 43,1 %. The energy content at 90° is 23,9 % lower than that at 270°. There is also a 23,9 % difference between the energy content at 135° and 315°.

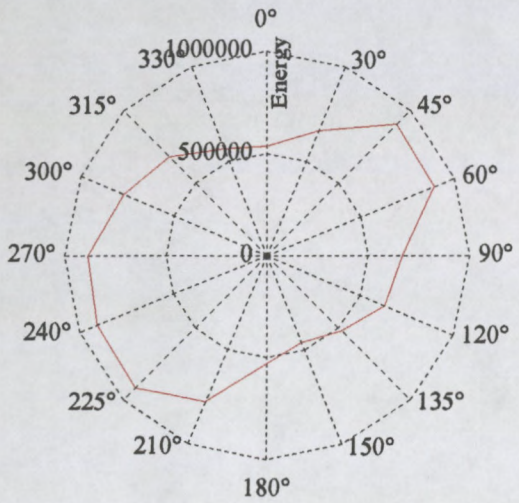

Figure 3.11.3. Variation of energy content in laminate 452.

3.11.4 Central Frequency

The most notable feature of the central frequency graph (figure 3.11.4) is the large difference between the central frequency at 150° and 180°. The highest central frequency (298 kHz) was recorded at 150° while the lowest central frequency (244 kHz) was recorded at 180°. This range, expressed as a percentage is equal to 18 %. The central frequency plot is not very symmetric and there are large differences between the values at 0° and 180°, 90° and 270° and between 150° and 330°.

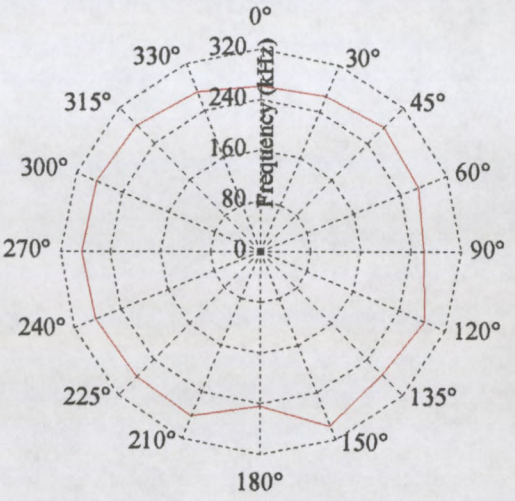

Figure 3.11.4. Variation of central frequency in laminate 452.

3.11.5 Arrival Time

The shape of the arrival time graph (figure 3.11.5) is oval, indicating that in the 315° to 0° region and in the 135° to 180° region the wave has a longer travel time. These regions of longer times coincide with the alignment of the 1st and 2nd layers. The shortest times were recorded in the 45° to 120° region and in the 225° to 300° region. These shorter times coincide with the alignment of the 3rd and 4th layers.

The longest travel time (31,9 μs) was recorded in the direction of the top layer (at 0°). The shortest travel time (26,23 μs) was recorded at both 240° and at 120° (both directions that are between the alignment of any of the layers). The range between the longest and shortest travel time, expressed as a percentage is 17,8 %.

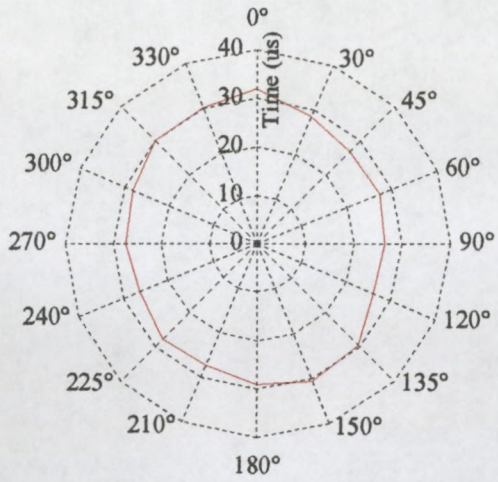

Figure 3.11.5. Variation of arrival time in laminate 452.

3.11.6 Summary of Main Features

In general, the peak voltage, ringdown counts and energy content plots have higher values in direction of the 3rd layer (45° / 225°). The peak voltage, ringdown counts and energy content have large percentage ranges; 56,7 %, 38 % and 43,1 % respectively. However the range of the central frequencies and arrival times is much less at 18% and 17,8 % respectively. The arrival time graph indicates that wave's travel time will be highest in the direction of the 1st and 2nd layers and lowest in the direction of the 3rd and 4th layers.

3.12 Correlation between Parameter Range and Anisotropy

A correlation between the relative anisotropy of the laminates and the range of the energy contents and arrival times has been observed. The laminates that are most anisotropic have the highest range of energy content and arrival time. This correlation has been summarized in table 3.12.1, where the laminates have been listed from the most to the least anisotropic.

There is a similar correlation between the laminate's anisotropy the parameters peak voltage, ringdown counts and central frequency. However these parameters do not reflect the anisotropy as consistently as do the energy content and arrival time.

Laminate	Energy Content Range	Arrival Time Range
UD3b	83,8 %	60,5 %
UD3	74 %	43,6 %
UD5	68,2 %	41,3 %
909	64,2 %	22,7 %
090	70,9 %	22,2 %
45	60,8 %	18,4 %
452	43,1 %	17,8 %

Table 3.12.1. Comparison between parameter's range and anisotropy

3.13 Conclusions

3.13.1 Fibre Orientation

In a glass fibre reinforced plastic laminate the magnitude of an acoustic wave's peak amplitude, ringdown counts, central frequency and energy content will be highest when the wave travels parallel to the fibre direction. In terms of energy content, this is identical to the findings of Kiernan and Duke [18, 48]. However Kiernan and Duke found that the central frequency would be at a maximum when the wave travelled at 15° to the fibre direction. This phenomenon was not observed in this study since tests on the uni-directional laminates were conducted at 30° increments meaning that the high central frequency at 15° was missed. The arrival time will be lowest when the wave travels parallel to the fibre direction and highest when the wave travels perpendicular to the fibre direction.

3.13.2 Resin Content

A lower resin content will cause a reduction in the magnitudes of peak voltage, ringdown counts, energy content.

The variation of central frequency with respect to fibre orientation in a laminate with a low resin content differs to that in a laminate with a higher resin content. A lower resin content will cause, the wave to have a higher central frequency when the it travels

perpendicular to the fibre direction. This phenomenon may be used to identify regions that have a low resin content.

An increase in a laminate's resin content will also have a moderating effect on the wave's travel time. In other words, at parallel to the fibre direction in a laminate with a high resin content the arrival time will be less than in a laminate with a low resin content. Likewise at perpendicular to the fibre direction the arrival time in a laminate with a low resin content will be less than that in a laminate with a higher resin content.

3.13.3 Anisotropy

From a radial testing pattern, the range of the parameters energy content and arrival time can be used as a measure of the laminate's anisotropy. The more anisotropic a laminaite is the greater the difference will be in the arrival time and energy content when these parameters are measured parallel to and then perpendicular to the direction of the laminate's greatest strength.

3.13.4 Laminate Thickness

In a thick laminate, the magnitude of an acoustic wave's peak amplitude, ringdown counts and energy content will be higher than in a thinner laminate. However the wave's arrival time and central frequency will be lower in a thicker laminate. A comparison of the frequency components present in the waveforms recorded in laminates UD3 and UD5 has revealed that each laminate transmits the same frequencies. This contradicts the findings of Kiernan and Duke [18] who found that the frequencies excited within a plate are inversely proportional to the plate thickness. This anomaly may be due to the frequencies excited in the laminate being outside the receiving transducer's sensitivity range.

Several peaks are present in the Fourier transforms of waveforms recorded in laminates UD3 and UD5. This correlates with the work of Egle and Brown [17] and Kiernan and Duke [18], which showed that much of the energy in the received signal is concentrated at certain frequencies.

3.13.5 Depth of Wave Penetration

There are peaks in all curves at both 0° and 90° for laminates 090 and 909. Thus, in a 3 layer laminate, the waves penetrate beyond the surface and are influenced by the layer orientation right through the thickness of the laminate.

In laminate 452, the highest values of peak voltage, ringdown counts and energy content were observed in the direction of the 3rd and 4th layers. This while the shortest arrival times were in the direction of these layers. Thus, the lower layers of a thin laminate appear to be more efficient at the transmission of acoustic energy than the upper layers.

There is no clear relation between the magnitude of any of the 5 parameters, calculated from a wave travelling in the direction of a particular layer, and that layer's depth below the laminate's surface. It is thus likely that the efficiency of wave propagation of a particular layer is affected by not only the layer's depth below the laminate's surface but also the orientation of its adjacent layers.

Chapter 4

The Testing of Landing Bay Doors

4.1 Introduction

In an effort to apply the AU method in a realistic situation, a set of experiments was conducted on composite landing bay doors. Two doors were supplied, one of which had been repaired. As well as providing an opportunity for detecting defects in a realistic component, these experiments were to show whether the AU method can detect differences in material properties between the repaired and unrepaired regions.

The doors are a prototype, made by Kentron (Pty) Ltd. and are intended to replace an aluminium equivalent on a 'Cheetah[2]' aircraft. They are of sandwich construction with a foam core and skins made of glass fibre and a nylon resin system. The repair was effected through the use of glass fibre and an 'Epolam' epoxy resin system.

A visual inspection of the unrepaired region showed that the skin's outer layer is bi-axial mat. However it is not possible by visual examination to determine the fibre orientations in the repaired region.

These AU tests were conducted in the early stages of the project, before the researcher was aware of the parameters energy content, ringdown counts and central frequency. At this stage, AU waveforms were characterized in terms of their speed and the amplitude of certain frequencies. Furthermore, these tests were conducted before the source generator (PAC 3000) was being used emit acoustic waves into the specimen. The method of breaking of pencil leads on the test specimen's surface was being used for generating acoustic waves when these tests were conducted. A resonant receiving

[2] A highly modified 'Mirage 3000'.

transducer (R6-127) with a sensitivity range of between 35 kHz and 100 kHz was used to record the waveforms.

4.2 Test Methods

Both doors have been x-rayed and the radiograph of the unrepaired door shows the presence of a delamination between the skin and the core.

A radial test pattern has been used for the AU testing of the landing bay doors. Pencil leads were broken on the door's surface at 30° increments on a 90 mm radius around the recording transducer. A trigger sensor, located close to the point at which the lead was broken was used to determine the time taken for the wave to travel to the recording transducer. From the wave's arrival time the velocity of the wave was calculated.

Four AU tests have been conducted on the bay doors. The first test was run on an un-repaired region, the second on a repaired region and the third was situated so as to cover part of the repaired and part of the unrepaired regions. The objective of the fourth test was to determine whether, and if so to what extent, a skin to core delamination affects an acoustic wave.

The Fourier transforms of the recorded waves all feature peaks at between 20 kHz and 30 kHz and a second peak at between 90 kHz and 100 kHz. The waveforms have been characterized by noting the amplitudes of these peaks. These amplitudes have been plotted as a function of the wave's direction of travel.

4.3 Unrepaired Door

4.3.1 Wave speed

The wave speed versus fibre angle curve for the unrepaired bay door is fairly symmetric and shows well-defined peaks at 0°, 90°, 180° and 270°. The difference between the velocities in the 0°/180° direction and the 90°/270° direction is only 1,3%. This indicates that there is an equal amount of fibre in these directions and this correlates with the visual inspection that shows the skins to be made of bi-axial mat. The velocities

recorded at 210° and 240° are higher than what would be expected for the curve to be symmetric.

4.3.2 Amplitude

20 to 30 kHz

Figure 4.3.2 shows the variation of the amplitudes and the wave speed recorded in the test on the unrepaired bay boor. The highest amplitude recorded was 75.4 dB (at 210°) and the lowest was 65.7 dB (at 60°), resulting in a percentage range, of 12.9%. The shape of the curve is not symmetric and does not show peaks in the directions of the fibre angles. The amplitudes at 210° and 240° are noticeably high.

90 to 100 kHz

The highest amplitude recorded was 61.67 dB (at 180°) and the lowest was 51.7 dB (at 150°), resulting in a percentage range of 16.7%. The curve is not symmetric and the amplitudes at 210° and 240° are higher than the amplitudes at 120° and 150°.

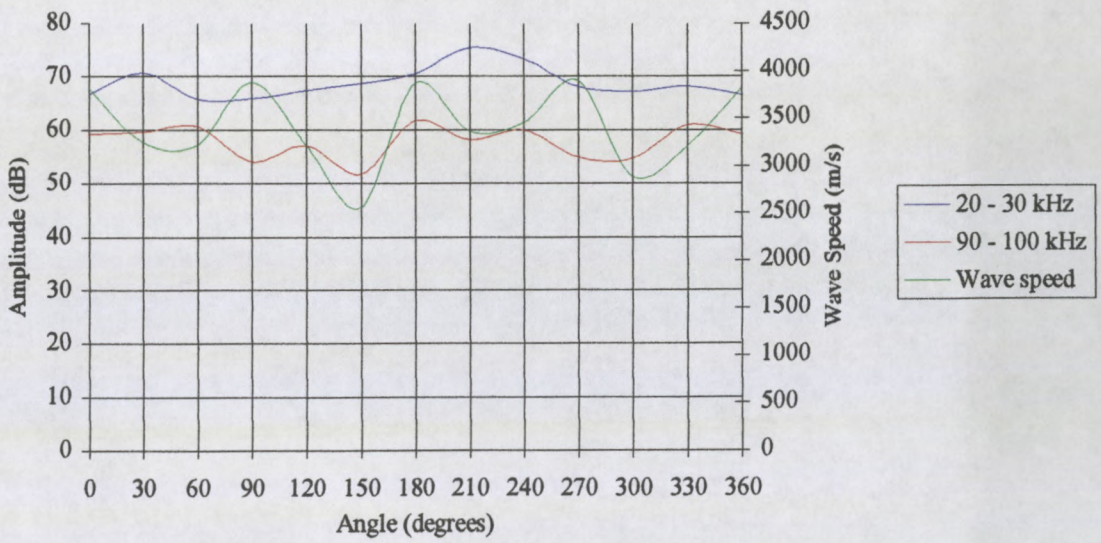

Figure 4.3.2. Amplitude & Wave Speed in Landing Bay Door.

4.4 Radiograph

The white, doughnut shapes on the radiograph (figure 4.4.1) are 'Tufnol' inserts that surround and reinforce the door's attachment points. A number of dark patches are also visible in this radiograph. These dark patches are air gaps and indicate a poor bond or delaminations between the core and skin. The axes used in the radial AU testing of the door have been superimposed upon the radiograph. Within the area tested, there is a high concentration of delaminations at between 180° and 270°. These delaminations correlate with the higher amplitudes and wave speed that were noted at 210° and 240°.

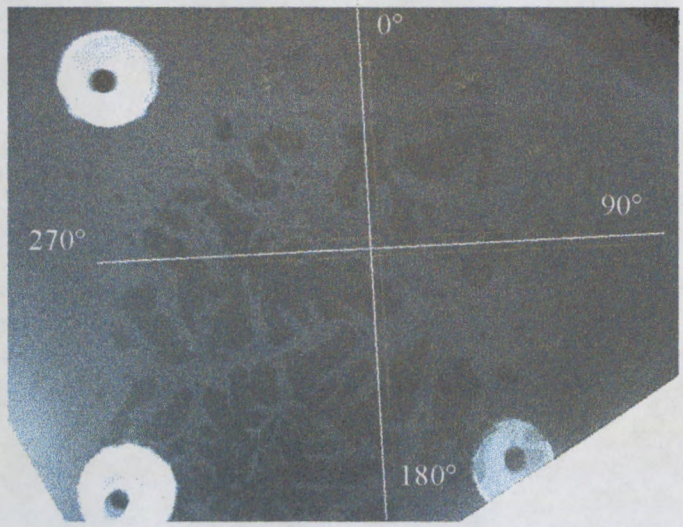

Figure 4.4.1. Radiograph of delaminated region of landing bay door.

4.5 Attenuation Characteristics of a Skin to Core Delamination

Figure 4.5.1 compares a waveform recorded in the delaminated area to a waveform recorded in a correctly bonded area. Both waveforms were recorded with a 60mm distance between the pencil lead break point and the recording sensor and with the fibre angle parallel to the direction of wave travel.

The Fourier transforms of these two waveforms have been determined and are shown in figure 4.5.2. Furthermore, the wave speeds for both the delamination and correctly

bonded areas have been measured. The wave speed determined for the delaminated area was 5009 m/s while that in the correctly bonded area was 3899 m/s.

The most obvious difference between the waveforms in figure 4.5.1 is that the wave from the correctly bonded region has a significantly lower amplitude. Furthermore, the shapes of the two waves are markedly different.

The wave from the delaminated area consists of two main frequency components that are visible in the Fourier transform as peaks at 25 kHz and 90 kHz. The waveform plot shows the higher frequency component at the front of the waveform, thereby indicating that it travels at a higher speed. The two components are the flexural and the extensional wave modes where the extensional mode has the higher velocity and frequency.

The wave from the correctly bonded area consists predominately of a single wave mode and thus only has one main peak (at 30 kHz) in its Fourier transform. This mode is the flexural mode. Since only the lower speed flexural mode is present in this wave, the wave speed measured in the correctly bonded region is lower than the speed measured on the delamination.

Both waves recorded in this experiment feature the flexural wave mode. However the wave recorded on the delamination also features an extensional wave mode. Furthermore, the attenuation of the flexural mode in the delaminated area is lower than its attenuation in the correctly bonded area. It is the presence of the delamination between the core and the skin that has caused these differences.

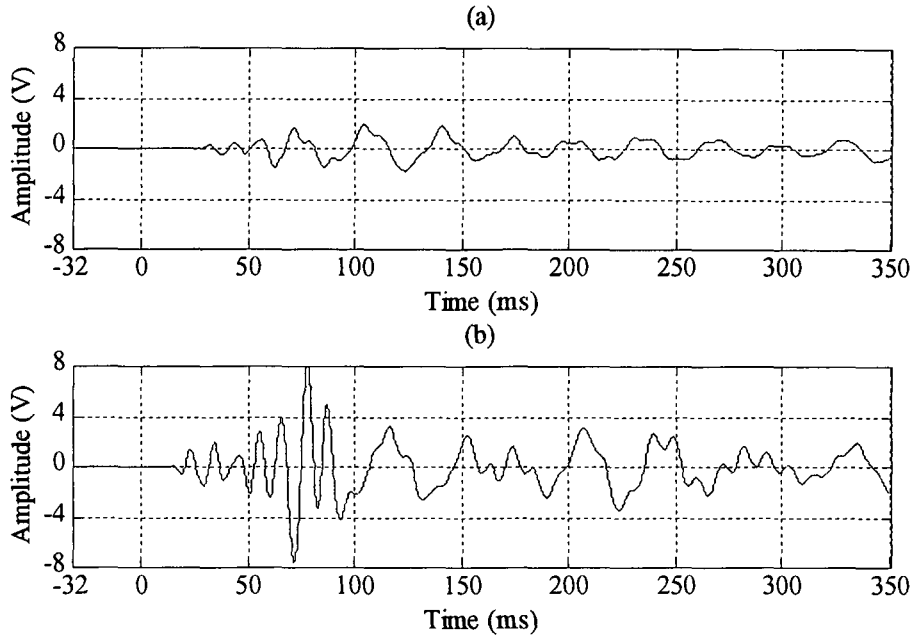

Figure 4.5.1. Waveforms recorded in (a) the correctly bonded area and (b) delaminated area of a landing bay door.

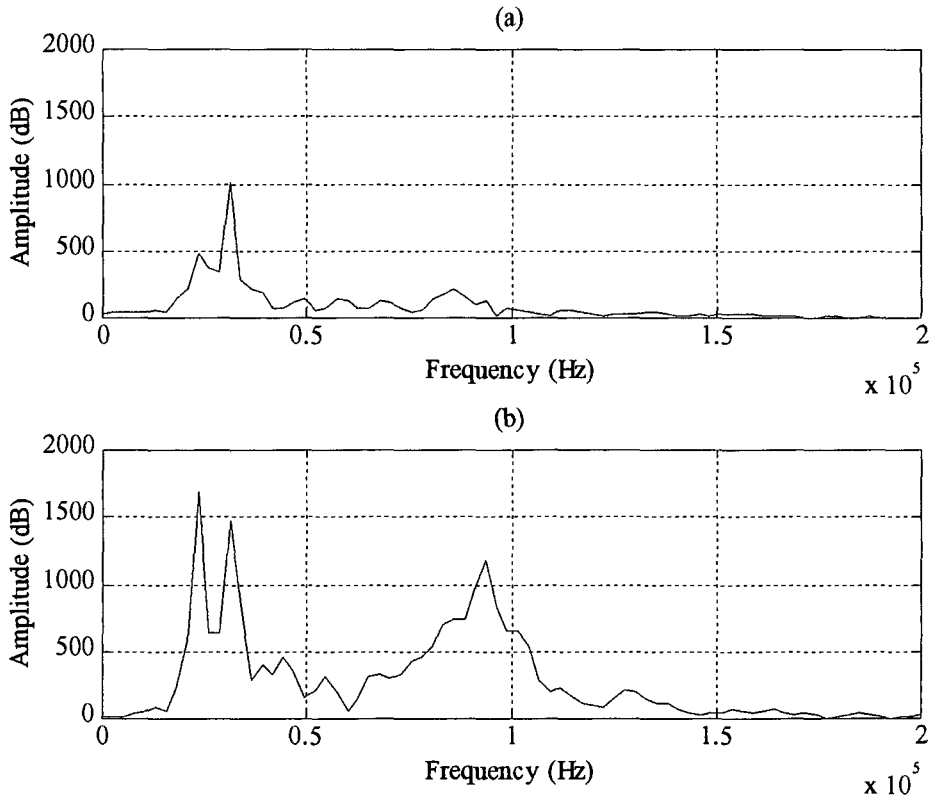

Figure 4.5.2. Fourier transforms of waveforms recorded in (a) the correctly bonded area and (b) delaminated area of a landing bay door.

4.6 Repaired Region of Landing Bay Door

The test region on the repaired area of the bay door was situated as is shown in figure 4.6.1. Inserts have, as part of the repair, been included below the skins within the core. The testing region has been situated such that the waves travelling at angles between 30° and 180° will have to travel over these inserts.

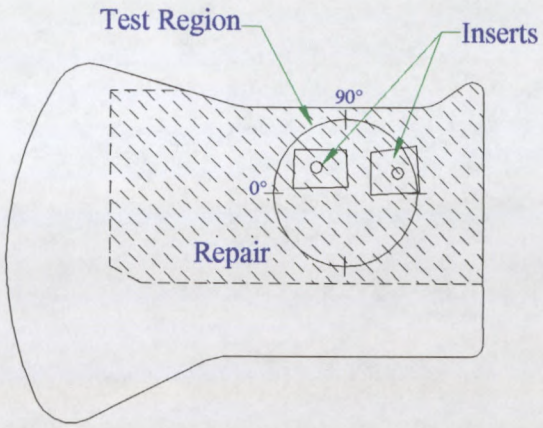

Figure 4.6.1. The Test Region on the Repaired Landing Bay Door.

4.6.1 Wave Speed

The wave speed versus fibre angle curve (figure 4.6.2) for the repaired region of the door is fairly symmetric. Well-defined peaks are present at 0°, 90°, 180° and 270° indicating that the fibres are aligned in these directions. The highest velocity recorded is 4072 m/s (at 90°) while the lowest is 3321 m/s (at 60°) which when expressed as a percentage represents a range of 18,4%. The velocities in the 90°/270° are only 2,6% higher than the velocities in the 0°/180° direction. This indicates that there is an equal amount of fibres in the 0°/180° and the 90°/270° directions.

The wave speed graph does not exhibit any significant differences between the region containing the inserts and the region that does not contain the inserts. Thus the wave speed is unaffected by the presence of the inserts below the skins. This may indicate that the wave being measured travels along the outer surface of the skin and is thereby unaffected by the inserts which are only in contact with the skin's inner surface.

4.6.2 Amplitude

20 to 30 kHz

The variation in the 20 to 30 kHz peak is shown in figure 4.6.2. It appears that the presence of the inserts below the repaired skin have affected the amplitude of the waves since the 20 to 30 kHz graph is not symmetric. Between 180° and 360° the graph is fairly flat, whereas between 0° and 180° the amplitude values occur over a larger range. The maximum amplitude recorded was 80,3 dB (at 90°), while the minimum recorded was 62,5 dB (at 120°), resulting in a percentage range of 22%.

90 to 100 kHz

The 90 to 100 kHz curve (figure 4.6.2) follows a similar pattern to the 20 to 30 kHz frequency curve. In other words the presence of the inserts has also affected the amplitudes in the higher frequency band. The maximum amplitude recorded was 69.23 dB (at 180°), while the minimum recorded was 53.67 dB (at 120°), resulting in a percentage range of 22%.

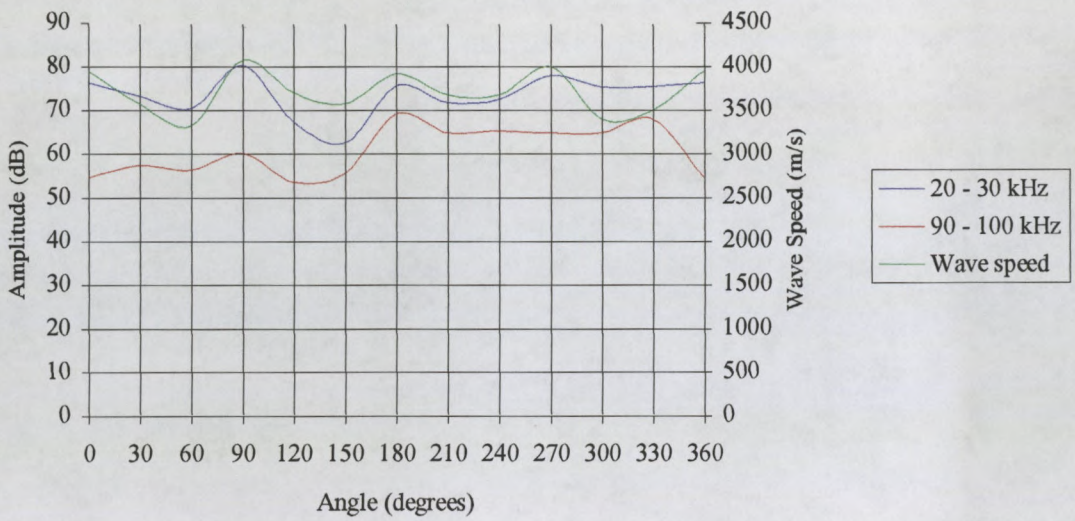

Figure 4.6.2. Acoustic Amplitude & Wave Speed to Repaired Region of Landing Bay Door.

4.7 Test Covering Both Repaired and Un-repaired Areas

The area tested, as shown in figure 4.7.1, covered part of the repaired as well as part of the un-repaired region. The test circle was situated such that the waves travelling at

between 30° and 150° would travel through the repair while those travelling at between 180° and 270° would be in unrepaired material.

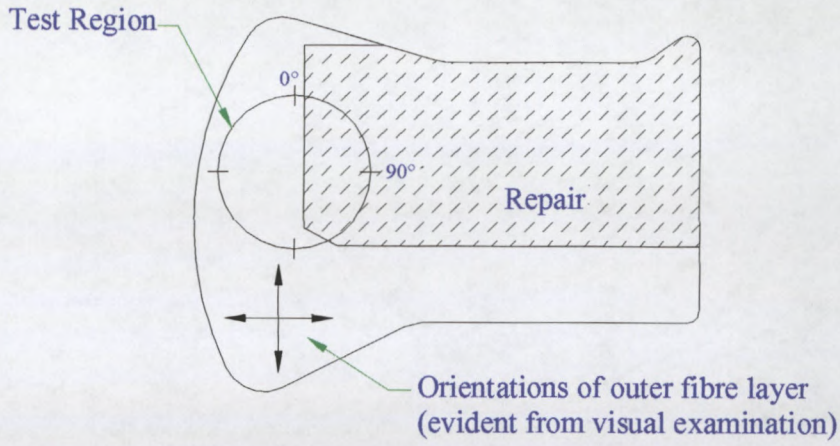

Figure 4.7.1. Region Tested on Repaired Landing Bay Door.

4.7.1 Skin Stiffness Test

The approximate stiffness of the repaired and the unrepaired skins of the bay doors have been determined. A load was applied to the surface of the repair until the skin had deflected 1 mm. This was repeated for the unrepaired door and in each case the resisting force at 1 mm deflection was noted.

This testing method is not a standard method and thus cannot be used to determine the exact flexural stiffness of the skins. However this method is suitable for comparison purposes.

The resisting force of the repair was 570 N and that on the unrepaired skin was 258 N. The resisting force of the repaired skin is greater, thereby indicating that it has a higher flexural stiffness than the unrepaired skin.

4.7.2 Wave speed

For the test that covers both the repaired and unrepaired regions of the bay door, the variation in wave speed is shown in figure 4.7.2. The wave speed curve is flatter in the repaired region (between 30° and 150°) than in the un-repaired region (between 180° and 360°) where there are large peaks present at 180°, 270° as well as at 360°. These peaks are to be expected since the fibres appear to be aligned in these directions. The

average velocity in the repaired region is 14,4 % higher than the average velocity in the un-repaired region. It is the increased stiffness of the repaired region has caused the higher wave speeds in the repaired region.

4.7.3 Amplitude

20 to 30 kHz

The 20 to 30 kHz amplitude curve (figure 4.7.2) for the repaired region (between 30° and 150°), apart from a peak between 120° and 150°, is fairly flat. For the un-repaired region (between 180° and 360°), there seems to be no relationship between amplitude and fibre angle. It was expected that amplitude peaks would feature at 180°, 270° and at 360° since the fibres appear to be aligned in these directions. However peaks are not present at these angles.

90 to 100 kHz

The variation in the amplitude of the peak at between 90 and 100 kHz is shown in figure 4.7.2. For the repaired region (between 30° and 150°), a large peak is present at 120° while the amplitude at 60° is especially low. For the un-repaired region (between 180° and 360°), as was the case for the low frequency band, there seems to be no relationship between amplitude and fibre angle. The amplitude recorded at 180° is especially low while there are peaks present at 300° and at 360°.

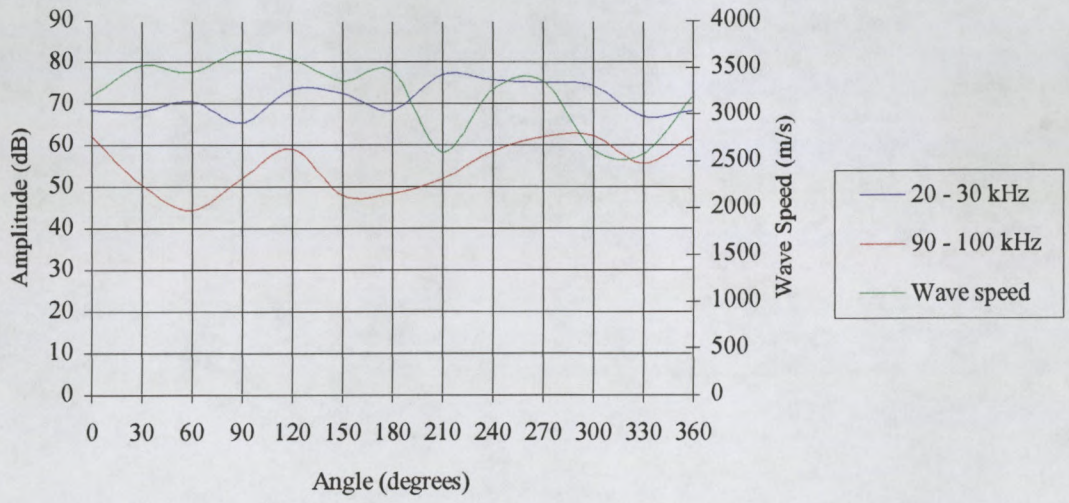

Figure 4.7.2. Acoustic Amplitude & Wave Speed to Repaired Region of Landing Bay Door.

4.8 Conclusions

The delaminations in the unrepaired door have reduced the flexural wave's attenuation and resulted in an additional mode ie. the extensional wave. The extensional mode travels at a higher velocity, thus the speed measured on the delaminated region was higher than that in the correctly bonded region. The reduced attenuation of the flexural mode and the stronger presence of the extensional mode are evident in the high amplitudes at 210° and 240° on figure 4.3.2. These angles coincide with areas with a large number of delaminations on the wave path. Thus in a component of sandwich construction, delaminations between core and skin may be identified by the combination of reduced attenuation, the presence of both the flexural and extensional wave modes and a higher wave speed.

Conventionally, in AU testing, defects and weaker material properties are associated with an increase in the rate of attenuation. However in the case of the bay door, the delaminations between the core and skin have caused a reduction in the rate of attenuation.

The wave speeds in the unrepaired region indicate fibre orientations that correlate with the directions that were determined from the visual examination.

The wave speed has been shown to be an indicator of the differing flexural stiffness between the repaired and unrepaired skins. Furthermore the wave speeds plotted for the repaired region of the door show the likely orientation of the fibres within the repair. This experiment has also shown that inserts within a sandwich structure affect the amplitude of the waveforms and not their speed.

Chapter 5

AU Test of a Damaged Wake-Board

5.1 Introduction

AU tests have been carried out on a damaged composite wake-board. As was the case with the landing bay doors, the purpose of the test was to apply to AU technique in a realistic situation and determine whether the damage can be detected.

5.2 Damage Description

The board is of sandwich constriction with a 'Divinicell' PVC foam core with skins made of hemp fibre and an epoxy resin. Exact details of the skin thickness and ply orientations are not available. A visual examination of the board indicated that the outer fibre layer is a bi-axial layer with the fibres at +45° and -45°, relative to the board's longitudinal axis.

While in use the board was bent excessively, causing a delamination between thecore and skin on the compression side of the bend. A crack was formed which extends across the width of the board, through the centre of the delamination. After the AU tests were conducted, for repair purposes, the skin in the region of the damage was removed and this allowed the delamination to be mapped. The extent of the delamination and the location of the crack in the skin are shown in figure 5.3.1. No damage to the 'Divinicell' core was evident.

5.3 Test Method

Preliminary tests indicated that in the board, the AU signal is very rapidly attenuated. Thus, so as to receive the strongest possible signal, the transducers were arranged such that the wave path from the source transducer to receiver was at 45° to the board's axis ie parallel to the fibre direction. For each recording position the distance between the

transducers was set to 80mm. As shown in figure 5.3.1, 6 waveforms were recorded in an undamaged region of the board and 6 waveforms were recorded across the damaged region.

From the recorded waveforms the energy content and central frequency of each signal was determined. The wave speed for each testing position was calculated from the arrival times. These 3 parameters have been plotted as a function of the position in which the waveform was recorded. At position 5 in the undamaged area and at positions 1 and 6 in the damaged region the attenuation of the signal was so great that it was not possible to record a signal. Hence the omission of bars in figures 5.4.1, 5.6.1 and 5.5.1 that correspond to these testing locations.

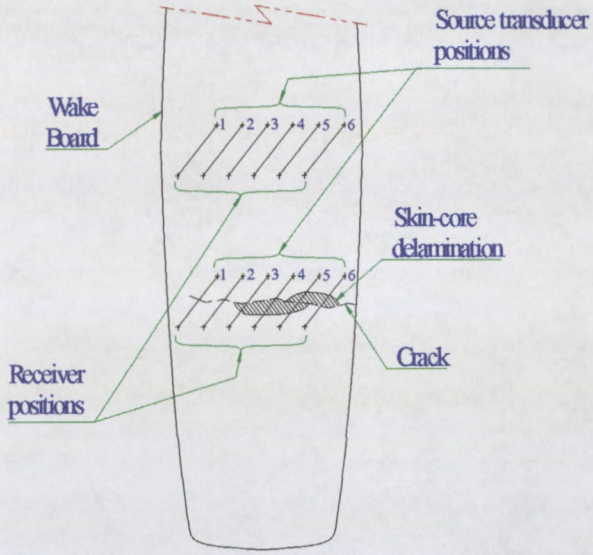

Figure 5.3.1. Wake-board damage and AU test configuration.

5.4 Energy Content

Figure 5.4.1 shows that the energy of the waves in the damaged region is significantly higher (33.1% on average) than in the undamaged region. Furthermore the range of energy contents in the damaged region is greater (45,4 % as apposed to 24,1 % in the undamaged region). The energy content recorded at position 2 of the damaged region almost equal to the average energy content recorded in the undamaged region. This may indicate that there is no severe damage present at position 2.

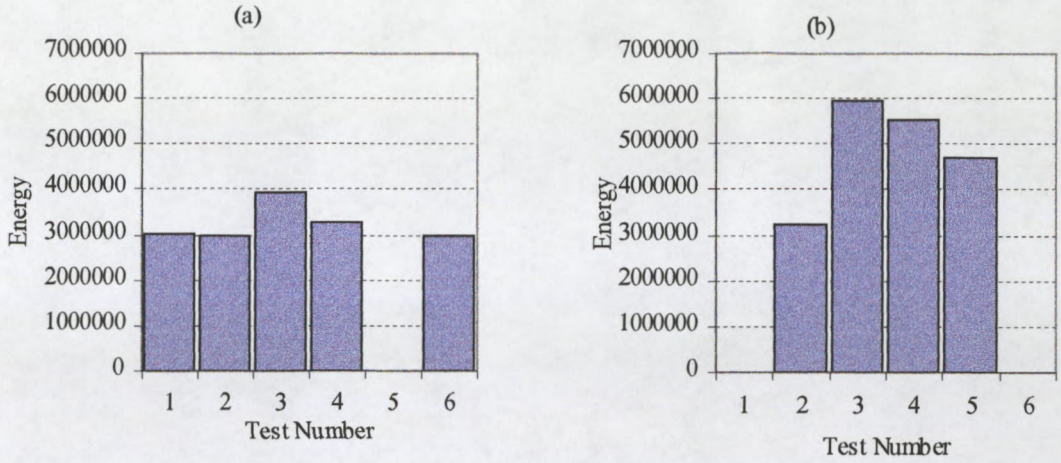

Figure 5.4.1. Variation of energy in (a) undamaged region of wake-board (b) damaged region of wake-board.

5.5 Central Frequency

Figure 5.5.1 shows that there is not much difference in central frequency when comparing waves recorded in damaged and undamaged material. The average central frequency recorded in the undamaged region is 365 kHz while that in the damaged region is 348 kHz. This difference when expressed as a percentage is 4.7%. Since this difference is small, it appears that the damage has not had a significant effect on the central frequency.

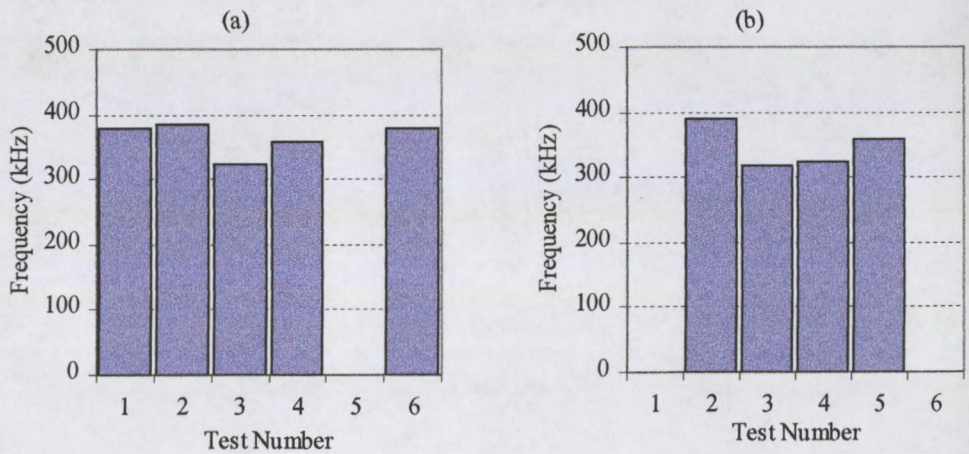

Figure 5.5.1. Central frequency in (a) undamaged region on wake-board (b) damaged region of wake-board.

5.6 Wave Speed

There is a striking difference between the wave speeds recorded in the damaged region when compared with the wave speeds recorded in the undamaged region (figure 5.6.1). The average of the wave speeds recorded in the damaged region is 69.1% greater than the average of the wave speeds recorded in the undamaged region. The wave speed recorded in position 2 of the damaged region is the lowest of the 5 wave speeds recorded in the damaged region. This reinforces the previously mentioned notion that the damage in position 2 is the least severe of the 4 test positions within the damaged region.

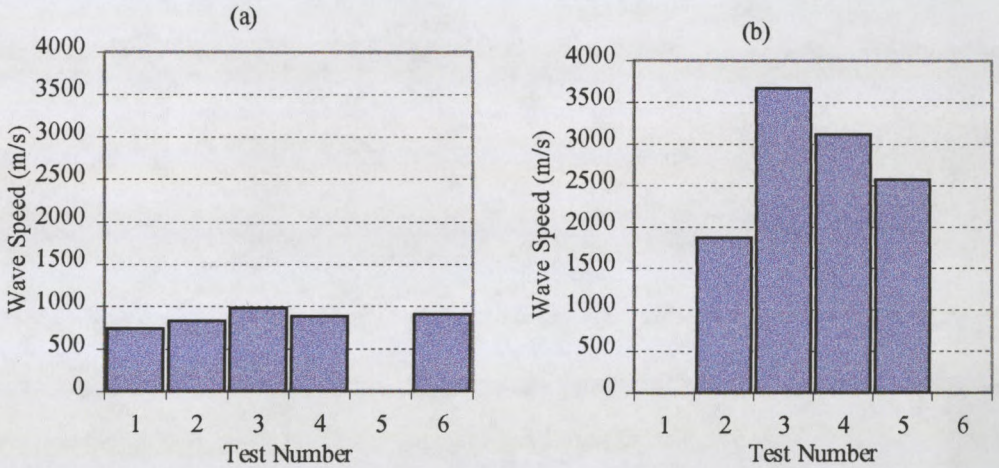

Figure 5.6.1. Wave speed in (a) undamaged region on wake-board (b) damaged region of a wake-board.

5.7 Waveform Comparison

Figure 5.7.1 shows a waveform recorded at position 3 of the damaged region and a waveform from position 3 in the undamaged region. The main difference between the two waveforms is that the waveform recorded in the damaged region has a number of high frequency oscillations at its leading edge. This high frequency component is an extensional wave and is the cause of the higher wave speed in the damaged region.

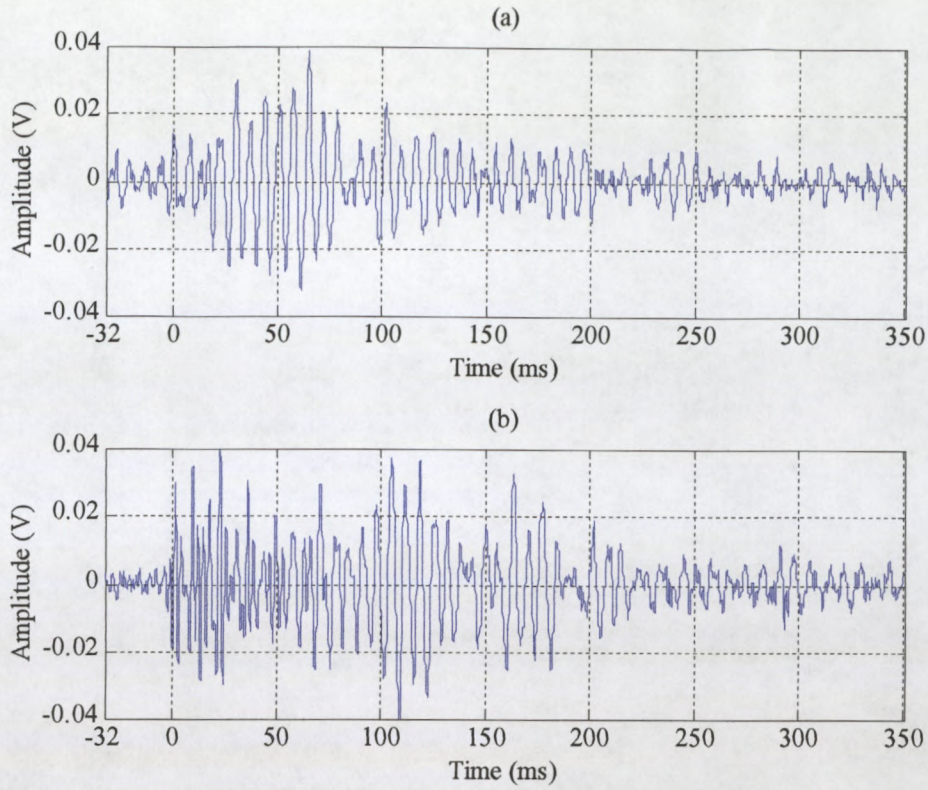

Figure 5.7.1. Waveforms recorded in test position 3 of (a) the undamaged material and (b) the damaged material.

5.8 Spectrum Comparison

So as to compare the frequency components that are transmitted in the damaged and undamaged material, Fourier transforms have been plotted. Figure 5.8.1 shows the Fourier transforms of the waves in position 3 ofthe damaged and undamaged regions.

When the 2 Fourier transforms are compared, it is clear that all of the frequency components at less than 300 kHz are present in both the damaged and the undamaged regions. However the components in the 200 to 300 kHz band are stronger in the damaged region. Furthermore, in the damaged region, there is an additional component at 370 kHz that is not present in the undamaged material.

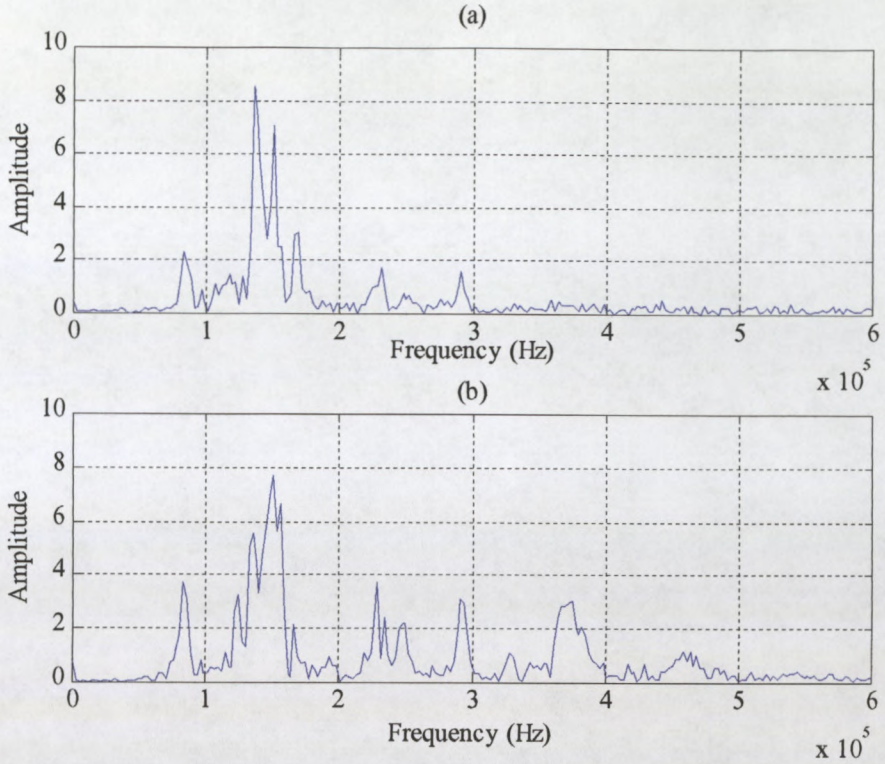

Figure 5.8.1. Fourier transforms of waves recorded in test position 3 of (a) the undamaged material and (b) the damaged material.

5.9 Conclusions

The damage in the wake board and the defect found in the landing bay door both feature a delamination between the skin and core. Thus the AU results have been affected in a similar manner.

A crack will normally cause in increase in the attenuation, however in this case the effect of the crack has been obscured by the reduction of attenuation associated with a skin to core delamination. Hence the energy of the waves recorded in the delaminated area is higher.

The skin to core delamination has also caused an increase in the speed of the AU waves. The reason for the increase in speed is due to an additional wave mode, an extensional wave, in the delamination. This mode is evident in the Fourier transform as a peak at 370 kHz which is not present in the undamaged region.

Of the 6 testing positions, position 2 differs least when the damaged region is compared to the undamaged region. This correlates with the mapping of the delamination that shows that in position 2 the wave does not pass through the delamination.

Chapter 6

Delamination Detection

6.1 Introduction

Delaminations are common defects in composites and can be introduced in the manufacture process or caused by applied loads or impacts. An attempt has therefore been made to use the AU technique to detect delaminations. To this end a laminate containing Teflon film patches, embedded between some of its plies, has been manufactured. The purpose of the Teflon is to simulate delaminations by preventing the adjacent fibre layers from bonding to one another. The use of embedded Teflon film is an accepted method for simulating delaminations for the purpose of evaluating testing methods and numerous researchers have used this technique [18, 53, 55, 68].

6.2 Specimen Details

A flat unidirectional glass fibre laminate was constructed from 3 layers of 440 g/m^2 glass fibre and the LR20 / SLC30 resin system. 5 Teflon film patches, with diameters ranging between 10 mm and 120 mm were included in the construction of this laminate. All of these patches were located between this laminates first and second layers such that the first layer is defined as the layer upon which the AU tests will be conducted. Thus only one layer of glass fibre separates the test surface from the Teflon.

6.3 Test Method

Four experiments have been run on the above laminate where each experiment has involved a differing transducer arrangement.

6.4 Experiment 1

6.4.1 Test Method

The source and receiving transducers were placed on the same side of the laminate, on either side of a patch of Teflon film. With this arrangement, waveforms were recorded across each of the 6 patches in turn. A 7th waveform was also recorded in which no Teflon was present between the transducers. Through the duration of the experiment the distance between the transducers was kept constant at 120 mm and all recordings were made such that the waves travelled parallel to the fibre direction.

5 parameters: energy content, central frequency, ringdown counts, peak voltage and wave speed have been calculated from the recorded waves. The reported results are an average of 3 waveforms.

6.4.2 Peak Voltage, Ringdown Counts and Energy Content

The graphs showing the variation in peak voltage, ringdown counts and energy content all show a similar trend (figure 6.4.2 (a), (b) and (c)). This trend suggests that at larger Teflon patch sizes these 3 parameters will have lower values. The exceptions to this trend are for the 40 mm and the 120 mm patches, both of which have a higher than expected peak amplitude, number of ringdown counts and energy content. It would be expected that, for them to conform to the general trend, these 3 parameters in the 40 mm patch would be approximately half way between their values recorded in the 20 mm and 80 mm patches. However the values of peak voltage, ringdown counts and energy content in the 40 mm patch are higher by 4,8 %, 29,3 % and 20,5 % respectively than their expected values.

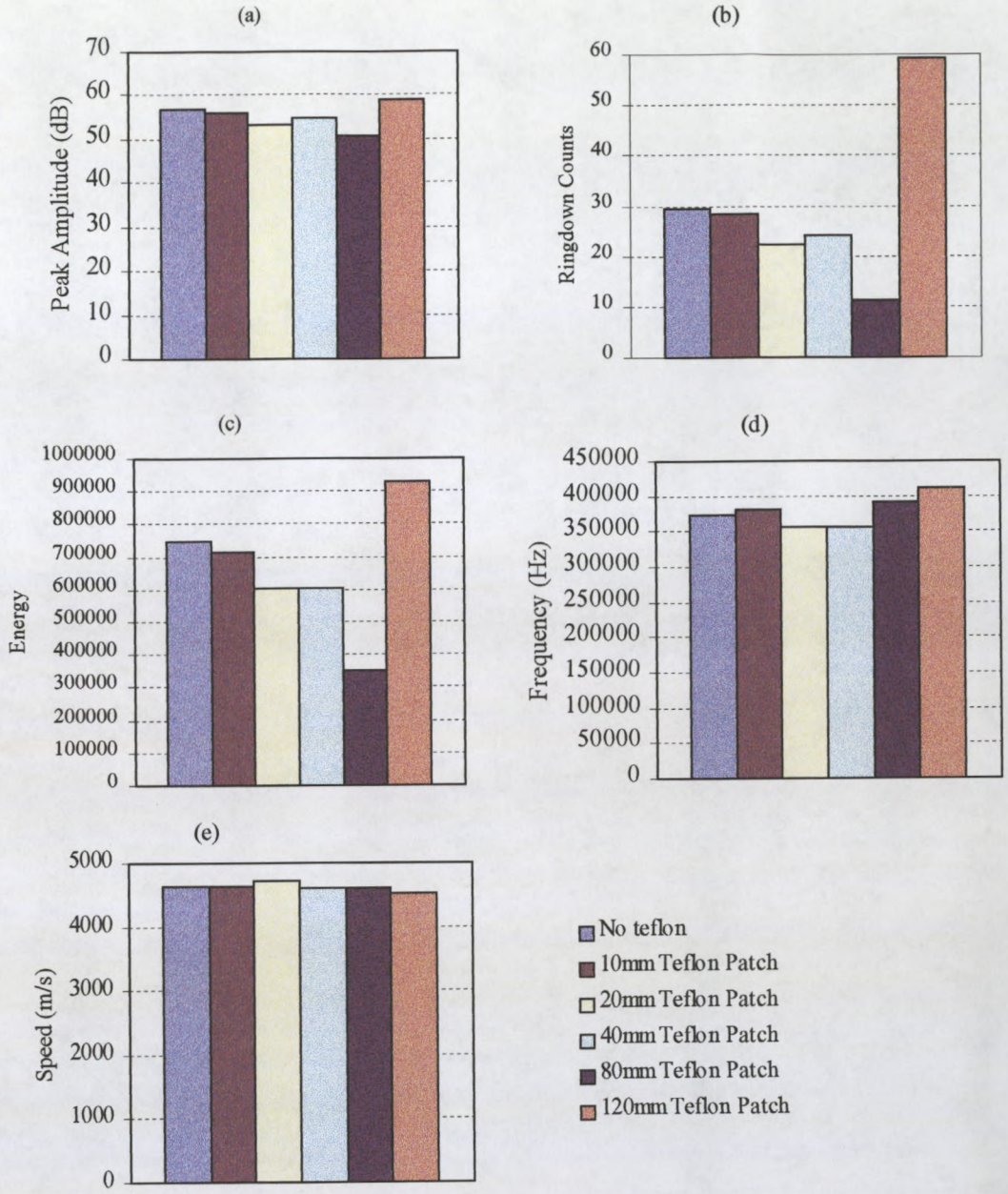

Figure 6.4.2. Variation of parameters (a) peak amplitude, (b) ringdown counts, (c) energy, (d) central frequency and (e) wave speed.

The peak amplitude, ringdown counts and energy content in the 120 mm patch deviate considerably from the general trend. For them to conform to the trend, these 3 parameters should have their lowest value at the 120 mm patch. However in the 120 mm patch they have their highest values.

It was initially thought that the above deviations from the trends were due to inconsistencies in the test method. The entire experiment was consequently repeated and

this has revealed the same deviations, thereby leading theresearcher to conclude that the deviations are not as a result of test method inconsistencies.

Thereafter the possibility was considered that the exceptionally high values at the 120 mm patch were due to the fact that the transducers were spaced at 120 mm and were thus seated on the Teflon's circumference. The experiment was therefore repeated with a 140 mm transducer spacing to confirm or disprove this. The results of this repetition have, in the same way as the original test, indicated highest values atthe 120 mm patch. Thus it is the size of the patch that has caused the higher values and not the fact that the transducers were sitting on the edge of the Teflon.

6.4.3 Central Frequency

There does not appear to be a relation between the central frequency of the waveform and the size of the Teflon patch present in the wave's path (figure 6.4.2 (d)). The highest central frequency of 413 kHz was recorded in the 120 mm patch and the lowest of 356 kHz was recorded in the 20mm Teflon patch. This range, expressed as a percentage is equal to 13.9 %.

6.4.4 Wave Speed

Figure 6.4.2 (e) shows the variation of wave speed for across the Teflon patches. The wave speeds for different patch diameters are all similar and have a range of only 4,1 %. This indicates that the Teflon has not influenced the wave's speed.

6.4.5 Spectrum Comparison

To determine what frequency components have caused the deviations from the trends in the peak voltage, ringdown counts and energy content plots, a Fourier transform has been plotted from each waveform. The Fourier transforms of the waveforms recorded in the Teflon patches have been compared to the Fourier transform recorded in the material that does not contain any Teflon.

It is evident by comparing the Fourier transforms (figure 6.4.5) that all the frequency components that are present in the waveform recorded in the material that does not contain a Teflon patch are also present in the waveforms that were recorded at the 10 mm, 20 mm, and 40 mm patches.

At the 20 mm patch the frequency components between 200 kHz and 500 kHz have been attenuated to a large degree while there has been very little attenuation of the lower frequency components. Thus the central frequency of the wave at the 20 mm patch is fairly low (shown in figure 6.4.2 (d)). The presence of a strong low frequency component has kept this wave's energy content at a level that is comparable to the other energy contents.

All frequency components at the 40 mm patch have attenuated equally and to a small degree when compared to the Fourier transform of the wave in the material that contains no Teflon. It is the slight attenuation at the 40 mm patch that has caused ringdown counts, peak amplitude and energy content to be higher than expected and thus deviate from the general trend.

The frequency components in the 200 kHz to 500 kHz range of the wave at the 120 mm patch are far stronger than in the same frequency range in the material that contains no Teflon. It is the presence of these strong frequencies that have caused the waveforms at the 120mm patch to have the highest peak amplitude, ringdown counts, central frequency and energy content. In addition, the 120 mm patch has attenuated the frequencies in the 100 kHz to 200 kHz range more than the region of material that contains no Teflon.

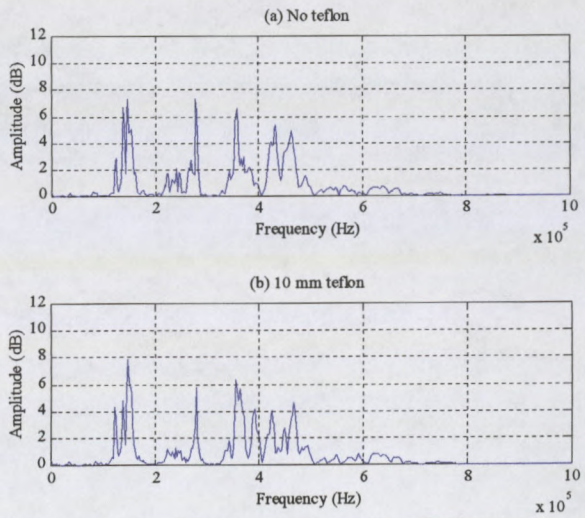

Figure 6.4.5. Fourier transforms of waves recorded across Teflon patches of diameter: (a) no Teflon, (b) 10 mm.

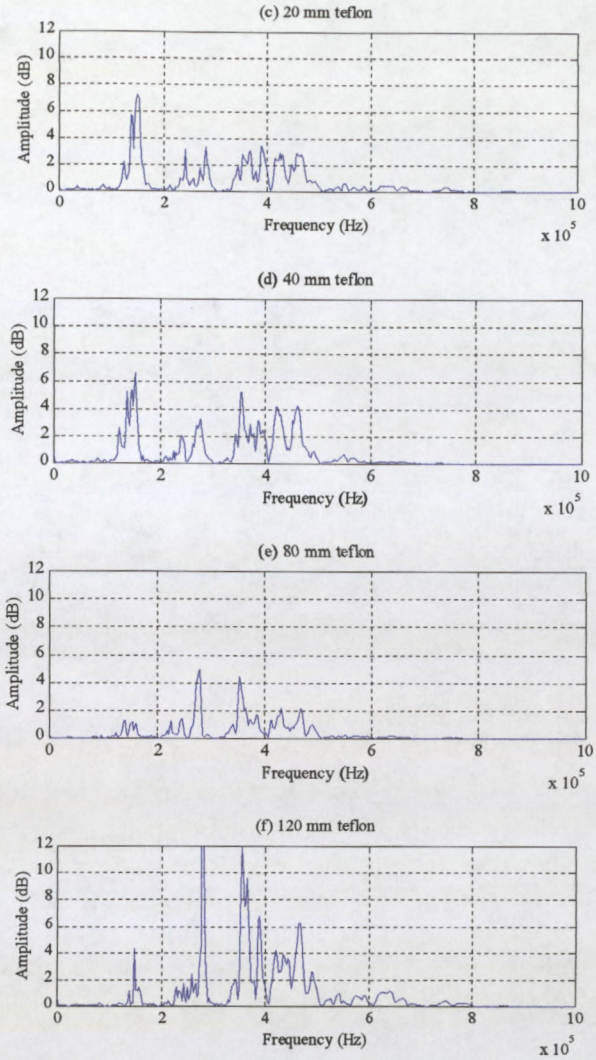

Figure 6.4.5 cont. Fourier transforms of waves recorded across Teflon patches of diameter: (c) 20 mm, (d) 40 mm, (e) 80 mm and (f) 120 mm.

6.5 Experiment 2

Experiment 2 was conducted to investigate differences in the waveforms recorded both on and off the Teflon patches.

6.5.1 Test Method

One wave was recorded on and one wave was recorded next to each Teflon patch as is indicated by figure 6.5.1. The first wave was recorded with the transducer spacing equal to the patch diameter such that the wave passed through the Teflon. The second, with the same transducer spacing, was recorded such that the wave passed through material that does not contain Teflon. This procedure, of recording a wave across the Teflon

containing material and then a second next to the Teflon, was repeated for each of the 5 patches. The peak voltage, ringdown counts, energy content, wave speed and central frequency have been determined for each of the recorded waves.

To simplify the discussion of the results, the waveforms that were recorded such that the acoustic wave passed through material that contained a Teflon patch will be referred to as 'data set A'. Likewise, the waveforms that were recorded in material that does not contain Teflon will be termed 'data set B'.

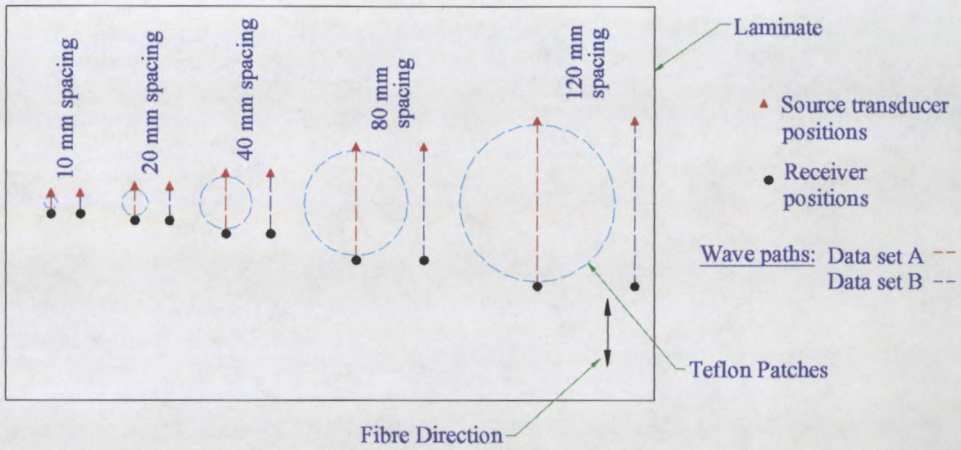

Figure 6.5.1. Transducer locations for experiment 2.

6.5.2 General Observations

The shapes of the curves depicting the variation in peak amplitude, ringdown counts and energy content (figure 6.5.2 (a), (b) and (c)) as functions of sensor spacing have several points in common. For data set A (recorded across Teflon patches), the value of peak amplitude, ringdown counts and energy content all decrease as the sensor spacing is increased from 10 mm to 80 mm. At the 120 mm patch however, the values for peak amplitude, ringdown counts and energy content are all greater than the values at 80 mm.

For data set B (recorded in non-Teflon containing material), the value of peak amplitude, ringdown counts and energy content all decrease as the sensor spacing is increased. The exception to this trend is between the 20 mm and 40 mm spacing where the peak amplitude, ringdown counts and energy content all have a higher value at 40 mm than at 20 mm.

At 10 mm, 40 mm and 80 mm sensor spacings, the percentage differences between data sets A and B, in ringdown counts and energy content are large i.e. in the order of 30 %. While at 20 mm and 120 mm the percentage differences in ringdown counts and energy content are much smaller i.e. in the order of 5 %.

6.5.3 Peak Amplitude

The general trend in the peak amplitude curves (figure 6.5.2 (a)) indicates that for larger sensor spacings, the peak amplitude will be lower. At the 10 mm and 20 mm sensor spacings, the peak amplitudes in data set A are 4,1 % and 2,4 % greater than the peak amplitudes determined from data set B. At the 40 mm and 80 mm spacings there is a reversal of this trend and the peak amplitudes in the data set B are 6,7 % and 6,8 % greater than the peak amplitudes determined for data set A. At 120mm spacing the peak amplitude from data set A is equal to that of data set B. The range of the peak amplitudes in data set B is less than the range in data set A. Expressed as a percentage these ranges are 18,4 % for data set A and 10,2 % for data set B.

6.5.4 Ringdown Counts

The differences in the number of ringdown counts between data sets A and B are shown in figure 6.5.2 (b). At the 10 mm, 20 mm and 120 mm sensor spacings, the ringdown counts in data set A are 14,1 %, 1,7 % and 3,7 % greater respectively than the ringdown counts determined for data set B. At the 40 mm and 80 mm spacings there is a reversal of this order and the ringdown counts in data set B are 29,3 % and 46,4 % greater than the ringdown counts determined for data set A. The range of the ringdown counts in data set B is less than that for data set A. Expressed as a percentage these ranges are 38 % and 55,3 %.

6.5.5 Energy Content

The differences in energy content between data sets A and B are shown in figure 6.5.2 (c). At the 10 mm, 20 mm and 120 mm sensor spacings, the energy content of the waves of data set A are 27,7 %, 9,8 % and 3 % greater respectively than the energy contents determined for data set B. At the 40 mm and 80 mm spacings there is again a reversal of this order and the energy contents in data set B are 37,5 % and 39,7 % greater than the peak voltages determined from data set A. The range of energy content in data set B is

less than that for data set A. Expressed as a percentage these ranges are 55,3 % and 77,4 %.

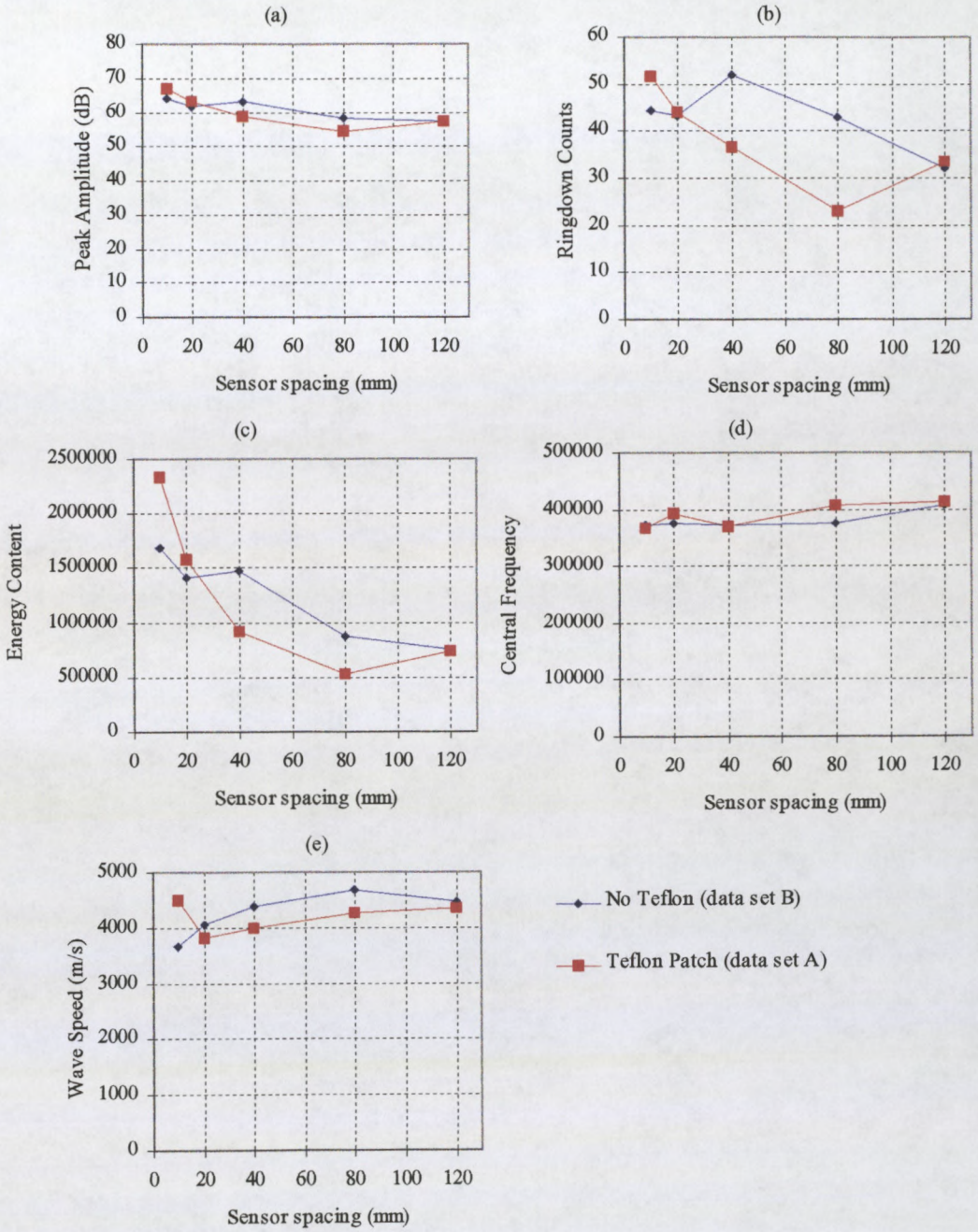

Figure 6.5.2. Variation of parameters (a) peak amplitude, (b) ringdown counts, (c) energy content, (d) central frequency and (e) wave speed.

6.5.6 Central Frequency

The central frequencies (figure 6.5.2 (d)) of all of the waveforms recorded in this experiment are between 366 kHz and 413 kHz. The general trend for both data sets is that at larger sensor spacings the central frequency becomes higher. The only exception to this trend is in data set A at the 40 mm patch where the central frequency is lower than that determined for the 20 mm patch. At the 20 mm, 80 mm and 120 mm sensor spacings, the central frequencies in the data set A are 3,8 %, 8,1 % and 1,4 % greater respectively than the central frequencies determined for data set B. At the 10 mm and the 40 mm sensor spacings, the central frequency of data set B is higher by 1,7 % and 0,6 % than those of the waves recorded in data set A. The range over which the central frequencies of data set A exist is 11,4 % while the range of the central frequencies of data set B is 8,6 %.

6.5.7 Wave Speed

The wave speeds (figure 6.5.2 (e)) of data set B are generally higher than those of data set A. The only exception to this is at the 10 mm spacing where wave speed in data set A is 18,4 % higher than that determined from data set B. It is likely that the wave speeds determined at the closer sensor spacings will be inaccurate because the wave travel time is not much greater than the sampling interval. Thus the difference in wave speed at the 10 mm spacing has been omitted from the following discussion. On average, the wave speed in data set A is 6,6 % higher than the wave speeds of data set B. Both wave speed, as a function of sensor spacing, curves indicate that at larger sensor spacings the wave speed is higher. The exception to this is at the 120 mm patch where the wave speed in this patch is 4,6 % less than the wave speed in the 80 mm patch. The apparent increase in wave speed as the test was moved to the larger Teflon patches may be as a result of measurement inaccuracies present at the closer sensor spacings.

6.6 Experiment 3

The aim of experiment 3 was to investigate the effect that placing either one or both of the transducers on the Teflon patch has on the recorded signals.

6.6.1 Test Method

Four waveforms were recorded, each with the sensor spacing at 80 mm and such that the wave travelled parallel to the fibre direction. Wave 1 was recorded with both the transducers situated on the 120 mm Teflon patch. Wave 2 was recorded with both transducers on a region of material that does not contain Teflon and far enough away from the patches for them to not interfere with the wave. Wave 3 was recorded with the pulser on the Teflon and the receiving transducer on the material that does not contain a patch. The positions of the transducers were exchanged for the recording of wave 4 so that the receiving transducer was on the Teflon patch and the pulser was on the region of material that does not contain Teflon. For recordings 3 and 4 the transducers were arranged such that the wave travelled for 40 mm in the Teflon containing material and for 40 mm in material that does not contain Teflon. So as to compare the frequency components transmitted in each of the 4 transducer arrangements, the waveforms and their Fourier transforms have been plotted.

6.6.2 Waveform Comparison

Figure 6.6.2 shows the waveforms of the 4 waves recorded in this test. The most evident difference between the 4 waveforms is that there is a large difference in signal strength. Wave 1 has the lowest peak amplitude (0.127 V) while wave 2 has the highest (1.1621 V). Note that the y-axis of wave 2 has been extended to 1 V whereas the maximum value on the y-axes of the other graphs is only 0.4 V.

Waves 2 and 4 can be divided into 2 clearly defined parts. The oscillations in first part of each wave have high amplitudes and a high frequency while the second part has a lower amplitude and lower frequency. The first part is the extensional wave mode and the second is the flexural mode. The peak amplitude of the extensional mode of wave 4 is significantly higher than the peak amplitude of the flexural wave mode. The amplitude of wave 2's extensional mode is only slightly higher its flexural mode.

Waves 1 and 3 do not feature well-defined wave modes and it is thought that this may be as a result of the pulser being on the material that contains Teflon.

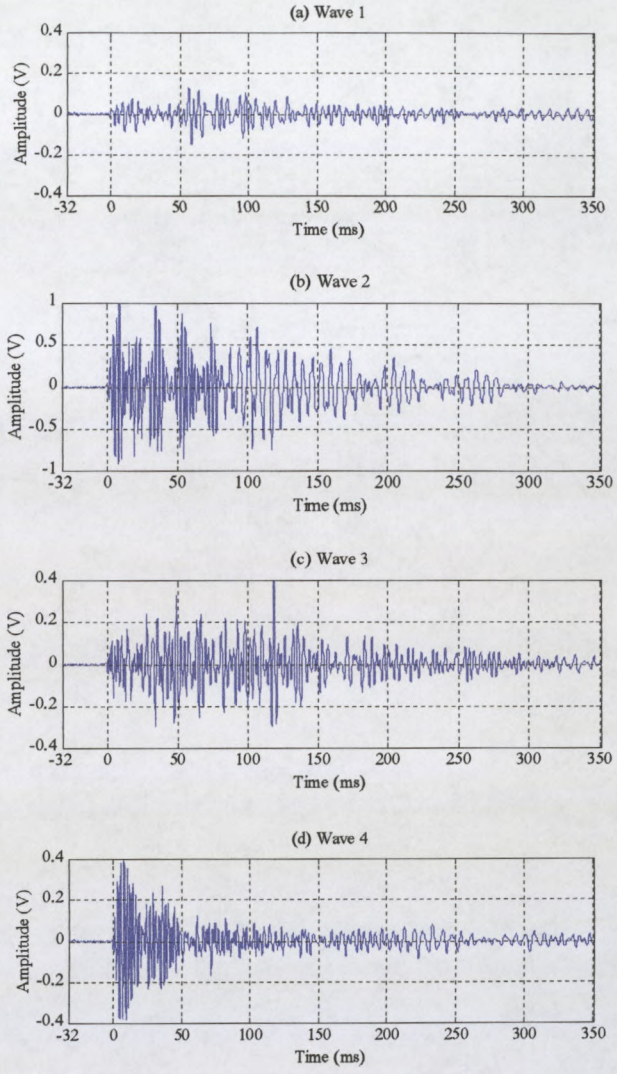

Figure 6.6.2. Waveforms recorded in various locations relative to a Teflon insert: (a) both transducers on Teflon, (b) both transducers off Teflon, (c) source transducer on Teflon and (d) receiver on Teflon.

6.6.3 Spectrum Comparison

The Fourier transform of each of the 4 waves is shown in figure 6.6.3. Wave 2 consists predominately of a frequency component at about 150 kHz and several components at between 300 kHz and 500 kHz.

The Fourier transform of wave 1 shows that the component at 150 kHz is still present in the signal, and the components at between 300 kHz and 500 kHz have been almost entirely eliminated. For this transducer arrangement a large proportion of the signal is between 200 kHz and 300 kHz.

For wave 3, the 150 kHz component and the components above 400 kHz were found to be weak while the majority of the signal consists of components at between 200 kHz and 400 kHz.

The frequency spectrum of wave 4 shows that the 150 kHz component and the 200 kHz to 400 kHz components are present at a low strength. This signal consists predominately of frequencies at between 400 kHz and 500 kHz.

The frequency spectra of waves 2 and 4 contain strong high and strong low frequency components while their mid frequency components have a moderate strength. It is because of this separation on the frequency axis of the 2 major components that the 2 wave modes are visible in the waveforms. The high frequency components are the extensional wave and the lower components are the flexural wave.

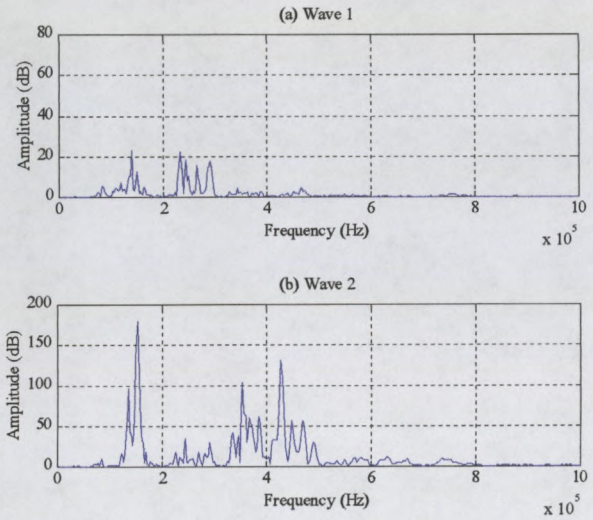

Figure 6.6.3. Fourier transform of waveforms recorded in various locations relative to a Teflon insert: (a) both transducers on Teflon, (b) both transducers off Teflon.

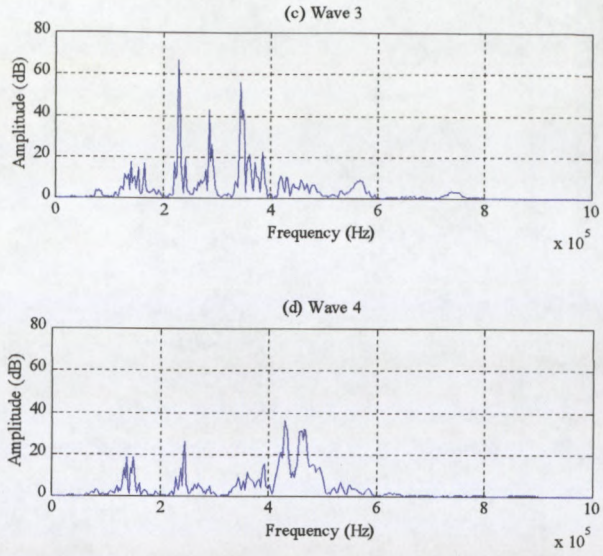

Figure 6.6.3. cont. Fourier transform of waveforms recorded in various locations relative to a Teflon insert: (c) source transducer on Teflon and (d) receiver on Teflon.

6.7 Experiment 4

Experiment 4 was run so as to investigate the effects of the wave travelling through differing lengths of Teflon.

6.7.1 Test Method

9 waveforms were recorded in this experiment, each with the source transducer on a region of material that does not contain Teflon and the receiving transducer positioned on Teflon containing material. The distance between the transducers was kept constant at 80 mm and all waves were recorded parallel to the fibre direction. After the recording of each wave the transducers were both moved 10 mm in the same direction so as to increase the amount of Teflon containing material through which the wave had to travel. Thus the first wave was recorded with no Teflon in its path, the second with 10 mm of Teflon in its path and the so on until the 9^{th} wave's entire 80 mm travel distance was through Teflon containing material. Figure 6.7.1 shows the location of the transducers for the recording of waves 1, 4 and 9. The remainder of the transducer positions have been omitted from this figure for the sake of simplicity.

Each of the recorded waveforms and their Fourier transform have been plotted and compared. The waveform's peak voltage, ringdown counts, energy content, central frequency and speeds have also been determined.

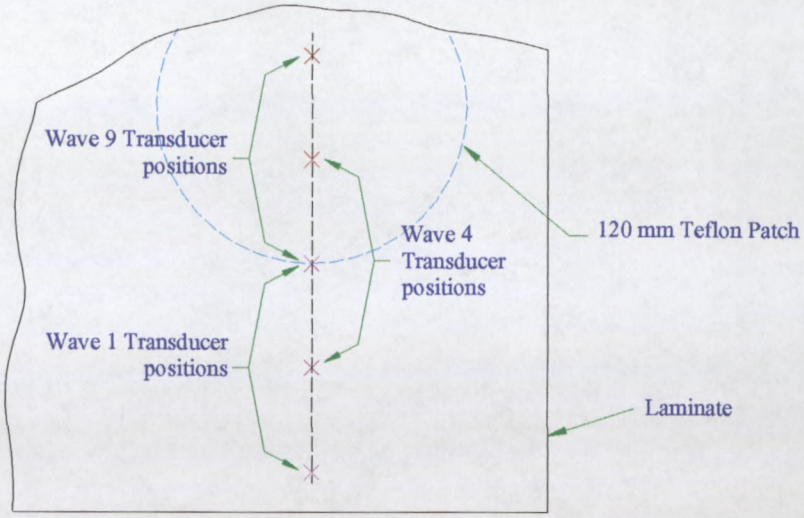

Figure 6.7.1 Transducer locations for experiment 4.

6.7.2 Waveform Comparison

Figure 6.7.2 shows the waveforms that were recorded as part of experiment 4. Both the flexural and the extensional wave modes are visible in these waveforms. In waves recorded with lesser lengths of Teflon in their path (up to 30 mm) these 2 modes have approximately the same amplitude. However for lengths of Teflon of between 40 mm and 80 mm the extensional component has a greater amplitude than the flexural component.

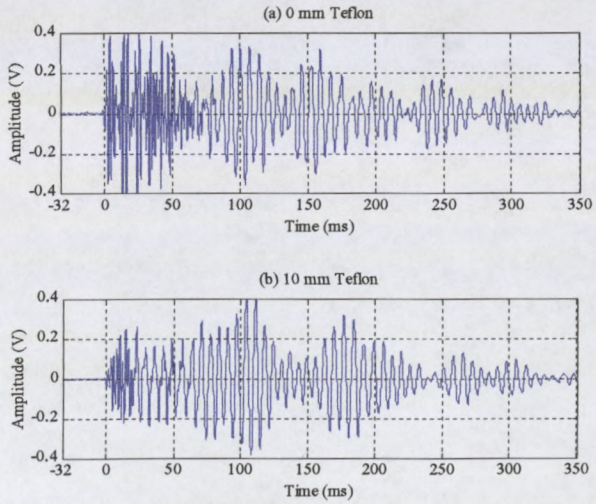

Figure 6.7.2. Waveforms recorded across differing lengths of Teflon: (a) 0 mm, (b) 10 mm.

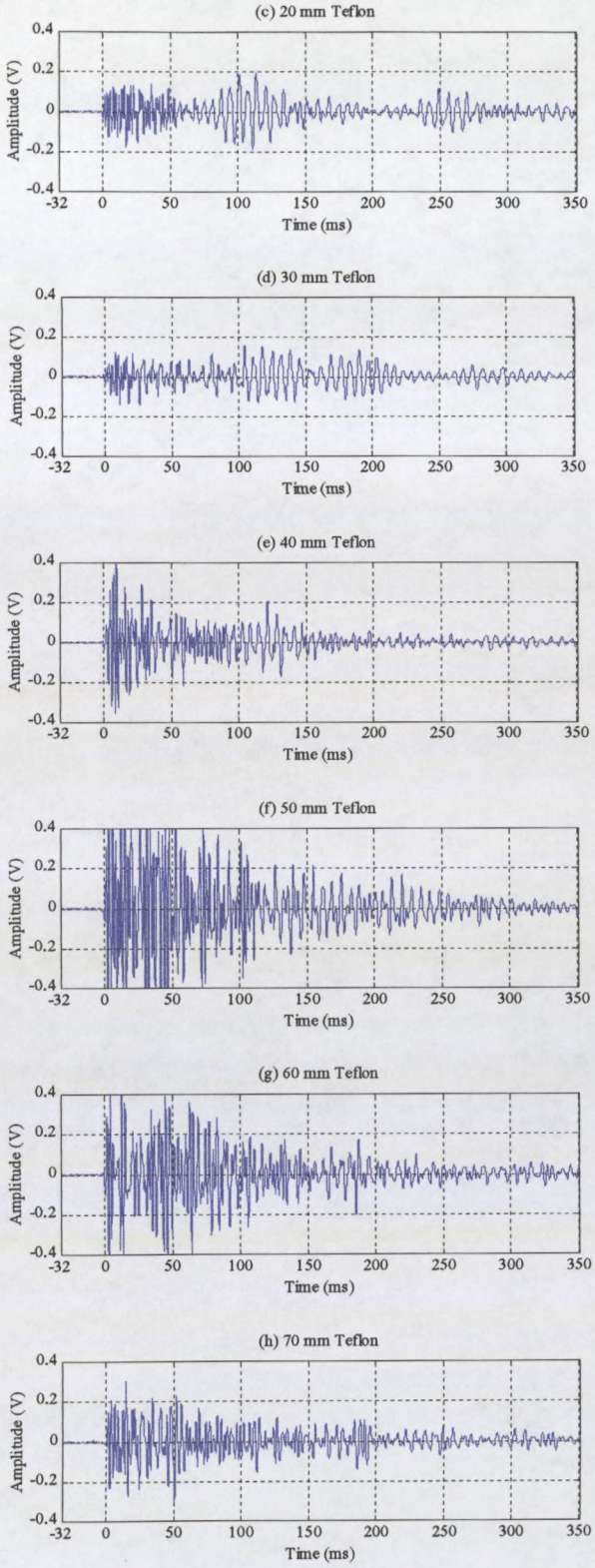

Figure 6.7.2 cont. Waveforms recorded across differing lengths of Teflon: (c) 20 mm, (d) 30 mm, (e) 40 mm, (f) 50 mm, (g) 60 mm, (h) 70 mm.

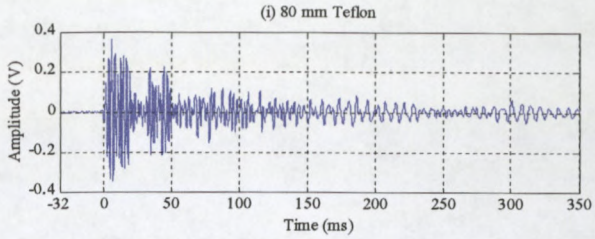

Figure 6.7.2. cont. Waveforms recorded across differing lengths of Teflon: (i) 80 mm.

6.7.3 Spectrum Comparison

The Fourier transforms of the waves recorded in experiment 4 have been plotted and are shown in figure 6.7.3. The waves recorded with between 0 mm and 30 mm of Teflon on the wave's path all have a frequency component at 150 kHz and at 450 kHz. It is because of these 2 strong components, with their large separation on the frequency axis that the 2 wave modes are clearly visible in the waveforms.

The Fourier transform of the waves recorded with between 40 mm and 80 mm of Teflon in the wave's path, as well as having components at 150 kHz and at 450 kHz, also have frequencies at between 200 kHz and 400 kHz. It is because of the presence of these mid range frequencies that 2 distinct wave modes are not clearly visible when viewing the waveforms.

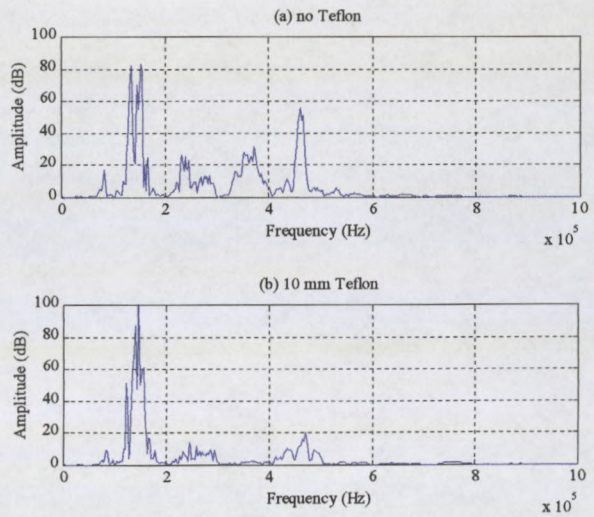

Figure 6.7.3. Fourier transforms of waveforms recorded across differing lengths of Teflon: (a) 0 mm, (b) 10 mm.

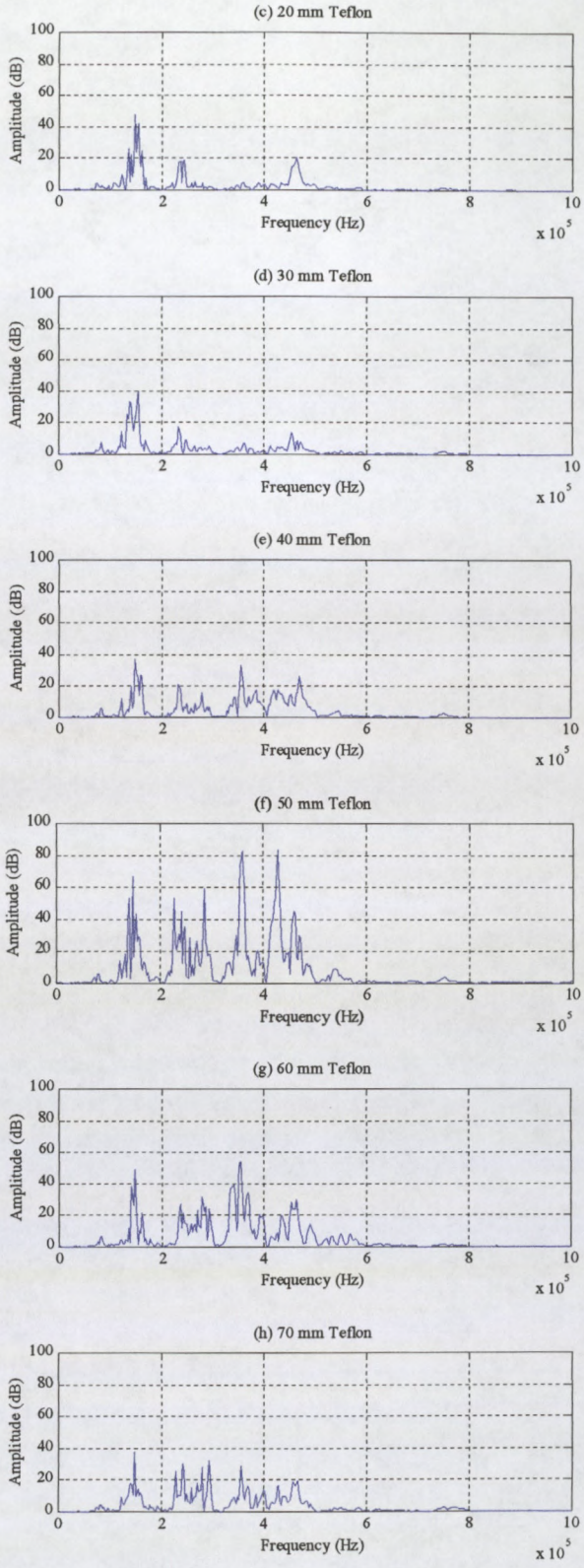

Figure 6.7.3. cont. Fourier transforms of waveforms recorded across differing lengths of Teflon: (c) 20 mm, (d) 30 mm, (e) 40 mm, (f) 50 mm, (g) 60 mm, (h) 70 mm.

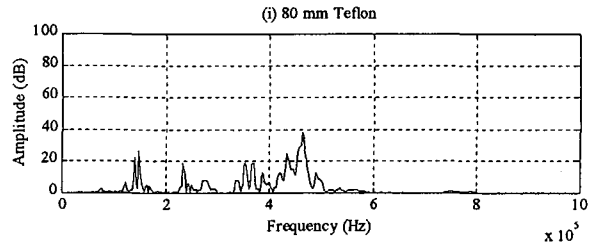

Figure 6.7.3. cont. Fourier transforms of waveforms recorded across differing lengths of Teflon: (i) 80 mm.

6.7.4 Discussion of Parameters

The value of each of the 5 parameters, determined from the waves that were recorded in experiment 4 is shown in figure 6.7.4. The variation in energy content and the variation in peak voltage follow similar patterns as the amount of Teflon containing material in the wave's path is increased. Both parameters exhibit a decreasing trend between 0mm and 30 mm, their highest value at 50 mm and then another decreasing trend between 50 mm and 80 mm. The most plausible explanation for the presence of the high energy content and peak voltage when there is 50 mm of Teflon in the wave's path is that in this arrangement resonance has occurred.

The general trend in the ringdown counts graph (figure 6.7.4 (b)) is that with greater lengths of Teflon in the wave's path, the ringdown counts will be higher. There are however several exceptions to this trend.

The signal with the lowest central frequency was recorded with 10 mm of Teflon in its path. The frequency spectrum of this wave shows that a component at 150 kHz has the greatest magnitude. Because this low frequency component is much stronger than the higher frequencies this wave's central frequency is low.

The signal with the highest central frequency was recorded with 50 mm of Teflon in the wave's path. The reason for this signal's high central frequency is that the frequency components in the 300 kHz to 500 kHz band are especially strong when compared to this frequency band of the other spectra.

There is a trend present in the wave speed graph (figure 6.7.4 (e)) that indicates that as the length of Teflon in the wave's path is increased, wave speed will be reduced. The wave speed when there is no Teflon within the wave's path is significantly higher than the speeds of the waves that passed through material that contained Teflon. The presence of Teflon within the wave's path appears to slow the wave.

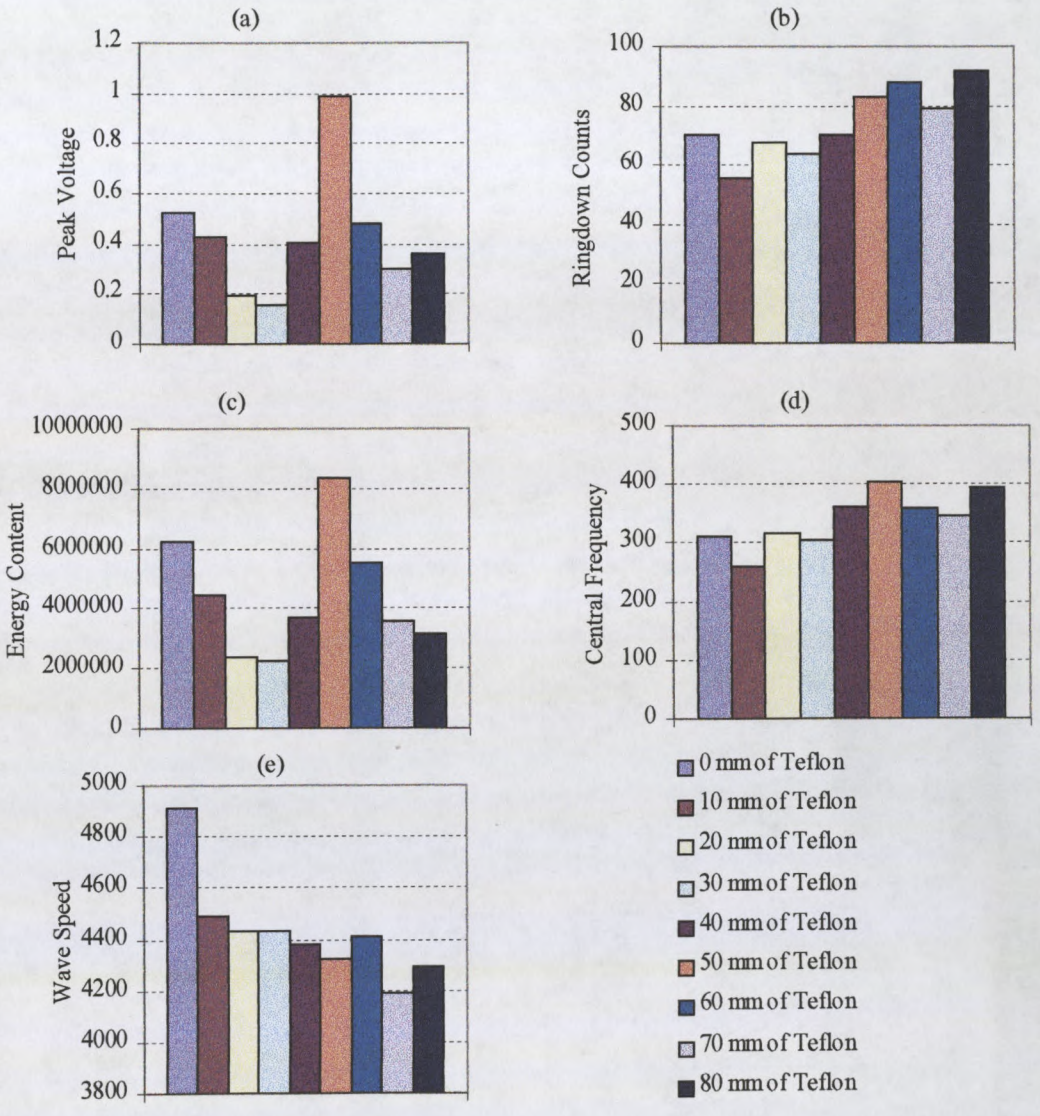

Figure 6.7.4. Variation of AU parameters (a) peak amplitude, (b) ringdown counts, (c) energy content, (d) central frequency and (e) wave speed for differing amounts of Teflon in the wave's path.

6.8 Conclusions

6.8.1 Experiment 1

The trends present in the peak amplitude, ringdown counts and energy content indicate that the AU technique has potential to be used to find delaminations. However the deviation from the trends, present at the 40 mm and 120 mm patches, indicate that the application of the AU method for delamination detection may be more difficult than originally envisioned.

The frequency content of the waveform recorded across the 120 mm patch has high amplitudes in the 200 kHz to 500 kHz band and is in this way different to the other waves recorded in this test. This difference is possibly due to resonance that has occurred at this patch. A second possibility is that the geometry of the Teflon within the laminate has caused a wave mode conversion.

6.8.2 Experiment 2

For the ringdown counts and energy content there is a large difference between data sets A and B at 10 mm, 40 mm and 80 mm. Thus these parameters may be used to identify delaminations that are these sizes. However the ability to only identify patches of a certain size and not of other sizes is not particularly useful and will limit the flexibility of a testing operation.

Apart from the wave speed at 10 mm, there is a consistent difference in wave speeds of data sets A and B. Thus wave speed has shown itself to be the most reliable indicator of the presence of Teflon within the laminate.

It was expected that the presence of the Teflon would have a consistent effect on the derived parameters as the test is moved to Teflon patches of greater diameter. The presence of a Teflon patch has at some sensor spacings caused the value of a parameter calculated from data set A to have a larger value than that derived from data set B. However at other sensor spacings this order has been reversed and the parameter calculated from data set B is has a greater value than that calculated from data set A. The above experiment has shown that AU method is not capable of detecting Teflon

patches of various sizes in a consistent manner. The cause of this inconsistency is not obvious and the following 2 possibilities have been suggested:

1. There may at some of the patches be a bond between the Teflon and the resin that is not present at other patches. The presence of a bond will have an effect on the wave transmission and may be responsible for the observed inconsistencies.
2. The geometry of the patches and the frequency of the pulser may cause resonance in some cases. The resonance can cause an increase in the peak voltage, ringdown counts and the energy content as well as affect the frequency content and wave speeds.

6.8.3 Experiment 3

The waveforms and frequency spectra can differ greatly depending on the transducers' position relative to the Teflon. For the 2 waves that were recorded with the source transducer positioned on the Teflon, only 1 wave mode was evident in the signal. The possibility therefore exists for using this phenomenon to establish whether the source transducer is positioned on a delamination.

6.8.4 Experiment 4

An analysis of the frequencies present in the waveforms recorded in experiment 4 shows that the signal's frequency content varies, depending on the length of Teflon between the transducers. It is because of the varying frequency content that there are no clear trends in the ringdown counts, peak voltage and energy content plots.

6.8.5 General Conclusions

Assuming that a Teflon patch is an accurate simulation of a delamination then the use of the parameters peak voltage, ringdown counts, central frequency and energy cannot be reliably used to locate delaminations. However a Teflon patch between layers of a laminate is merely a simulation of a delamination. The accuracy of this simulation is questionable when one compares the smooth surface of the Teflon to the irregular interfaces that are present in a delamination. Therefore these results do not necessarily imply that these parameters cannot be used for detecting realistic delaminations.

The presence of Teflon has consistently had a slowing effect on the wave speed. Thus wave speed seems to be the best parameter for detecting delaminations.

Chapter 7

Impact Damaged Laminate

7.1 Introduction

Composites a prone to damage from impacts. Some of the causes of impact damage are the impact of tools during maintenance, hail and in the case of aircraft, bird strikes. Thus, the ability of the AU method to detect and quantify the severity of impact damage has been evaluated. In order to do this, an FRP laminate has been manufactured and then subjected to a number of controlled impacts. The AU technique was then applied to this damaged laminate and the effect of the damage on the value of the AU parameters was observed.

7.2 Specimen Details

A flat fibre glass laminate was constructed from 5 layers of 440 g/m² uni-directional glass fibre and the LR20 / SLC30 resin system. The stacking sequence used is as follows: 0°/90°/0°/90°/0°.

The above laminate was impacted with a drop impact tester at 22 different locations such that each impact had a differing amount of energy. The laminate was supported (unclamped) on a hollow steel cylinder of 50 mm internal diameter. The striker used had a hemispherical striking surface of 12,7 mm diameter. After each impact the laminate was moved so that the striker aligned with a fresh, undamaged region of material. The weighted striker was then dropped from a greater height so that the following impact struck an undamaged part of the laminate with slightly more energy. Each impact was located far enough away from previous impacts to prevent the overlap of damage. This process was repeated, each time increasing the energy of the impact by 1,87 J until the striker had sufficient energy to pierce through the laminate.

7.3 Description of the Damage

All impacts caused delaminations that are visible in the form of a light coloured area surrounding the point of impact. The delaminations have a circular shape on the laminate's top surface and an oval shape on the laminate's bottom face. The major axis of the oval delaminated area is oriented in the direction of the 90° layers.

As an approximate measure of the damage, the length of each delamination's major axis has been measured and plotted as a function of the energy of the impact (figure 7.3.1). The general trend of this plot is a straight line. However several points deviate considerably from the trend. This indicates that an increase in the in the energy of an impact will not always result in a proportionate increase in the damage size. Variations in the laminate's properties may be the cause of the disproportionate relationship between impact energy and damage size.

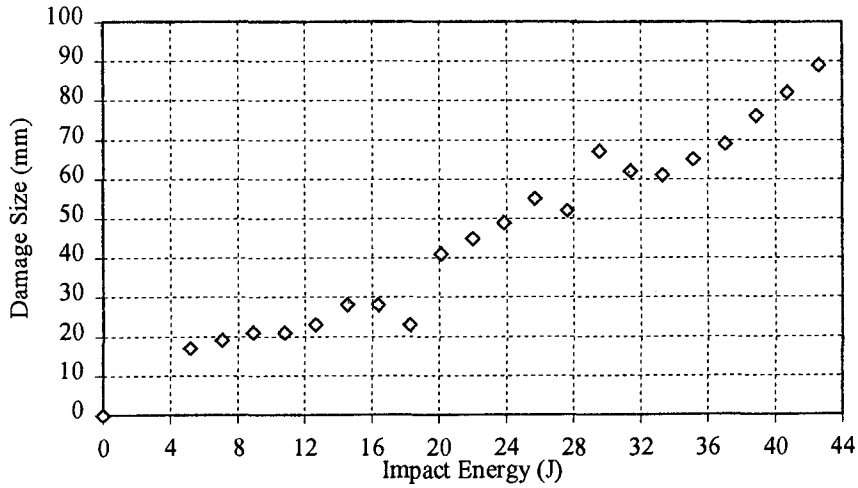

Figure 7.3.1. Relationship between impact damage and energy of the impact.

Impacts with energies of up to 24 J caused a very slight depression on the laminate's top face. Above 24 J of impact energy resin cracks become visible on the top surface and the depressions become more noticeable. A bulge first appears on the laminate's bottom face at an impact energy of 20 J. As the impact energy is increased, the bulges become more prominent and at above 26 J, cracks are visible in the laminate's bottom face. At 31 J, long and narrow delaminations appear in the laminate's 0° direction. As the energy

of the impacts is further increased the delaminations grow in size, the cracks and depressions in the laminate's top surface become more evident and at 43 Jthe striker pierced through the laminate.

The amount of impact energy sustained by the laminate in this test is comparable to the energy of a 0.05 m diameter hailstone at a free-fall velocity of 33 m/s (35J).

7.4 Testing Procedure

An AU testing procedure was devised to investigate the relation between the degree of impact damage and the value of the AU parameters. This procedure involved running AU tests across each impact in turn.

The source and receiving transducers were placed at either side of an impact so that a wave travelling between the transducers would travel through the impact-damaged region. Through the duration of the test the distance between the transducers was kept constant at 50 mm and 3 waveforms were recorded across each impact. Between the recording of each wave the transducers were removed form the laminate before being re-adhered with fresh glycerine. It was necessary to record 3 waves at each impact so as to allow averaging of the variations that arise as a result of coupling inconsistencies. The average value of the parameters peak voltage, ringdown counts, energy content, central frequency and arrival time have been plotted as a function of the energy of the impact across which the waves were recorded.

7.4.1 Peak Voltage

Figure 7.4.1 shows the variation in peak voltage of waves recorded across various impacts. At the left-hand side, where the impacts had a small amount of energy, there is a lot of scatter in the data points. This scatter is due to the poor repeatability of the peak voltage parameter. When impacted with a greater amount of energy, toward the right-hand side of the graph, there is less scatter and thus the data points form a clearly defined trend. The percentage difference between the maximum and minimum peak voltages is 84,5 %.

The peak voltage data can be divided into 3 portions, each with a differing trend. Although there is a lot of scatter in the first portion (impacts from 0 to 25 J) its general trend indicates that the peak voltage is approximately constant. Thetrend of the second portion shows that the peak voltage of the waveforms decreases rapidly as the impact energy is increased from 25 J to 34 J. The trend of the third portion (above 34 J) has a shallow downward gradient and thus indicates small reductions in the level of the peak voltage as the impact energy is increased.

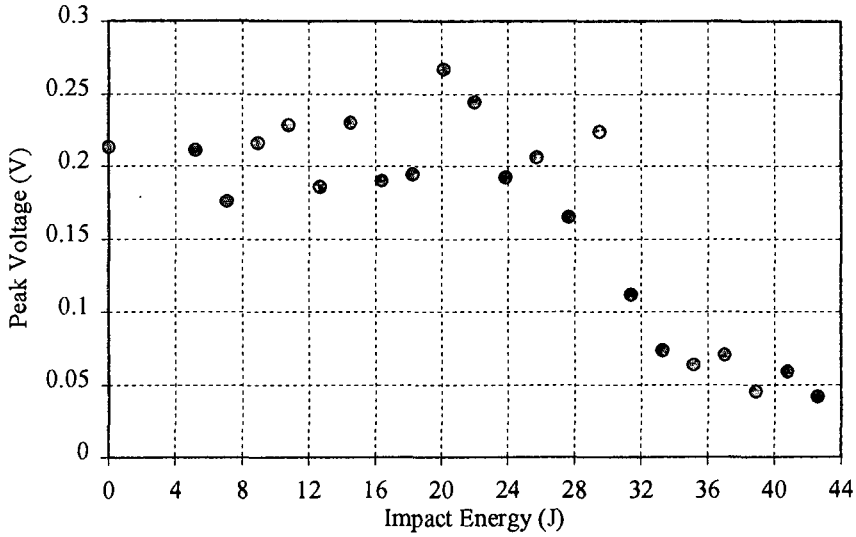

Figure 7.4.1. Relationship between peak voltage and impact energy.

7.4.2 Ringdown Counts

Initially, the ringdown counts for each waveform were calculated with a threshold level of 0,01 V. After graphing the ringdown counts that were determined with this threshold level, the researcher suspected that a better indication of the trends would be achieved if a different threshold level were selected. Thus the ringdown counts were recalculated with a 0,005 V, 0,02 V and then a 0,04 V threshold level. Table 7.4.2 has been included to illustrate the effect that various threshold levels have on the number and range of the ringdown counts.

Threshold Level (V)	Ringdown counts Maximum	Ringdown counts Minimum	Range
0,005	70,67	51,33	19,34
0,01	60,67	33,33	27,34
0,02	51,67	14,33	37,34
0,04	31,67	0,33	31,34

Table 7.4.2. The effect of various threshold voltages on the number of ringdown counts.

Table 7.4.2 confirms that a higher threshold level will result in a lower number of ringdown counts. This is to be expected since a given signal will cross a higher threshold fewer times than it would cross a lower threshold.

The variation in ringdown counts determined with each of the 4 different threshold settings is shown in figure 7.4.2. The representations of the ringdown counts based on the 0,02 V and 0,01 V thresholds show a smoother downward trend over a larger range than the representation based on the 0,005 V or 0,04 V thresholds. Thus only the ringdown counts for the 0,02 V and 0,01 V thresholds have been discussed.

0,01 V Threshold

The ringdown counts determined for a 0,01 V threshold is shown in figure 7.4.2 (b). The number of ringdown counts in the undamaged material (0 J) is less than the number of ringdown counts for most impacts between 5 J and 28 J. As the energy of the impacts is increased from 0 J to 16 J the number of ringdown counts remains approximately constant at 57. Thereafter there is a steady increase in the number of ringdown counts from 51 counts at 18 J to 60 at 24 J. Between the impacts of 24 J and 39 J there is a steady decrease in the number of ringdown counts to 33. Above 39 J the number of ringdown counts remains approximately constant. The percentage range between the minimum and maximum number of ringdown counts is 45,1 %.

0,02 V Threshold

For impacts of up to 24 J the number of ringdown counts remain approximately constant (figure 7.4.2 (c)). The average number of ringdown counts between 0 and 24 J is 43,7. The number of counts for the undamaged region (0 J) is less than in many of the

impacts up to 24 J. Between impacts of 24 J and 39 J there is a steady decrease in the number of ringdown counts from 43 to 14. In the more severely damaged material (impacts between 39 J and 43 J) the number of ringdown counts remains approximately constant. The percentage range between the minimum and maximum number of ringdown counts is 72,3 %.

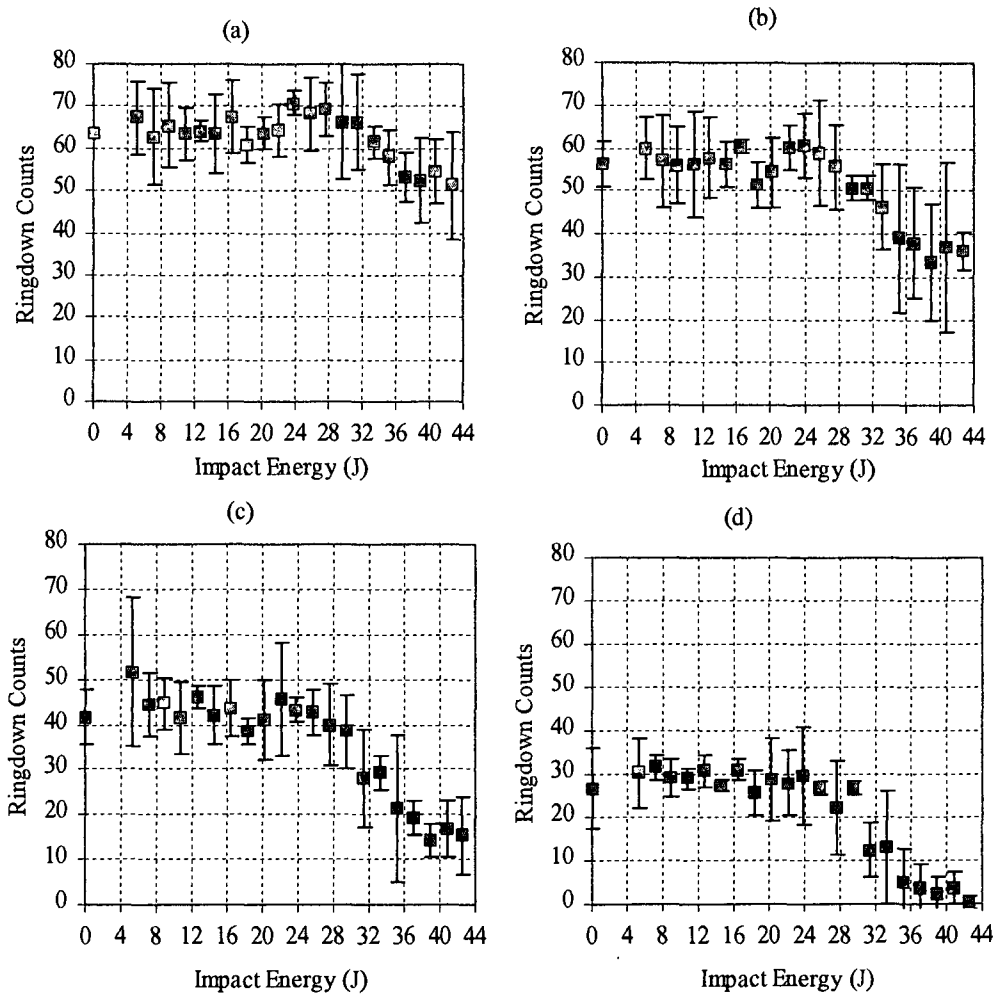

Figure 7.4.2. Ringdown counts in impact damaged laminate determined with threshold levels of: (a) 0,005V, (b) 0,01 V, (c) 0,02 V and (d) 0,04 V. The error bars represent a 95 % confidence interval.

7.4.3 Energy Content

Similar to the peak voltage graph, where the impact energy is low (figure 7.4.3), there is a lot of scatter in the data points. With higher amounts of impact energy, toward the right-hand side of the graph, there is less scatter and the data points are aligned.

The energy content graph can be divided into 3 portions. The trend of the first portion, with impacts ranging from 0 to 25 J, indicates that as the impact energy is increased the energy content of the waveforms remains approximately constant. In the second portion, as the energy of the impacts is increased from 25 J and 34 J, there is a rapid reduction in the energy content of the waveforms. The trend of third portion indicates that, as the impact energy is further increased, there is a small reduction in the energy content of the waveforms. The percentage difference between the maximum and minimum energy contents is 77,8 %.

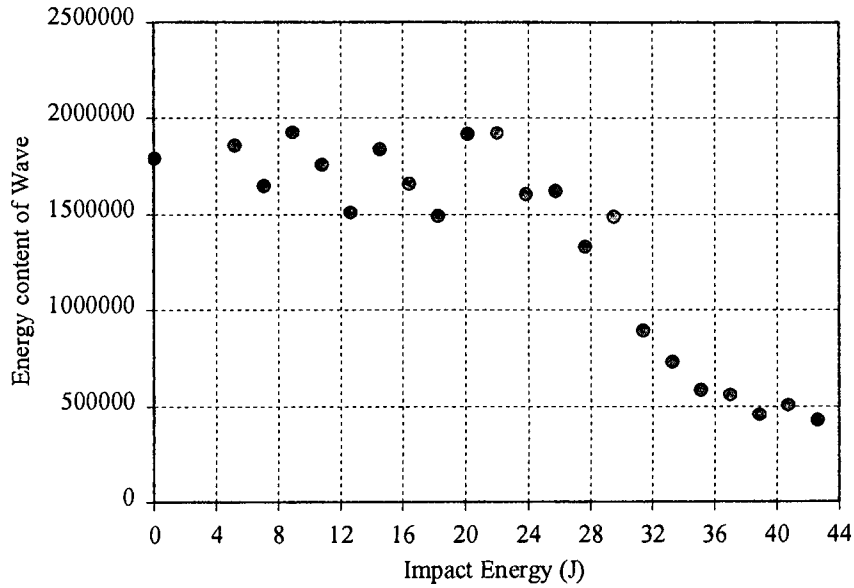

Figure 7.4.3. Relationship between energy content and impact energy.

7.4.4 Central Frequency

All the central frequency values on the graph lie in an approximately horizontal line (figure 7.4.4). The maximum central frequency of the 22 waveforms recorded was 301 kHz and the minimum was 284 kHz. The percentage difference between the maximum and minimum central frequencies in 5,7 %.

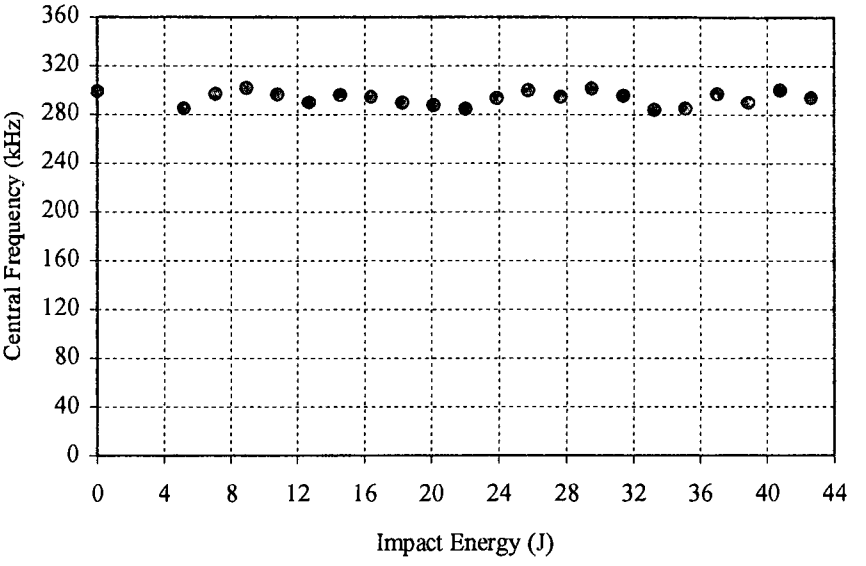

Figure 7.4.4. Relationship between central frequen cy and impact energy.

7.4.5 Arrival Time

The arrival time graph (figure 7.4.5) indicates an increase of the energy of the impact will cause an increase in the wave's travel time. However, during the running of the test it was evident to the researcher that the arrival time remained constant. The reason for the apparent increase in arrival time is that in the more severely damaged regions the amplitude of the signals were low and thus the first few voltage oscillations were below the threshold level. Since the first threshold crossing point has been used as the wave's arrival time, the weaker signals will appear to have a longer time of travel.

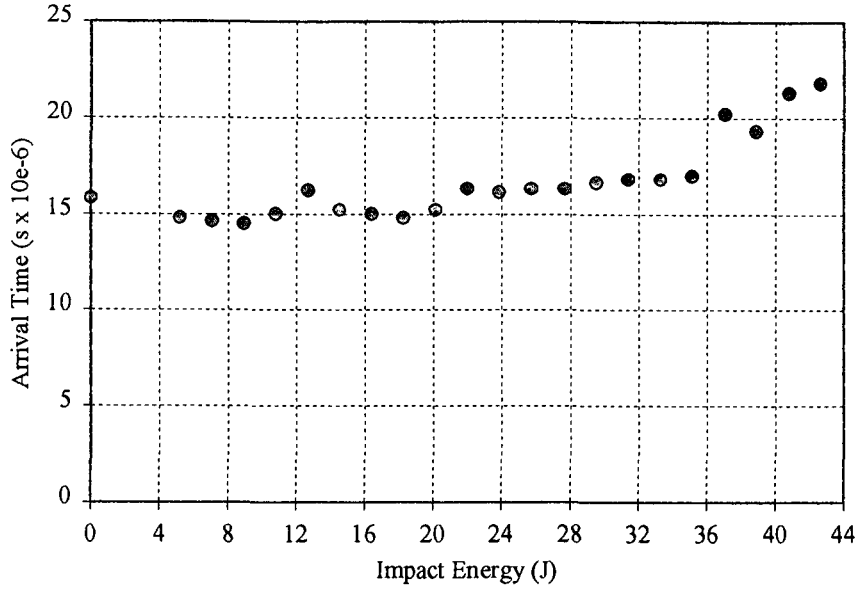

Figure 7.4.5. Relationship between arrival time and impact energy.

7.5 Conclusions

Since the peak voltage, energy content and ringdown counts are all approximately constant for impacts with energies below 25 J, these parameters are limited in terms of the degree of impact damage that they are sensitive to. At above 25 J, cracks were first observed in the laminate's top and bottom faces and the peak voltage, energy content and ringdown counts showed a declining trend, as the energy of the impacts was further increased. Thus it is only when the energy of an impact is sufficient to cause cracks in both the top and bottom faces of a laminate that a significant effect can be observed on the value of peak voltage, energy content and ringdown counts.

The central frequency and arrival time of a wave are not affected by the presence of impact damage within the wave's path. Since the central frequency remains constant, the impact damage attenuates the waveform's low and high frequency components to the same degree. Central frequency and arrival time can thus not be used to locate impact damage.

Four different threshold levels have been used for the calculation of ringdown counts. This exercise has drawn attention to the necessity for selecting an appropriate threshold setting, depending on the signal amplitudes.

Chapter 8

Dispersion Curves

8.1 Introduction

Typically acoustic energy consists of a broad range of frequencies, however when emitted into a plate, the frequencies excited exist within a few narrow bands. These frequency bands are governed by the both the properties and thickness of the plate. Furthermore the elastic wave energy within a plate exists in an infinite number of modes where each mode is characterized by a unique displacement field.

In terms of sound wave propagation, a fibre reinforced plastic plate is an example of a dispersive medium. This dispersive nature causes each frequency component to travel at a unique velocity. Equations, called 'the Rayleigh-Lamb frequency relations' can be used to determine the velocity at which a wave with a particular frequency thickness product will propagate within the plate. The graphical display of these relations, called dispersion curves, shows the wave modes present and the frequency thickness product above which each mode exists.

The governing equations of elastodynamics for waves in plates are presented in this chapter. The derivation of the Rayleigh-Lamb frequency relations, as per Rose [15], has been shown. The extensional and flexural wave speeds in a glass fibre laminate have been determined experimentally. These wave speeds have then been substituted into the Rayleigh-Lamb frequency relations and the relations have been solved numerically, as has been done in [15]. This has enabled dispersion curves for a unidirectional glass fibre laminate to be plotted. These dispersion curves have been used to determine cutoff frequencies from which the wave modes present in the WD transducer's sensitivity range have been determined. Thereafter number of wave modes predicted by the dispersion curves has been compared to the number of modes visible in Fourier transforms.

8.2 The Rayleigh-Lamb Frequency Relations

Recall from the theory of elasticity (using Cartesian tensor notation):

$\sigma_{ij,j} + \rho f_i = \rho \ddot{u}_i$ 3 equations of motion (i = 1, 2, 3); (1)

$\varepsilon_{ij} = \frac{1}{2}(u_{i,j} + u_{j,i})$ 6 independent strain displacement equations; (2)

$\sigma_{ij} = \lambda \varepsilon_{kk} \delta_{ij} + 2\mu \varepsilon_{ij}$ 6 independent constitutive equations (isotropic materials). (3)

The first 2 equations are valid for any continuous medium; the specific type of medium is introduced via (3). If we eliminate the stress and strain factors from these equations, then we have

$$\mu u_{i,jj} + (\lambda + \mu) u_{j,ji} + \rho f_i = \rho \ddot{u}_i \tag{4}$$

The boundary conditions take the form of prescribed tractions and displacements and are as follows:

$u(x,t) = u_0(x,t)$ on surface displacements; (5)

$t_i = \sigma_{ij} n_j$, on surface tractions; (6)

$u(x,t) = u_0(x,t)$ on S_1

and $t_i = \sigma_{ij} n_j$, on S_2 as a mixed boundary condition. (7)

8.2.1 The Free Plate Problem

The geometry of the free plate problem is illustrated in figure 8.2.1. The problem is governed by the equations of motion (4), with boundary conditions of type (6). The surfaces at the coordinates $y = d/2 = h$ and $y = -d/2 = -h$ are considered traction-free. The exact solution of this problem has been obtained by the method of displacement potentials.

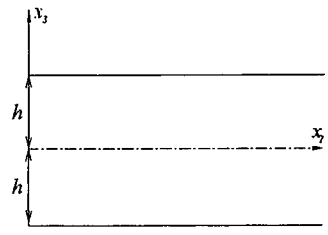

Figure 8.2.1. Geometry of the free plate problem.

8.2.2 Solution by the Method of Potentials

The two uncoupled wave equations for plane strain are

$$\frac{\partial^2\phi}{\partial x_1^2}+\frac{\partial^2\phi}{\partial x_3^2}=\frac{1}{c_L^2}\frac{\partial^2\phi}{\partial t^2} \qquad \text{governing longitudinal waves;} \qquad (5)$$

$$\frac{\partial^2\psi}{\partial x_1^2}+\frac{\partial^2\psi}{\partial x_3^2}=\frac{1}{c_T^2}\frac{\partial^2\psi}{\partial t^2} \qquad \text{governing shear waves;} \qquad (6)$$

The case of plane strain is not the most general for the problem at hand, but the analysis is greatly simplified in this case. Achenbach [19] shows that taking the general state of strain as the starting point results in the same set of solutions presented here plus additional modes (infinite in number), known as horizontal shear modes, that can exist independently of other wave modes.

As a result of our assumption of plain strain, the displacements and stresses can be written in terms of potentials as

$$u_1 = u = \frac{\partial\phi}{\partial x_1}+\frac{\partial\psi}{\partial x_3} \qquad (7a)$$

$$u_2 = v = 0 \qquad (7b)$$

$$u_3 = w = \frac{\partial\phi}{\partial x_3}-\frac{\partial\psi}{\partial x_1} \qquad (7c)$$

$$\sigma_{31} = \mu\left(\frac{\partial u_3}{\partial x_1}+\frac{\partial u_1}{\partial x_3}\right) = \mu\left(\frac{\partial^2\phi}{\partial x_1\partial x_3}-\frac{\partial^2\psi}{\partial x_1^2}+\frac{\partial^2\psi}{\partial x_3^2}\right) \qquad (8a)$$

$$\begin{aligned}\sigma_{33} &= \left(\frac{\partial u_1}{\partial x_1}+\frac{\partial u_3}{\partial x_3}\right)+2\mu\frac{\partial u_3}{\partial x_3}\\ &= \left(\frac{\partial^2\phi}{\partial x_1}+\frac{\partial^2\phi}{\partial x_3^2}\right)+2\mu\left(\frac{\partial^2\phi}{\partial x_3^2}-\frac{\partial^2\psi}{\partial x_1\partial x_3}\right)\end{aligned} \qquad (8b)$$

where λ and μ are Lamé constants.

We begin the analysis by assuming the solutions in the form

$$\phi = \Phi(x_3)\exp[i(kx_1 - wt)], \qquad (9)$$

$$\psi = \Psi(x_3)\exp[i(kx_1 - wt)]. \qquad (10)$$

Substitution of these assumed solutions into (5) and (6) yields equations governing the unknown functions Φ and Ψ. The solutions to these equations are

$$\Phi(x_3) = A_1\sin(px_3) + A_2\cos(px_3), \qquad (11)$$

$$\Psi(x_3) = B_1 \sin(qx_3) + B_2 \cos(qx_3), \tag{12}$$

where:

$$p^2 = \frac{w^2}{c_L^2} - k^2 \qquad \text{and} \qquad q^2 = \frac{w^2}{c_T^2} - k^2, \tag{13}$$

c_L is the extensional wave velocity

c_T is the flexural wave velocity.

With these results, the displacements and stresses can be obtained directly from (7) and (8). Omitting the term $\exp[i(kx_1 - wt)]$ in all expressions, the results are as follows:

$$u_1 = \left[ik\Phi + \frac{d\Psi}{dx_3} \right], \tag{14}$$

$$u_3 = \left[\frac{d\Phi}{dx_3} - ik\Psi \right]; \tag{15}$$

$$\sigma_{33} = \left[\lambda\left(-k^2\Phi + \frac{d^2\Phi}{dx_3^2} \right) + 2\mu\left(\frac{d^2\Phi}{dx_3^2} - ik\frac{d\Psi}{dx_3} \right) \right], \tag{16}$$

$$\sigma_{31} = \mu\left(2ik\frac{d\Phi}{dx_3} + k^2\Psi + \frac{d^2\Psi}{dx_3} \right). \tag{17}$$

Now, since the field variables involve sines (resp. cosines) with argument x_3, which are odd (resp. even) functions about $x_3 = 0$, we split the solution into two sets of modes: symmetric and antisymmetric modes. Specifically, for displacement in the x_1 direction, the motion will be symmetric (with respect to the midplane of the plate) if u_1 contains cosines but will be antisymmetric if u_1 contains sines. The reverse is true for displacements in the x_3 direction. Thus we split the modes of wave propagation into two systems:

$$\frac{\tan(qh)}{\tan(ph)} = -\frac{4k^2pq}{\left(q^2 - k^2\right)^2} \qquad \text{for symmetric modes.} \tag{18}$$

$$\frac{\tan(qh)}{\tan(ph)} = -\frac{\left(q^2 - k^2\right)^2}{4k^2pq} \qquad \text{for antisymmetric modes} \tag{19}$$

Recall that p and q are defined in (13).

The wave number k, is equal to $\frac{\omega}{c_p}$, where c_p is the phase velocity of the Lamb wave mode and ω is the circular frequency.

These equations are known as the Rayleigh-Lamb frequency relations and can be used to determine the velocity at which a wave at a particular frequency will propagate within a plate.

It should be noted that the separation of waves into symmetric and antisymmetric modes is an exception rather than a rule. In hollow cylinders, the lack of structure symmetry does not allow this separation. Plate wave modes do exist in an anisotropic plate, but the separation into symmetric and antisymmetric modes is not possible unless the wave propagates along a symmetry axis of the plate. The dispersion relations for off axis directions in an anisotropic plate have additional modes known as shear horizontal modes.

8.3 Determining the Extensional and Flexural Wave Velocities

The value of p and q in the Rayleigh-Lamb frequency relations are dependent on the material's flexural and extensional wave speeds. Therefore to solve these relations, the extensional and flexural wave velocities need to be determined experimentally. These velocities were determined for wave travel at parallel to the fibre direction of a unidirectional glass fibre/epoxy laminate. Since this is a symmetry axis of an anisotropic plate, the separation into symmetric and antisymmetric modes is valid.

Extensional waves are characterized by particle motion that is parallel to the plane of the plate. To excite and record pure extensional waves it is therefore necessary to couple the transducers to the edge of a laminate. To provide sufficient contact area for the transducers, a laminate whose thickness is greater than the diameter of the transducers was required. A 24-layer glass fibre laminate was made and had sufficient thickness to allow the transducers to be attached to its edge. The source transducer and a trigger transducer were coupled to one edge of the laminate and the receiving transducer was coupled to the opposite edge (figure 8.3.1) such that a wave travelling between the transducers would travel parallel to the fibre direction. With this transducer arrangement the wave's travel time between them was determined and from this time the velocity of the extensional wave was calculated. The extensional wave velocity was found to be 4067 m/s.

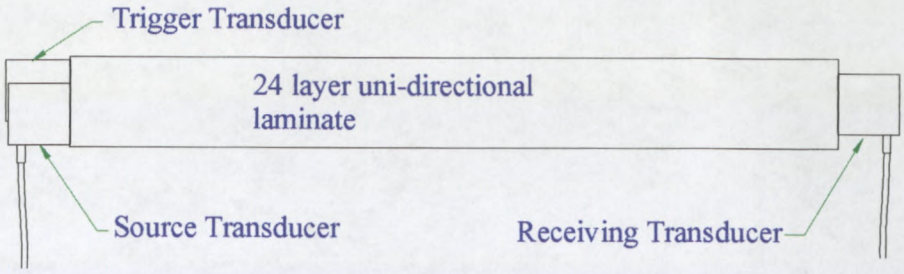

Figure 8.3.1. Transducer arrangement for determining the extensional wave velocity.

The velocity of the flexural wave was determined in a similar manner to that used for determining the extensional wave velocity. Flexural waves are characterized by particle motion that is perpendicular to the plane of the plate. Therefore to measure the flexural wave speed, the source, trigger and receiving transducers were coupled as shown in figure 8.3.2. The wave's travel time between the source and receiving transducers was determined and from this time the flexural wave's velocity was calculated. The flexural wave velocity was found to be 5169 m/s.

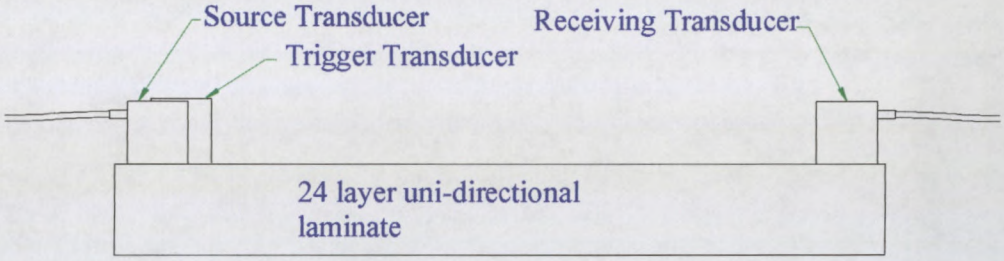

Figure 8.3.2. Transducer arrangement for determining the flexural wave velocity.

8.4 Numerical Solution of the Rayleigh-Lamb Frequency Equations

We are only interested in the real solutions of the Rayleigh-Lamb frequency relations. The real solutions represent the undamped propagating modes of the structure. Thus the relations should be rewritten so that they take on only real values for real or pure imaginary wave numbers k. This is achieved through the following set of equations:

$$\frac{\tan(qh)}{q} + \frac{4k^2 p \tan(ph)}{\left(q^2 - k^2\right)^2} = 0 \qquad \text{for symmetric modes,} \qquad (20)$$

$$q\tan(qh)+\frac{(q^2-k^2)^2\tan(ph)}{4k^2p}=0 \qquad \text{for antisymmetric modes.} \qquad (21)$$

The procedure followed for the solution of equations (20) and (21) is that suggested by Rose [15] and is shown below.

A frequency thickness (ωh) product was first chosen. With the values of ω and h known, p, q and k were then written in terms of c_p and substituted into (20). The software package 'Mathematica' was then used to solve equation (20). Thus the values of c_p were found that would satisfy equation (20) and these solutions were plotted versus their corresponding frequency thickness product ($f d$) (figures 8.4.1 and 8.4.2). Note that the units $f d$ on x axis have been converted to MHz.mm. The dispersion curves were plotted for both the symmetric modes and the antisymmetric modes for frequency thickness products ranging between 0 and 13 MHz.mm.

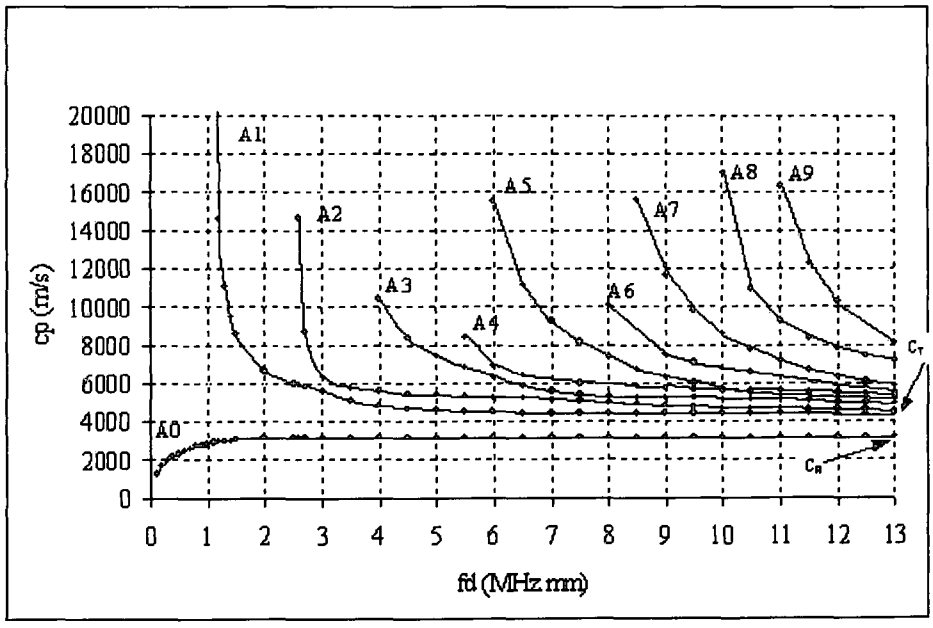

Figure 8.4.1. Dispersion curves of a glass fibre plate (antisymmetric modes)

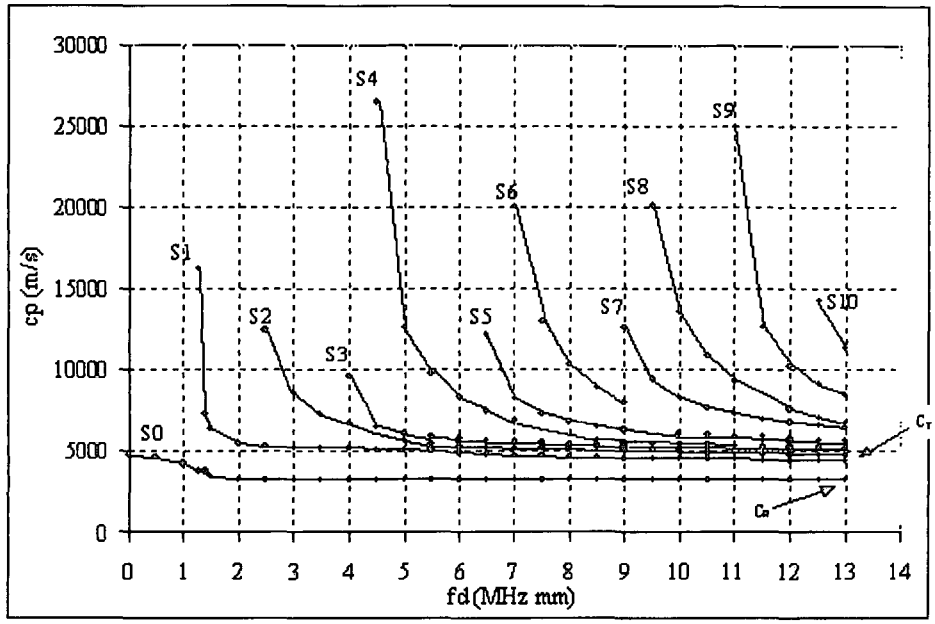

Figure 8.4.2. Dispersion curves of a glass fibre plate (symmetric modes)

8.5 Discussion

Each of the curves in figures 8.4.1 and 8.4.2 refer to a particular wave mode. All modes, apart from the A0 and S0 modes have a cut-off frequency, below which that mode does not exist. On the dispersion curves, the cut-off frequencies are found where $c_p \to \infty$ ie. where the curve becomes vertical. The A0 and S0 modes converge to the Rayleigh surface wave velocity, c_R, while the higher modes converge to c_T, the shear velocity.

To illustrate the use and interpretation of dispersion curves, the cutoff frequencies of the S1, S2, A1 and A2 modes have been determined for a 3 layer and a 5 layer glass fibre laminate. The thickness of the 3 layer laminate is 1,3 mm and that of the 5 layer laminate is 2,165 mm. The $f\,d$ product that corresponds to the cutoff frequencies of the S1, S2, A1 and A2 modes has been read off the dispersion curves. These values were obtained where the curves where the curves become vertical and are listed in the table 8.5.1.

Wave Mode	Frequency Thickness Product (MHz.mm) at Cutoff Frequency
S1	1,2
S2	1,925
A1	1,1
A2	1,2

Table 8.5.1. Frequency thickness products corresponding to various wave modes.

With the laminates thickness and the $f\ d$ product that corresponds to the cutoff frequencies known, the cutoff frequencies can be determined (table 8.5.2). These cutoff frequencies only apply to a 1,3 mm and a 2,165 mm unidirectional glass fibre laminate in the case where the wave travels parallel to the fibre direction.

	Cutoff Frequency (kHz)	
Wave Mode	3 Layer Laminate	5 Layer Laminate
S1	924	554
S2	1,925	1,155
A1	846	508
A2	2000	1200

Table 8.5.2. Cutoff frequencies for various wave modes.

The WD transducer, was found to respond to frequencies in the 90 kHz to 800 kHz range. Thus, according to the above theory, apart from the A0 and S0 modes (which do not have cutoff frequencies), the only mode that exists in the sensitivity range of the WD transducer is the S1 mode in the 5 layer laminate.

If the dispersion curves from which the cutoff frequencies were calculated are accurate then only the A0 and S0 modes will be detectable with the WD transducer in the 3 layer laminate. Thus the Fourier transform of a waveform recorded in the 0° direction of the 3 layer laminate should have 2 peaks, 1 of which corresponds to the A0 mode and the

other corresponding to the S0 mode. However figure 3.5.1 (a), which shows the Fourier transform of a wave recorded at 0° in UD3, has more than 2 peaks. Thus, additional wave modes besides the A0 and S0 modes have been detected.

Likewise, in the 5 layer laminate only the A0, S0 and S1 modes should be detectable and there should thus be 3 peaks in the Fourier transform. However figure 3.5.1 (b), which shows the Fourier transform of a wave recorded at 0° in UD5 has more than 3 peaks.

Thus there is an inconsistency between the number of wave modes observed in the experimental results and the number predicted by the dispersion curves. The cause of this difference is most likely the dispersion curves being inaccurate and this is probably as a result of inaccurate measurement of the extensional and flexural wave speeds on which the dispersion curves have been based.

8.6 Conclusions

Insight into the dispersive nature of waves in plates has been gained through the plotting of dispersion curves. These plots have been used to determine the cutoff frequencies and the wave modes that are within the WD transducer's sensitivity range for a 3 layer and a 5 layer laminate. This has shown that the upper limit of the WD transducer's response range is lower than the cutoff frequencies of most of the wave modes in 3 and 5 layer glass fibre laminates.

In an effort to correlate the theory with the experimental results, the number of wave modes that should be present in the WD transducer's sensitivity range has been compared to the number of peaks in the Fourier transforms. Since the number of wave modes, as predicted by the dispersion curves, does not correlate with the number of modes seen in the Fourier transforms, the accuracy of the dispersion curves is questionable.

It is possible that, as suggested by Ditri [16], the use of a specific wave mode would provide a better indication of the material's condition. Future experiments should therefore investigate the use of a variety of receiving transducers so as to determine

which modes are the most sensitive to defects. To do this a receiving transducer with the appropriate sensitivity range would have to be selected in accordance with accurate dispersion curves.

Chapter 9

Control of the Input Frequency

9.1 Introduction

In all of the previously conducted experiments an acoustic emission computer (PAC 3000) has been used to power the source transducer. However the frequency and amplitude of the signal output by this instrument cannot be varied and no specifications of the output signal are available. An important aspect of AU testing is the frequency of the input signal. Experiments have thus been run, using a variable waveform generator (Hewlett Packard 33120A) to power the source transducer. With the use of this generator, the frequency of the input signal can be controlled and this has been investigated in the following experiments.

Specifically the aims were to:

1. characterize the response of the WD sensor and determine its response range
2. investigate the differences in transmission characteristics of laminates of different thickness
3. investigate the differences in between a signal travelling parallel to and a signal travelling perpendicular to the fibre direction
4. investigate the effect that simulated defects (Teflon patches) within the laminate have on the frequencies transmitted.

9.2 Repeatability Experiment

A signal repeatability experiment has been run to determine the expected variations due to coupling inconsistencies and whether certain the frequencies are more susceptible to coupling variations than others.

9.2.1 Test Method

In this experiment, the source and receiving transducers were coupled to a 3 layer laminate at a 50 mm spacing. The input frequency was increased in 50 kHz increments

from 100 kHz to 800 kHz and the amplitude response at each frequency was noted. The transducers were then removed and the couplant was wiped off the laminate and transducers. With fresh couplant, the transducers were re-adhered and the amplitude response to input frequencies between 100 kHz to 800 kHz was again noted. This process was repeated 6 times and the amplitude as a function of the input frequency was plotted for each data set (figure 9.2.2). Because the couplant was renewed after obtaining each data set while all other conditions (sensor spacing and locations, instrument settings etc.) were kept constant, any differences between the each of the 6 amplitude plots are an indication of the coupling inconsistencies. The standard deviation of the amplitude readings at each frequency has been determined and is also included on figure 9.2.2.

9.2.2 Results and Discussion

Referring to figure 9.2.2, it is clear that at some frequencies the 6 amplitude plots are closely bunched while at other frequencies they are more spaced apart. The standard deviation illustrates this by varying as the input frequency is increased. Thus the repeatability of amplitude readings is dependent on the frequency of the input signal. The frequencies that provide the most repeatable results are those at which the standard deviation is lowest. Hence when the WD transducer is used the testing frequency should be 150 kHz or between 400 kHz and 650 kHz.

At the 3 best frequencies in terms of repeatability (150 kHz, 400 kHz and 550 kHz), the percentage range in the recorded amplitudes are 7,8 %, 4,3 % and 5,6 % respectively.

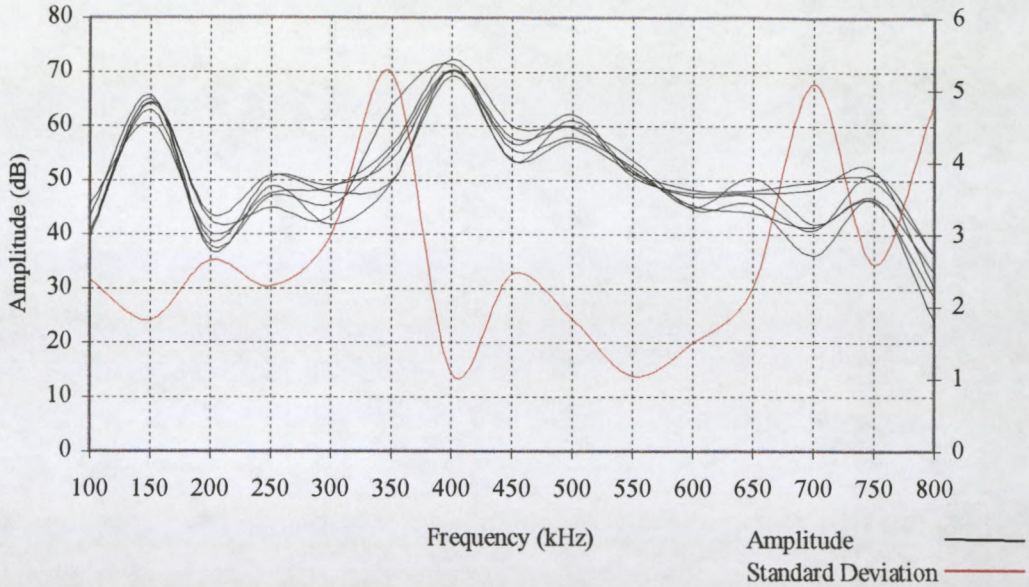

Figure 9.2.2. Six data sets, each recorded with new couplant.

9.3 Characterizing the WD Sensor

9.3.1 Test Method

A response curve for the WD transducer has been plotted. This was achieved by coupling the WD sensor directly to the source transducer such that their mounting faces were in contact. With this arrangement, the adjustable waveform generator was used to supply the source transducer with a range of frequencies.

The Mistras AE system was used to graphically display the Fourier transform of the WD sensor's response. This Fourier transform was observed to have a peak at the frequency of the input signal. The magnitude of this peak is the response of the sensor to the input frequency.

The WD sensor was found to respond to inputs of between 90 kHz and 800 kHz. The input frequency was thus increased from 90 kHz to 800 kHz and the amplitude of the peak, as displayed in the Fourier transform, was noted at 10 kHz increments. These amplitudes have been plotted as a function of the input frequency (figure 9.3.1).

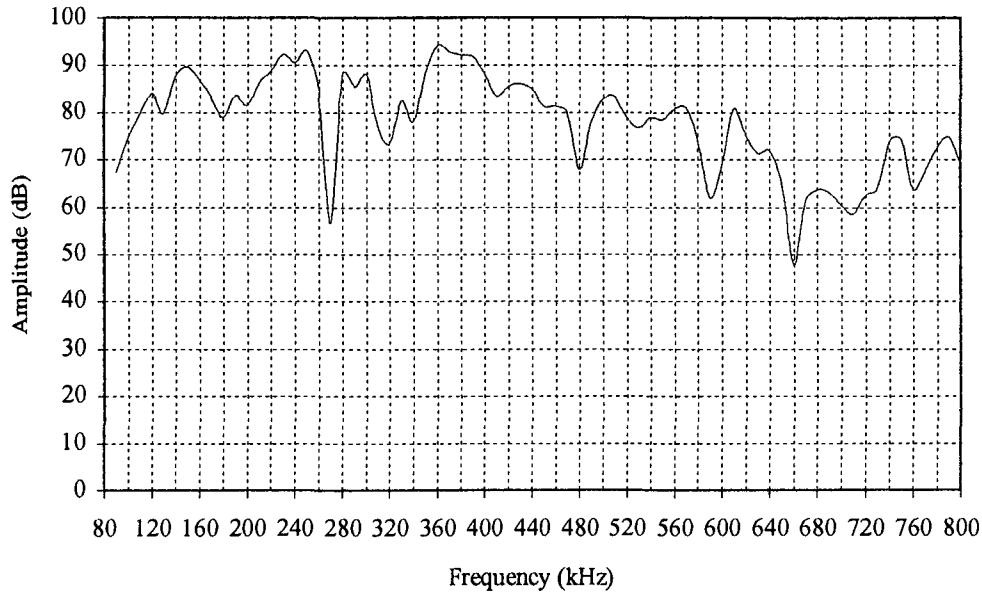

Figure 9.3.1. Response of WD sensor.

9.3.2 Results and Discussion

Figure 9.3.1 shows how its the response differs for different input frequencies. Although this sensor is classified as wide band, implying that its response is flat over a wide frequency range, a number of resonant peaks are evident in the response curve.

It should be noted that this response curve is not entirely accurate and solely a reflection of the characteristics of the WD transducer. Other factors such as the constraining effect of the source transducer on the WD's mounting face and the characteristics of the source transducer will have affected this curve. For more accurate transducer calibration, methods such as the helium gas jet technique, the reciprocity technique and the step-force calibration technique have been suggested [33, 65].

9.4 Comparison of Waveforms Travelling Parallel and Perpendicular to Fibre Direction

The response of a 3-layer uni-directional laminate to a range of input frequencies has been compared for when the wave travels parallel to and then perpendicular to the fibre direction.

9.4.1 Test Method

With the source and receiving transducers coupled to a 3 layer unidirectional glass fibre laminate, the frequency of the input was increased from 90 kHz to 800 kHz in 10 kHz increments. This experiment was conducted twice; once with the transducers arranged such that the wave travelled parallel to the fibres and a second time such that the wave travelled perpendicular to the fibre direction. The Mistras AE system was used to monitor the WD sensor's response and display the Fourier transform of the received signal. A curve depicting the amplitude as a function of the input frequency has been plotted for both the parallel to the fibres and the perpendicular to the fibres test.

9.4.2 Results and Discussion

Figure 9.4.2 shows the amplitudes for a range of input frequencies when the wave travelled either parallel to or perpendicular to the fibre direction. The amplitude when the wave travels perpendicular to the fibre direction is lower, at almost all frequencies, than the amplitude of the wave that travels parallel to the fibres. The curves have peaks and troughs at identical locations and there is a larger separation between them at higher frequencies.

Between 90 kHz and 320 kHz, the amplitude when the wave travels perpendicular to the fibre direction is on average 9,2 % lower than the amplitude when the wave travels parallel to the fibre direction. At above 320 kHz, there is a greater difference between the two as the amplitudes for waves that travel perpendicular to the fibre direction drop to 38,5 % below those for waves that travel parallel to the fibres.

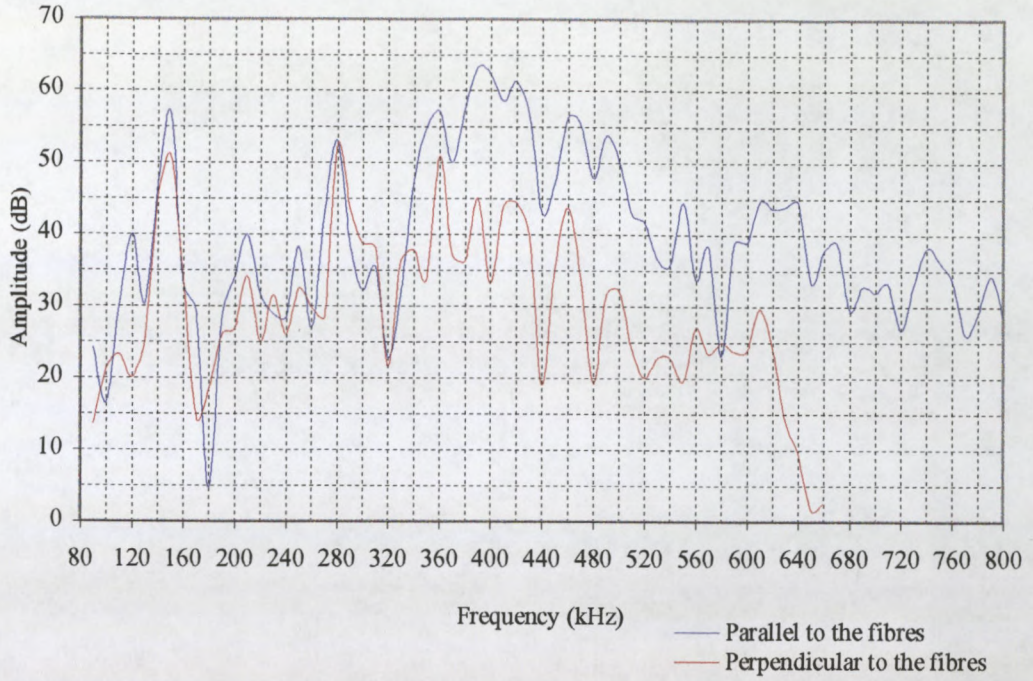

Figure 9.4.2. Comparison of amplitudes for waves travelling parallel to and perpendicular to the fibre direction.

9.5 Comparison of Response of Laminates of Different Thickness

The response of a 3 layer uni-directional laminate to a range of input frequencies has been compared to that of a 5 layer uni-directional laminate.

9.5.1 Test Method

Following a similar method as in the previous experiment, the transducers were coupled to the laminate and the input frequency was increased in 10 kHz increments from 90 kHz to 800 kHz. The amplitude of the received signal at each frequency was noted and this procedure was applied to both a 3 layer and a 5 layer laminate. In each case the transducers were arranged such that a wave travelling between the transducers would travel parallel to the fibres. A curve depicting the amplitude as a function of the input frequency has been plotted for the test on each laminate (figure 9.5.2). The response curve of the WD sensor has been superimposed on this figure so as to show how much the laminates attenuate each frequency.

9.5.2 Results and Discussion

Figure 9.5.2 shows the amplitudes over a range of input frequencies when the wave travelled in either a 3 or a 5 layer laminate. In terms of the location of peaks and troughs, the curves for the 3 and 5 layer laminates and the response curve of the WD transducer are similar. Below 330 kHz the amplitudes in the 5 layer laminate are consistently higher than those in the 3 layer laminate. Between 330 kHz and 610 kHz the amplitudes for the two laminates are at similar levels. Above 610 kHz, the amplitudes in the 5 layer laminate drop well below those in the 3 layer laminate.

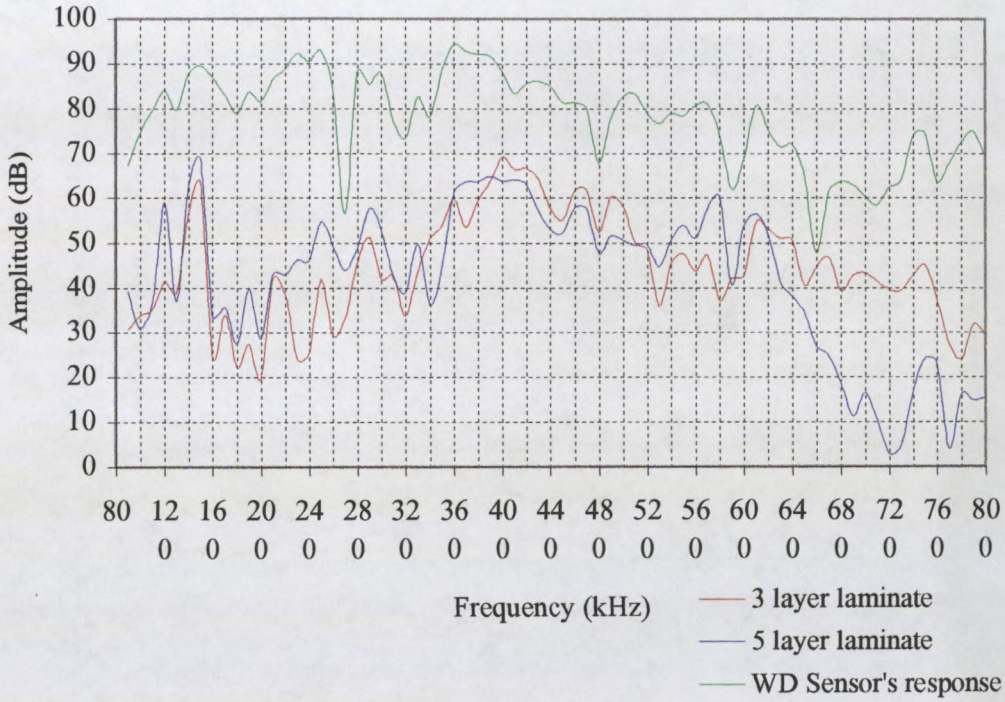

Figure 9.5.2. Comparison of response of laminates different thickness.

9.6 Detection of Teflon Patches

When the acoustic emission computer (PAC 3000) was used to supply the source transducer, the results from the testing on the Teflon containing laminate were ambiguous. In other words no consistent relation between the patch size and the AU parameters was found and the ability of the method for detecting delaminations could not be confirmed.

In an effort to establish a relationship between the AU parameters and the Teflon patch size the variable function generator has been used to supply the pulser. A 3 layer uni directional glass fibre laminate containing Teflon patches of diameter 10 mm, 20 mm, 40 mm, 80 mm and 120 mm was used in these experiments.

9.6.1 Selection of Testing Frequency

With 100 mm separation, the transducers were first placed on a region of the laminate that does not contain any Teflon. The input frequency was then increased in 10 kHz increments from 90 kHz to 800 kHz. The amplitude response of the receiving transducer was noted and plotted as a function of the input frequency. Thereafter the transducers were moved so as to straddle the 20 mm patch and the amplitudes for input frequencies between 90 kHz and 800 kHz were again plotted. This process was also applied to the 40 mm and then the 80 mm Teflon patch.

9.6.2 Results and Discussion

In many of the testing instances the received signal was below the AE system's threshold level, meaning that a reading could not be taken. Therefore the curves of figure 9.6.2 have breaks in them. The omission of a data point thus indicates that the amplitude was very low.

There is a correlation between the patch size and the signal amplitude. The correlation indicates that for larger patch sizes the amplitude will be lower. However the relationship between patch size and amplitude is not consistent and the curves cross at many locations.

Also evident from figure 9.6.2 is the fact that certain frequencies may be better suited to detecting Teflon patches. The frequencies that appear to be best are 150 kHz, 280 kHz, 610 kHz and frequencies between 480 kHz and 520 kHz since there is a good spacing between the amplitudes for each patch at these frequencies.

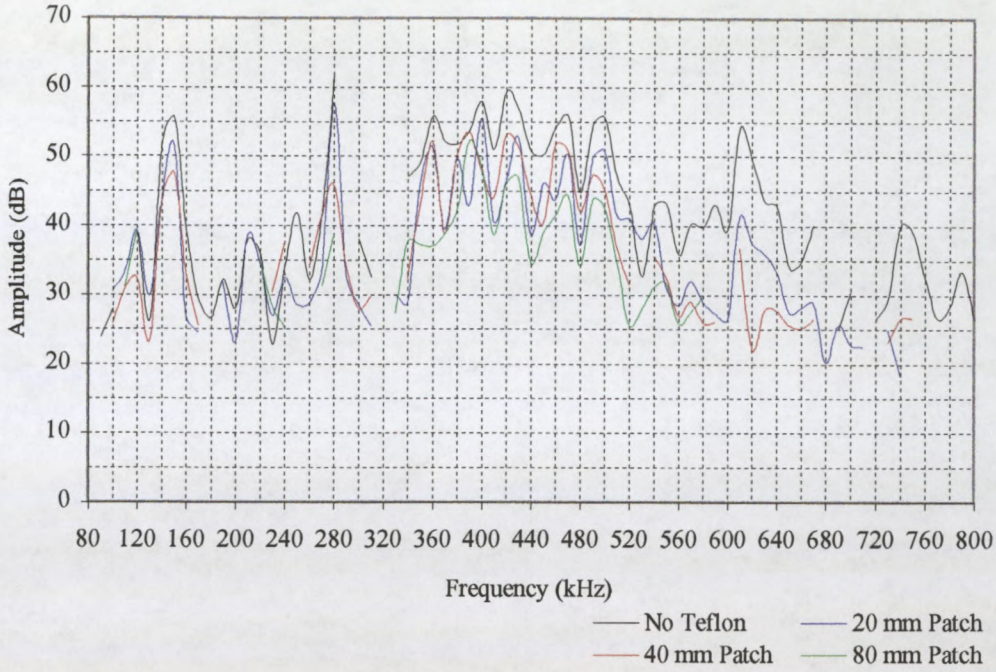

Figure 9.6.2. Amplitudes at several Teflon patches.

9.7 Single Frequencies for the Detection of Teflon Patches

Based on the findings of the previous experiment, input frequencies of 150 kHz, 492 kHz, 500 kHz and 610 kHz have been used on the Teflon patch containing laminate.

9.7.1 Test Method

The source and receiving transducers were coupled at 130 mm spacing to a region of the laminate that does not contain Teflon. The input frequency was set to 150 kHz, 492 kHz, 500 kHz and then 610 kHz and at each frequency the amplitude of the receiving transducer's response was noted. The transducers were then removed from the laminate before being re-adhered with fresh couplant. A second set of amplitude readings were then taken in an identical manner with the same transducer positions. This process was repeated 5 times, thereby obtaining 5 sets of amplitude readings on the region of the laminate that does not contain Teflon. Thereafter the transducers were moved so as to straddle a Teflon patch and 5 sets of amplitudes were, in the same way as before, recorded across the Teflon. In this way 5 sets of readings were taken at each patch and the average value was reported in each case to reduce the effects of coupling inconsistency and improve the accuracy of the results.

The average amplitudes have been plotted as a function of the patch size across which the amplitude readings were taken (figure 9.7.2). The error bars represent a 95 % confidence interval for individual readings.

9.7.2 Results and Discussion

In figure 9.7.2 many of the error bars are long enough for them to extend above and below their adjacent points. The cause of these long error bars is inconsistencies in the coupling.

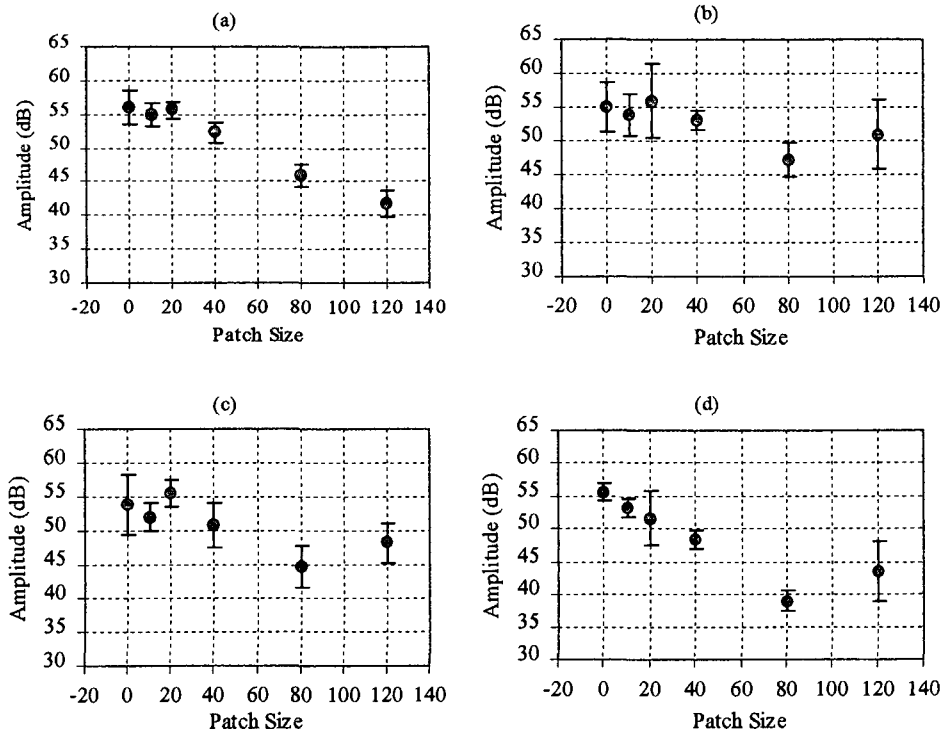

Figure 9.7.2. Average amplitude at Teflon patches of various sizes when the input frequency is set to: (a) 150 kHz, (b) 492 kHz, (c) 500 kHz and (d) 610 kHz.

The amplitude of the 150 kHz input signal (figure 9.7.2 (a)) is approximately the same for the case where there is no Teflon, the 10 mm Teflon patch and the 20 mm patch. However, as the patch diameter was increased from 20 mm to 120 mm, the amplitude decreases. For these patch sizes, with a 150 kHz input frequency, there is an approximately linear relationship between the amplitude and the patch diameter.

When the input frequency was set to 492 kHz and 500 kHz (figures 9.7.2 (b) and (c)) there is no consistent relation between the patch size and the amplitude.

Figure 9.7.2 (d) shows the amplitudes when the input frequency was set to 610 kHz. For the patches of up to 80 mm diameter the amplitude decreases linearly as the patch size increases. However the amplitude at the 120 mm patch deviates from the trend shown at the smaller patches.

9.8 The Effect of Sensor Spacing

When a 150 kHz input frequency and a 130 mm sensor spacing were used, there is an obvious relation between patch size and amplitude (figure 9.7.2 (a)). To verify that this trend will remain even when the sensor spacing is changed, the above experiment was repeated but with a 50 mm sensor spacing. Only the 3 smaller patches as well as a region of the laminate that does not contain Teflon were used in this case. Only the smaller patches were used so as to avoid the meaningless result that would arise if the transducer spacing were less than the patch diameter.

9.8.1 Method

With a 50 mm sensor spacing the transducers were located either side if the 10 mm, 20 mm and then 40 mm patch in turn. The input frequency was set to 150 kHz and, in an identical manner to the previous tests, an amplitude reading was taken 5 times with the renewal of the couplant between each reading. This process was then repeated with a 130 mm sensor spacing. The average of the 5 amplitudes have been plotted as a function of the patch size across which the amplitudes were recorded (figure 9.8.2). The error bars represent a 95 % confidence interval for single readings.

9.8.2 Results and Discussion

The main difference between figures 9.8.2 (a) and 9.8.2 (b) is that the amplitudes in 9.8.2 (a) are higher. This is to be expected and is due to the closer sensor spacing that has resulted in reduced attenuation. However the trends shown in figures 9.8.2 (a) and figure 9.8.2 (b) are the same ie. the average amplitudes are in the same relative positions in the two graphs.

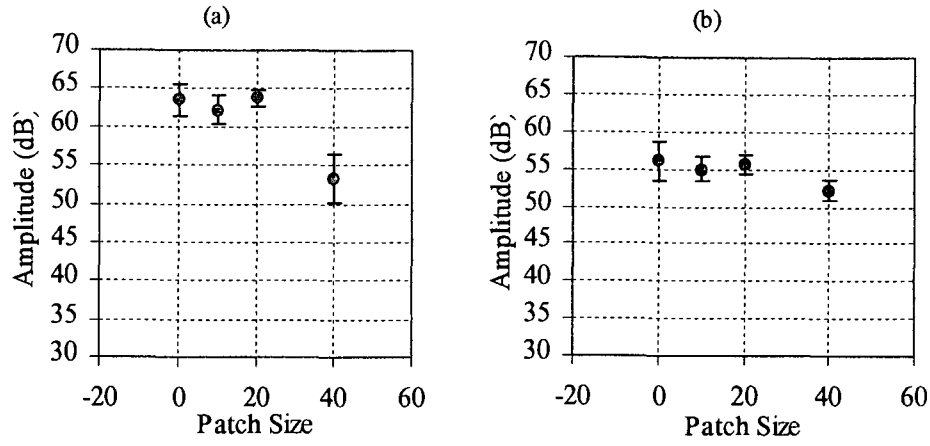

Figure 9.8.2. Average amplitude at Teflon patches of various sizes when the input frequency is 150 kHz and the sensor spacing is: (a) 50 mm and (b) 130 mm.

9.9 Conclusions

9.9.1 Repeatability

A repeatability experiment has shown the repeatability varies depending on the frequency of the input signal. The frequencies that will provide the most repeatable results are 150 kHz and those in the 400 kHz to 650 kHz range. At the frequencies that provide the optimum repeatability, the percentage range of the amplitudes was less than 8 % (or $^{+}/_{-}$ 4 %). Thus, with the use of single readings, it may not be possible to detect defects that cause a reduction in the amplitude of less than 10 %. In order to detect such defects, several readings would need to be taken and assessment would have to be based on their average.

At the three best frequencies in terms of repeatability, the amplitudes are within $^{+}/_{-}$ 4 %. This repeatability is better than that achieved by Henneke *et al* [63] who conducted a similar set of repeatability experiments and achieved an optimum repeatability of $^{+}/_{-}$ 10 % for stress wave factor values.

9.9.2 Characterizing the WD Sensor

The WD transducer's response curve shows numerous peaks. Thus the notion that this transducer has an equal response to a wide band of frequencies is not entirely true. This highlights the fact that the received signal is not necessarily an accurate indication of the particle motion within the material since the resonances of the sensor will affect the signal. Such a curve is nevertheless suitable for AU testing and should be considered when investigating the frequencies transmitted within a structure.

9.9.3 Comparison of Waveforms Travelling Parallel and Perpendicular to Fibre Direction

The same frequency components are transmitted by a laminate irrespective of whether the wave travels parallel to or perpendicular to the fibre direction. A wave that travels perpendicular to the fibre direction will experience a more rapid attenuation of its higher frequency components than a wave that travels parallel to the fibres. This correlates with earlier tests that showed that a wave that travels perpendicular to the fibre direction would have a lower central frequency.

9.9.4 Comparison of Response of Laminates of Different Thickness

Since in terms of the locations of their peaks and troughs the response curves for the 3 layer, 5 layer and WD sensor are similar, the received signal consists primarily of sensor resonances and the resonances of the laminate are not evident. The most likely reason for this is that the laminate's resonant frequencies are outside the WD sensor's sensitivity range. This observation correlates with the dispersion curves which show that the WD sensor's range of sensitivity is below the cutoff frequencies of the majority of the wave modes in a thin glass fibre laminate. This situation is not ideal and many authors have specified that for improved materials characterisation the input frequency should match the resonant frequency of the structure. Future work should be aimed at determining the laminate's resonant frequency and using a pair of transducers that are capable inputting and detecting this frequency.

The increased attenuation of the upper frequencies in the 5 layer laminate correlate with the findings of earlier tests in which it was shown that a wave in a thicker laminate will have a lower central frequency.

9.9.5 Detection of Teflon Patches

By using a single frequency as an input signal the detection of simulated delaminations has been improved. This correlates with the recommendation that the use of a specific wave mode would provide a better indication of the material's condition [16].

Two different sensor spacings have been compared for the detection of Teflon patches. Both spacing have yielded the same result. Therefore the capability of the AU technique for the detection of Teflon patches is independent of sensor spacing.

Variations due to coupling inconsistencies are present, and this highlights the need for assessment to be based the average of a number of readings.

There appears to be a relation between the Teflon patch size and the frequency that can effectively be used to detect the Teflon. An input signal of 150 kHz is suited to locating and sizing delaminations that are 40 mm and greater in diameter but cannot be used to discriminate between patches that are small than 40 mm in diameter. A 610 kHz input signal is suited to detecting and sizing delaminations that have diameters of less than 80 mm.

Chapter 10

Conclusions

10.1 Development of a Repeatable Test Method

The numerous factors that affect the results of AU experiments have been identified. Efforts to develop a repeatable test method have shown that variations to any of these factors can have an effect on an AU experiment's results. Thus for AU testing, as has been done in this study, a testing procedure that produces the most repeatable results must be identified and adhered to.

The major obstruction to achieving perfectly repeatable results is in the coupling of the transducers to the test specimen. Although much effort has been focussed on the improvement of this aspect of the testing procedure, inconsistencies due to coupling persist. Unless a means of improving the consistency of the coupling is found, then suitable reliability and accuracy can only be achieved by recording numerous waveforms from which the average value of each parameter can be calculated.

The 5 parameters used for characterising AU waveforms in this study each have a differing repeatability. Arrival time and central frequency are the most repeatable and thus, when possible, material assessment should be based on the value of these parameters. The parameter ringdown counts has the next best repeatability and should also be considered since not all defect conditions affect the arrival time and central frequency.

10.2 Thin Laminates

A composite laminate's fibre orientation, resin content and thickness all have a distinct influence on all 5 AU parameters. Thus the AU method can be used to gauge a composite's anisotropic nature and thickness as well as locate resin-starved regions. AU

waves are affected by the orientation of all of the fibre layers of a thin laminate, which shows that the waves penetrate right through its thickness.

10.3 Landing Bay Door

The AU method has been proved in a realistic situation by applying it to a landing bay door. The fibre orientations, as indicated by the wave speeds, correlate with the orientations determined from a visual inspection. A defect within the door's structure caused the introduction of an additional wave mode and affected the attenuation and wave speed. Thus with the knowledge gained of these effects, defects of this type can be identified.

An AU test, conducted on both repaired and unrepaired regions of the bay door, indicated higher wave speeds in the repair. A mechanical test shows that the repair has a greater flexural stiffness and this is thought to correlate with the higher wave speeds. Thus the AU method can be used to determine whether the properties of a repair match those of the unrepaired material.

10.4 Wake-board

A damaged wake-board has been subjected to AU tests. The damage in the wake-board is of a similar nature to that in the landing bay door and has thus has a similar effect on the AU results. The skin to core delamination has caused an increase in the wave's speed and energy content and resulted in an additional wave mode.

10.5 Dispersion Curves

The theory underlying the propagation of waves in plates has been reviewed. Dispersion curves have been plotted from which the cutoff frequencies of thin glass fibre laminates have been determined. When these frequencies were compared to the sensitivity range of the receiving transducer, it was found that most of the wave modes exist outside of the transducer's range. However the accuracy of the dispersion curves is questionable since the number of wave modes that they predict is different to the number of modes observed in the Fourier transforms.

Accurate dispersion curves should be used in future work to select a receiving transducer that is sensitive to a particular wave mode. The use of a particular mode may improve the AU method's sensitivity to defects.

10.6 Impact Damage Detection

The AU method has been applied to a laminate that has been impact damaged. The parameters peak voltage, ringdown counts and energy were found to be affected by the impact damage while central frequency and arrival time were unaffected. The reliable detection of impact damage is limited to the cases where the damage is severe and the discrimination between small impacts and undamaged material is not possible.

10.7 Delamination Detection

Delaminations have been simulated by including Teflon film patches of various sizes between the layers of a glass fibre laminate. In an AU test, the arrival time was the most consistent indicator of the presence of the Teflon. The parameters peak voltage, ringdown counts and energy were affected by the presence of the Teflon but a relation between the diameter of the Teflon patch and the value of these parameters was not evident. It is likely that resonance or wave mode conversion at certain patches has caused this.

10.8 Input Frequency Control

The effect of controlling the frequency of the wave input into the specimen has been investigated. These experiments have shown that an increase in the thickness of a laminate will cause an increase in the attenuation of the upper frequencies. Likewise, the upper frequencies of a wave will attenuate more when a wave that travels at perpendicular to the fibres as compared to when it travels parallel to the fibres.

In a repeatability experiment it was found that certain frequencies are more susceptible to variations due to coupling inconsistencies. Thus the repeatability can be improved by selecting the frequency of the input accordingly.

Certain frequencies were found to be more reliable indicators of the presence of Teflon patches than others. By testing at these frequencies the detection of Teflon patches was improved. A relation was observed between the diameter of the patch and the frequency that can be used to detect it. It was found that to discriminate between small diameter patches a high frequency is required whereas a lower frequency is necessary for the detection of larger patches. Thus in order to detect delaminations of a range of size several pulses, each with a differing frequency will have to be used.

Generally speaking, defect detection and materials characterisation has been improved through the use of a single frequency input. The most effective frequencies will be those that provide the best repeatability and also depend on the structure's natural frequencies and the instruments and transducers used. The selection of the testing frequencies should be based on preliminary experiments that determine the frequencies transmitted by the structure.

The AU method is suited to being used in a portable device for detecting damage, manufacturing flaws, assessing repairs and locating material property variations. However the method has a number of complexities such as wave mode conversion, resonance, surface and substrate effects, sensitivity to coupling variations and the effect of specimen constraints. Before the method can be effectively implemented in a portable device, these complexities need to be investigated further.

References

1. Smith, W. F. 1993. *Foundations of Materials Science and Engineering.* New York: McGraw-Hill.
2. *S P Systems ® Composite Engineering Materials.* Guide to Composites, http://www.spsystems.com
3. Gürdal, Z., Haftka, R. T. and Hajela, P. 1999. *Design and Optimization of Laminated Composite Materials.* New York: Wiley Interscience.
4. Rose, J. L. 1999. *Ultrasonic Waves in Solid Media.* United Kingdom: Cambridge University Press. pp. 262.
5. Fowler, K. A. and Papadakis, E. P. 1972. Observation and Analysis of Simulated Ultrasonic Acoustic Emission Waves in Plates and Complex Structures. *Acoustic Emission,* **505**: 222-237.
6. Lamb, N. 1917. On Waves in an Elastic Plate. *Proceedings of the Royal Society,* 1917: A93:114-28.
7. Graff, K. 1976. *Elastic Wave Motion in Solids.* Ohio State University Press.
8. Prosser, W. H. and Dorighi, J. 1992. Extensional and Flexural Waves in a Thin-Walled Graphite/Epoxy Tube. *Journal of Composite Materials,* **26**(14): 2016-2027.
9. Gorman, M. R. *Journal of Composite Materials,* Submitted for publication.
10. Gorman, M. R. and Prosser, W. H. 1991. AE Source Orientation by Plate Analysis. *Journal of Acoustic Emission,* **9** (4): 283-289.
11. Dunegan, H. L. 1997. *Modal Analysis of Acoustic Emission Signals.* Dunegan Engineering Company Inc. Technical Report, October 1997 [online]. Available from: http://www.deci.com/oct97.htm. [Accessed May 2000].
12. Mindlin, R. D. and Medick, M. A. 1959. Extensional Vibrations of Elastic Plates. *Journal of Applied Mechanics,* **26**: 561-569.
13. Kane, T. R. and Mindlin, R. D. 1956. High-Frequency Extensional Vibration of Plates. *Journal of Applied Mechanics,* **23**: 277-283.
14. Prosser, W. H. and Dorighi, J. 1992. Extensional and Flexural Waves in a Thin-Walled Graphite/Epoxy Tube. *Journal of Composite Materials,* **26**(14): 2016-2027.

15. Rose, J. L. 1999. *Ultrasonic Waves in Solid Media.* United Kingdom: Cambridge University Press. pp. 101-130.

16. Ditri, J., Rose, J. L. and Chen, G. 1991. Mode Selection Guidelines for Defect Detection Optimisation Using Lamb Waves. *In: proceedings of the 18th Annual Review of Progress of Quantitative NDE.* New York: Plenum. 11: 2109-15.

17. Egle, D. M. and Brown, A. E. 1975. Considerations for the Detection of Acoustic Emission Waves in Thin Plates. *The Journal of the Acoustical Society of America,* 57(3):591-597.

18. Kiernan, M. T. and Duke, J. C. Jr. 1988. Acousto-Ultrasonics as a Monitor of Material Anisotropy. *Materials Evaluation,* 46: 1105-1113.

19. Achenbach, J. D. 1973. *Wave Propagation in Elastic Solids,* American Elsevier. New York, NY.

20. Talreja, R. 1988. Application of Acousto-Ultrasonics to Quality Control and Damage Assessment of Composites. *In*: Duke, J.C. Jr. (ed.). *Acousto-ultrasonics: Theory and Application: proceedings of a workshop held at the Virginia Polytechnic Institute and State University, July 1987.* New York: Plenum Press. pp. 177-190.

21. Kroll, J. R., Stress Waves in Test Specimens due to Simulated Acoustic Emission. Ph.D. dissertation, Michigan State University, 1962.

22. Halmshaw, R. 1991, *Non Destructive Testing.* Second edition. Edward Arnold: London.

23. Li, L. and Zhao, J. H. 1986. The Monitoring of Damage Growth Process in Glass Fibre Reinforced Composite by Amplitude Analysis. *In: Second International Symposium on Acoustic Emission for Reinforced Composites,* Society of the Plastics Industry. Montreal, Canada, New York, pp. 90-95.

24. Berthelot, J. M. 1986. Relation Between Amplitudes and Rupture Mechanisms in Composite Materials, *Second International Symposium on Acoustic Emission for Reinforced Composites,* Society of the Plastics Industry, Montreal, Canada, New York, pp. 126-133.

25. Valentin, D., Bonniau, Ph. and Bunsell, A. R. 1983. Failure Mechanism Discrimination in Carbon Fibre-Reinforced Epoxy Composites. *Composites,* 14 (4): 345-351.

26. Ono, K. 1986. Acoustic Emission Behaviour of Flawed Unidirectional Carbon Fibre-Epoxy Composites. *Second International Symposium on Acoustic*

Emission from Reinforced Composites, Society of the Plastics Industry. Montreal, Canada, New York, pp. 22-28.

27. Guild, F. J., Phillips, M. G. and Harris, B. 1983. Acoustic Emission Studies of Damage in GRP. *NDT International,* October. pp. 209-218.
28. Pao, Y. H. 1978. Theory of Acoustic Emission. *Elastic Waves and Non-Destructive Testing of Composite Materials,* ASME AMD, New York, **29**:107-128.
29. Gorman, M. R. 1995. New Technology for Wave Based Acoustic Emission and Acousto-Ultrasonics, *Proceedings of the 41st International Instrumentation Symposium,* pp 471-480.
30. Breckenridge, F. R., Proctor, T. M., Hsu, N. N. and Eitzen, D. G. 1986. Some Notions Concerning the Behaviour of Transducers. *Progress in Acoustic Emission III,* The Japanese Society of NDI, pp. 675-684.
31. Hsu, N. N. and Eitzen, D. G. 1982. The Inverse Problem of Acoustic Emission – Explicit Determination of Acoustic Emission Source Time Functions. *In*: Thompson, D. O. and Chementi, D. E. (eds.) *Review of Progress in Quantitative Nondestructive Evaluation.* Plenum Publishing Corporation. pp. 405 -412.
32. Proctor, T. M., Jr. 1982. Some Details on the NBS Conical Transducer. *Journal of Acoustic Emission,* **1** (3).
33. Hsu, N. N. and Breckenridge, F. R. 1980. Characterisation and Calibration of Acoustic Emission Sensors. *Materials Evaluation,* **39**(1): 60-68.
34. American Society for Testing of Materials. 1996. *Standard Practice for Acoustic Emission Examination of Fibreglass Reinforced Plastic Resin Tanks/Vessels.* 1996. West Conshohocken, Pasadena, United States: American Society for Testing of Materials.
35. American Society for Testing of Materials. 1997. *Standard Guide for Acoustic Emission Examination of Small Parts.* West Conshohocken, Pasadena, United States: American Society for Testing of Materials.
36. Walker, M., Jonson, D and Dugmore, K. 2000. The use of Acoustic Emission Monitoring for Online Damage Assessment and Risk Management of GRP Pressure Vessels and Pipes. *Polifin Non-Metallics Conference on "Into the Future with Non-Metallic Engineering", May 2000,* Maccauvlei Conference Centre, Vereeniging. pp. 58-68.

37. Morrás, M. L., Rodriguez, M. and León, L. M. 1997. Acoustic Emission Applied to Pipes of GFRP that have been Exposed to Corrosive Mediums. *Journal of Composite Materials,* **31** (9): 896-909.

38. Cheng, R., Tozawa, T., Gen, M., Kato, H. and Takayama, Y. 1996. AE Behaviours with BP Neural Network. *Computers and Industrial Engineering,* **31** (3/4): 867-871.

39. Hill, R., Brooks, R. and Kaloedes, D. 1999. Transverse Cracking of Fibre Bundle Composites Studied by Acoustic Emission and Weibull Statistics – Effects of Postcuring and Surface Treatment. *Journal of Materials Science,* **34**: 5215-5226.

40. Barnes, C. A. and Ramirez, G. 1998. Acoustic Emission Testing of Carbon Fibre Composite Offshore Drilling Risers. In: *Proceedings of the Sixth International Symposium on Acoustic Emission from Composite Materials. American Society for Nondestructive Testing, Inc. San Antonio, Texas, June 1-4, 1998.* pp. 1322.

41. Shiwa, M., Carpenter, S. and Kishi, T. 1996. Analysis of Acoustic Emission Signals Generated during the Fatigue Testing of GFRP. *Journal of Composite Materials,* **30** (18): 2019-2041.

42. Qi, G., Barhorst, A., Hashemi, J. and Kamala, G. 1997. Discrete Wavelet Decomposition of Acoustic Emission Signals from Carbon-Fibre Reinforced Composites. *Composites Science and Technology,* **57**: 389-403.

43. Gorman, M. R. and Ziola, S, M. 1991. Plate Waves Produced by Transverse Matrix Cracking. *Ultrasonics,* **29**: 245-251.

44. Prosser, W. H. and Dorighi, J. 1992. Extensional and Flexural Waves in a Thin-Walled Graphite/Epoxy Tube. *Journal of Composite Materials,* **26**(14): 2016-2027.

45. Dunegan, H. L. 1997. *Modal Analysis of Acoustic Emission Signals.* Dunegan Engineering Company Inc. Technical Report, October 1997 [online]. Available from: http://www.deci.com/oct97.htm. [Accessed May 2000].

46. Vary, A. 1988. The Acousto-Ultrasonic Approach. *In*: Duke, J.C. Jr. (ed.) *Acousto-Ultrasonics Theory and Application: proceedings of a workshop held at the Virginia Polytechnic Institute and State University, July 1987.* New York: Plenum Press. pp. 1-21.

47. Vary, A. 1991. Acousto-Ultrasonics: Retrospective Exhortation with Bibliography. *Materials Evaluatio,.* **49** (5): 581-591.

48. Kiernan, M. T. and Duke, J. C. Jr. 1988. PC Analysis of an Acousto-Ultrasonic Signal. Materials Evaluation, pp 1344-1352.
49. Duke, J.C. Jr. 1988. Preface. In: Duke, J.C. Jr. (ed.) Acousto-Ultrasonics Theory and Application: proceedings of a workshop held at the Virginia Polytechnic Institute and State University, July 1987. New York: Plenum Press. pp. v.
50. American Society for Testing of Materials. 2000. *Standard Guide for the Acousto-Ultrasonic Assessment of Composites, Laminates and Bonded Joints.* West Conshohocken, Pasadena, United States: American Society for Testing of Materials.
51. American Society for Testing of Materials. 2000. *Standard Practice for Acousto-Ultrasonic Assessment of Filament-Wound Pressure Vessels.* West Conshohocken, Pasadena, United States: American Society for Testing of Materials.
52. Talreja, R. 1988. Application of Acousto-Ultrasonics to Quality Control and Damage Assessment of Composites. *In*: Duke, J.C. Jr. (ed.) *Acousto-Ultrasonics Theory and Application: proceedings of a workshop held at the Virginia Polytechnic Institute and State University, July 1987* New York: Plenum Press. pp. 177-190.
53. Sundaresan, M. J., Henneke, E. G. II. and Brosey, W. D. 1989. Acousto-Ultrasonic Investigation of Filament-Wound Spherical Pressure Vessels. *Materials Evaluation*, pp 601-606.
54. Lo, Y. J., Wu, S. K., Hwang, D. G. and Hsu, S. E. 1989. A Correlation Between Strength and Acousto-Ultrasonic Signal for a CFRP Laminate. *Proceedings 1st MRS International Meeting on Advanced Materials,* **5**: 475-480.
55. Talreja, R., Govada, A. and Henneke, A. A. 1984. Quantitative Assessment of Damage Growth in Graphite-Epoxy Laminates by Acousto-Ultrasonic Measurements. *In:* D. O. Thompson and D. Chimenti, (eds.) *Review of Progress in Quantitative Nondestructive Evaluation.* Plenum Press, New York.
56. Srivastava, V. K. 1983. Acousto-Ultrasonic Evaluation of Interface Bond Strength of Coated Glass Fibre-Reinforced Epoxy Resin Composites. *Composite Structures,* pp 281-285.
57. Phani, K. K. and Bose, N. R. 1987. Hydrothermal Ageing of Jute-Glass Fibre Hybrid Composites – an Acousto-Ultrasonic Study. *Journal of Materials Science,* **22**:1929-1933.

58. Vary, A. and Bowles, K. J., NASA TM X-73646, 1977.

59. Vary, A. and Bowles, K. J. 1979. An Ultrasonic-Acoustic Technique for Nondestructive Evaluation of Fibre Composite Quality. *Polymer Engineering and Science,* **19** (5): 373-376.

60. Fahr, A., Lee, S., Tanary, S. and Haddad, Y. 1989. Estimation of Strength of Adhesively Bonded Steel Specimens by Acousto-Ultrasonic Technique. *Materials Evaluation,* **47**: 233-241.

61. Tang, B., Lui, C. T. and Henneke, E. G. II. 1995. Acousto-Ultrasonic Technique Applied to Filled-Polymer Damage Assessment. *Journal of Spacecraft and Rockets,* **32**(5): 866-869.

62. Tiwari, A. and Henneke II, E. G. 1996. Recent Developments in Real-Time Acousto-Ultrasonic NDE Technique to Detect and Monitor Damage Modes under Compressive Load. *Materials Science Forum,* **210-213**: 573-580.

63. Henneke, E. G., II., Duke, J. C., Jr., Stinchcomb, W. W., Govada, A. and Lamoscon, A. 1983. A Study of the Stress Wave Factor Technique for the Characterisation of Composite Materials. *NASA CR-3670*

64. Dugmore, K. and Jonson, D. 2001. *Acousto-Ultrasonics for Defect Assessment in Composite Structures.* Presentation at Kentron Student Conference, Kentron, Irene, October 2001.

65. Breckenridge, F. R., Proctor, N. N., Hsu, N. N. and Eitzen, D. G. 1986. Some Notions Concerning the Behaviour of Transducers. *Progress in Acoustic Emission III, The Japanese Society of NDI,* pp. 675-684.

66. Physical Acoustics Corp., Mistras 2001 AEDSP-32/16 user's manual, 1995; Ch 3, 3.

67. Dugmore, K., Jonson, D and Walker, M. 2001. A Comparison of Signal Consistency using Common Ultrasonic Couplants. *Composites Part A: Applied Science and Manufacturing.* Submitted for publication.

68. Wooh, S. C. and Wei, C. 1999. A high-fidelity Ultrasonic Pulse-Echo Scheme for Detecting Delaminations in Composite Laminates. *Composites,* pp 433 -441.